DOUBLE-DIFFUSIVE NATURAL CONVECTION WITHIN A CLOSED ANNULUS

To My Family

NUMERICAL SIMULATION OF DOUBLE-DIFFUSIVE NATURAL CONVECTION WITHIN A CLOSED ANNULUS

By

PAUL W. SHIPP, B.ENG.

A Thesis

Submitted to the School of Graduate Studies

in Partial Fulfilment of the Requirements

for the Degree

Master of Engineering

McMaster University

MASTER OF ENGINEERING (1991)
(Mechanical)

McMASTER UNIVERSITY
Hamilton, Ontario

TITLE: Numerical Simulation of Double-Diffusive Natural Convection within a Closed Annulus

AUTHOR: Paul W. Shipp, B.Eng (McMaster University)

SUPERVISORS: Dr. M. Shoukri

Dr. M. B. Carver

NUMBER OF PAGES: xvii, 161

ABSTRACT

A numerical study for steady laminar double-diffusive natural convection within a vertical closed annulus is examined with a constant temperature and mass species (concentration) difference imposed across the vertical walls. System parameters are the thermal Rayleigh number, the buoyancy ratio, the Lewis number and the Prandtl number, with the aspect ratio and the curvature ratio as the physical enclosure parameters.

The effect of the buoyancy ratio, thermal Rayleigh number and Lewis number was investigated on the flow structure and the average Nusselt and Sherwood numbers. Resulting flow structures were found to fall into three categories: mass species buoyancy force dominated circulation, thermal buoyancy force dominated circulation and transitional flow. It was determined that the solutions in the flow reversal range are not unique, with two or three solutions for the same parameters depending on the original flow conditions. The extent of this flow reversal range is defined by upper and lower critical buoyancy ratios which are influenced by the Lewis and thermal Rayleigh numbers.

ACKNOWLEDGEMENTS

I would like to express my appreciation to Dr. M. Shoukri for his time, patience and guidance throughout the course of this study.

Sincere thanks are extended to all faculty members, staff members and graduate students within the Mechanical Engineering department, who have provided a friendly and pleasantly interesting working atmosphere.

Finally I would like to give special thanks to Dr. M. B. Carver for providing his insight and expertise despite the distances involved.

TABLE OF CONTENTS

NOMENCLATURE

a	Coefficient in discretization equation (SIMPLER)	
b	Source term in discretization equation (SIMPLER)	
Ar	Aspect ratio	[H/R]
C	Mass fraction of constituent	
C^*	Dimensionless concentration	$[(C - C_r)/(C_i - C_o)]$
d	Coefficient of pressure-difference term (SIMPLER)	
D	Mass diffusivity of constituent through the fluid mixture	
D	Diffusion conductance (SIMPLER)	
F	Flowrate through a control volume face (SIMPLER)	
g	Gravitational acceleration	
Gr_C	Mass species Grashof number	$[g\beta_C(C_i - C_o)R^3/\nu^2]$
Gr_T	Thermal Grashof number	$[g\beta_T(T_i - T_o)R^3/\nu^2]$
h	Convective heat transfer coefficient	
hm	Convective mass species transfer coefficient	
H	Height of enclosure	
k	Thermal conductivity	
K	Curvature ratio	$[r_o/r_i]$
i	Cell size increase percentage for non-uniform grids	
j"	Mass species flux	
J	Total (convection + diffusion) flux (SIMPLER)	
L	Characteristic length for two-dimensional test case	
Le	Lewis number	$[\alpha/D]$

m	Number of cells across enclosure	
n	Buoyancy ratio	$[\ \beta_C(C_i-C_o)/\beta_T(T_i-T_o)\ ]$
Nu	Local Nusselt number	$[\partial T^*/\partial r^*]$
$\overline{Nu}$	Average Nusselt number	
P	Pressure	
P^*	Dimensionless pressure	$[\ PR^2/\rho_r\alpha^2\ ]$
Pe	Peclet number	$[\ u\ \Delta r/\Gamma\ ]$, $[\ v\ \Delta z/\Gamma\ ]$
Pr	Prandtl number	$[\ \nu/\alpha\ ]$
q"	Heat flux	
r	Radial coordinate	
r^*	Dimensionless radial coordinate	$[\ r/R\ ]$
R	Radial difference	$[\ r_o-r_i\ ]$
R	Field equation residual	
Ra_C	Mass species Rayleigh number	$[\ g\beta_c(C_i-C_o)R^3/D\nu\ ]$
Ra_T	Thermal Rayleigh number	$[\ g\beta_T(T_i-T_o)R^3/\alpha\nu\ ]$
s	Number of thin cells for semi-uniform grids	
S	Source term (SIMPLER)	
Sc	Schmidt number	$[\ \nu/D\ ]$
Sh	Local Sherwood number	$[\partial C^*/\partial r^*]$
$\overline{Sh}$	Average Sherwood number	
t	Time	
T	Temperature	
T^*	Dimensionless temperature	$[\ (T-T_r)/(T_i-T_o)\ ]$
u	Radial velocity	
u^*	Dimensionless radial velocity	$[\ uR/\alpha\ ]$
v	Axial velocity	

v^*	Dimensionless axial velocity	[vR/α]
z	Axial coordinate	
z^*	Dimensionless axial coordinate	[z/R]

Greek Symbols

α	Thermal diffusivity
β_C	Mass species expansion coefficient
β_T	Thermal expansion coefficient
δ	Distance between two adjacent grid points (SIMPLER)
Δ	Difference, Width of control volume (SIMPLER)
ϕ	Dependent variable (SIMPLER)
Γ	Diffusion coefficient (SIMPLER)
ν	Kinematic viscosity
ω	Underrelaxation factor
η	Tridiagonal matrix algorithm (TDMA) overrelaxation factor
ρ	Fluid density
ψ	Streamfunction
ψ^*	Dimensionless streamfunction [$\psi/R\alpha$]

Subscripts

C	Mass species
e,w,n,s	East, west, north and south neighboring control volume faces
E,W,N,S	East, west, north and south neighboring grids points (SIMPLER)
i	Inner radial wall
I,J	Computational space coordinates
nb	General neighbor grid point (SIMPLER)
o	Outer radial wall

r	Reference
P	Central grid point under consideration (SIMPLER)
T	Thermal

Superscripts

*	Non-dimensional
'	Non-dimensional for flux boundary conditions, or Correction value (SIMPLER)
—	Average
~	Guessed value (SIMPLER)
^	Pseudo value (SIMPLER)
m	Iteration step

LIST OF FIGURES

LIST OF TABLES

CHAPTER ONE

INTRODUCTION

1.1 Introductory Remarks

The study of convection produced by unbalanced density gradients in a fluid, otherwise known as natural convection, has been extensively studied. When the unstable density gradient is subjected to a gravitation field, natural convective fluid flow will result. The density gradient can usually be created by a temperature gradient or a concentration gradient.

Most numerical studies have attended to cases of temperature variations due to heat transfer as the single driving force. However more recently, attention has been paid to the simultaneous presence of two components with different diffusivities. This type of flow is referred to as *double-diffusive* natural convection, in which a whole range of interesting phenomena can be studied and applied.

1.2 Configurations

Thermal natural convection studies have almost extensively examined all types of configurations for external and internal flows. External flow studies usually examine flow occurring around a submerged body. The heated or cooled vertical plate would be a more well known case, however other external flow configurations such as horizontal flat plates, vertical and horizontal cylinders, and spheres have also been

examined. The majority of numerical studies of internal flow have been limited to two dimensional rectangular enclosures. However, a few studies have been performed on vertical and horizontal closed cylinders, or other irregular geometries. In double-diffusive natural convection most, if not all, numerical studies have been performed with two dimensional rectangular coordinates. At the present time there is a need to expand this field to include other geometries. The present study attempts to do this by examining the heat, mass and laminar flow characteristics for a closed annulus in axi-symmetric coordinates.

1.3 Analogy of Heat and Mass Transfer

The concept of mass transfer is very similar to heat transfer, where as the temperature difference is the driving potential for heat transfer (Fourier's law), the concentration difference is the driving potential for mass transfer (Fick's law).

Fourier's law

$$q'' = - k \frac{\partial T}{\partial x}$$

Fick's law

$$j'' = - \rho D \frac{\partial C}{\partial x}$$

The similarity between heat and mass transfer is given in table 1.1.

Table 1.1 Similarity of Heat and Mass Transfer.

Variable	Heat	Mass
Potential	ΔT	ΔC
Flux	q''	j''
Flux (Non dimens.)	Nu	Sh
Diffusivity	α	D
Diffusivity (Non dim.)	Pr	Sc
Expansion Coef.	β_T	β_C

1.4 Double-Diffusive Applications

Natural convection is caused by the density gradient due to the concentration and temperature gradients. Many occurrences of double-diffusive natural convection are found in nature and technology. In nature, double-diffusive natural convection may be found in flows of water containing suspended particulate or dissolved materials which increase the local fluid density acting along with temperature gradients. A prime example of this is in the study of oceanography where thermal and salinity gradients drive the flow (an example of this is when sea water intrudes into fresh water), this is also known as *thermohaline* or *thermosolutal* convection [1]. Atmospheric flows also can be considered to be double-diffusive with temperature and water concentration gradients. Astronomers have suggested that double-diffusive convection occurs in large stars in which the helium rich core is heated from below while cooler hydrogen exists outside the core [2]. Double-diffusive convection can also be applied to the fields of geology and geophysics where chemical and thermal differences at the core-mantle boundary within the Earth drive magma flow [3].

Technological applications of double-diffusive natural convection are also as widespread. Examples include cleaning and drying operations, where residual fluids diffuse into a surrounding fluid medium at a different temperature. Liquid gas storage, transpiration cooling, energy storage in solar ponds [4], material processes such as solidification, oxidation of surface material [2] and the fouling of piping and fluid storage components also entail such flows. Recently, there has been an increased interest in the role double-diffusive

natural convection plays in crystal-growth techniques where temperature and concentration differences are evidently required for crystal growth [5]. Simultaneous heat and mass transfer is not only important for its engineering applications, but also for the understanding of the physics involved. Some of the examples are listed with the driving forces in table 1.2 [6].

Table 1.2 Simultaneous Heat and Mass Transfer Processes and Driving forces.

Application	Species	ΔC	ΔT
Evaporation of water	Water Vapour	$C_{surface} - C_{moist\ air}$	$T_{surface} - T_{moist\ air}$
Frost Formation	Water Vapour	$0 - C_{moist\ air}$	$T_{frost} - T_{moist\ air}$
Drying of Painted Surfaces	Solvent	$C_{wall} - C_{air}$	$T_{wall} - T_{air}$
Melting of Ice in Sea Water	Water	$1 - C_{sea\ water}$	$T_{ice} - T_{sea\ water}$
Chemical Leaching	Metallic Salt	$C_{surface} - C_{solute}$	$T_{solid} - T_{solute}$

1.5 Orientation of Driving Forces

Problems that involve the simultaneous presence of temperature and concentration gradients are considerably more complex than problems with a single driving force. For a single driving force in an enclosure (temperature and concentration gradients are interchangeable in this case), there are two modes of convection depending on the orientation of the density gradient with respect to the gravitational or body force

direction. If the density gradient is perpendicular to the body force (fig. 1.1a), flow will result and is referred to as *conventional natural convection*. If the density gradient is parallel and acting in the same direction as the body force no flow is possible due to the stratified stabilizing effect of the density gradient; heat or mass diffusion will occur as if the fluid is solid. However, if the body force and the density gradient are opposed, and a critical value for the density gradient is exceeded, flow will result in the form of rolling cells or vortices (fig. 1.1b), this is referred to as the *Bénard convection problem*.

With the simultaneous action of both temperature and concentration gradients more configurations for different orientations are possible. The combinations of the two gradients are displayed in figures 1.2a through 1.2d. In figures 1.2a and 1.2b the temperature and concentration gradients are parallel to each other. In case (a) the opposing concentration and temperature gradients augment the density gradient. A positive concentration gradient will tend to produce a positive density gradient, whereas a positive temperature gradient produces a negative density gradient. In case (b) the temperature and concentration gradients are aligned and suppress the resulting combined density gradient. If the strength of the concentration and temperature gradients are equal and the two components have matched diffusivities the flow will be impeded, resulting in heat conduction and mass transfer through molecular diffusion only. The effect of the temperature and concentration gradients on the buoyancy forces will be discussed later.

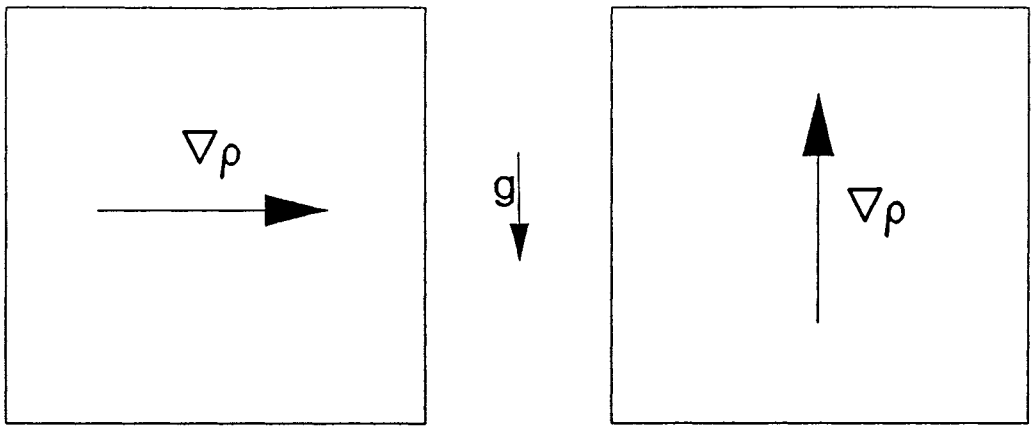

(a) Conventional Natural Convection

(b) Bénard Problem

Figure 1.1 Possible Directions of Single Density Gradients in an Enclosure

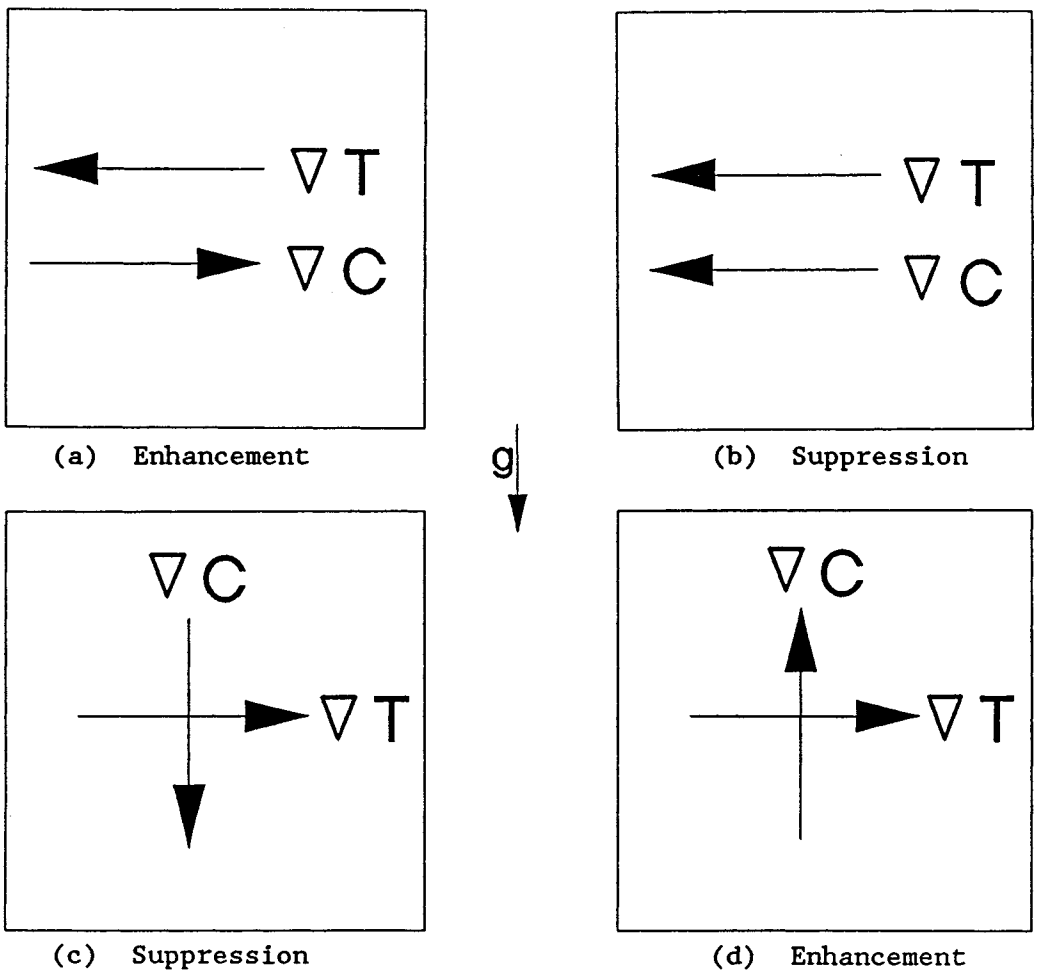

(a) Enhancement

(b) Suppression

(c) Suppression

(d) Enhancement

Figure 1.2 Orientation of the Temperature and Concentration Gradients

If the temperature and concentration gradients are perpendicular, two outcomes may result. In figure 1.2c the vertical stabilizing concentration gradient tends to retard the flow produced by the horizontal temperature gradient. When the temperature and concentration gradients are interchanged and the direction of the temperature gradient is reversed the same retarding influence will be generated. In case (d) the direction of the concentration gradient is reversed leading to a flow condition where the unstable influence of the concentration gradient will enhance the flow. Again, if the two components are interchanged and the direction of the temperature gradient reversed the same flow condition would follow.

1.6 Aiding and Opposing Flow Conditions

In this study we are only interested with the suppression and enhancement of the horizontal density gradient as depicted by case (a) and (b) in figure 1.2. The effect of the temperature and concentration gradients on the buoyancy forces are shown in figure 1.3. In figure 1.3a the enhancement of the concentration and temperature gradients create clockwise buoyant flow; this is known as *aiding* flow. However, in figure 1.3b the component of the density gradient influenced by the temperature gradient suppresses the other density gradient component caused by the concentration difference. The actual direction of the overall buoyancy force in this *opposing* flow condition is determined by the magnitudes of the temperature and concentration gradients (thermal and mass species Rayleigh numbers) along with the ratio of the thermal and mass species diffusivities (Lewis number).

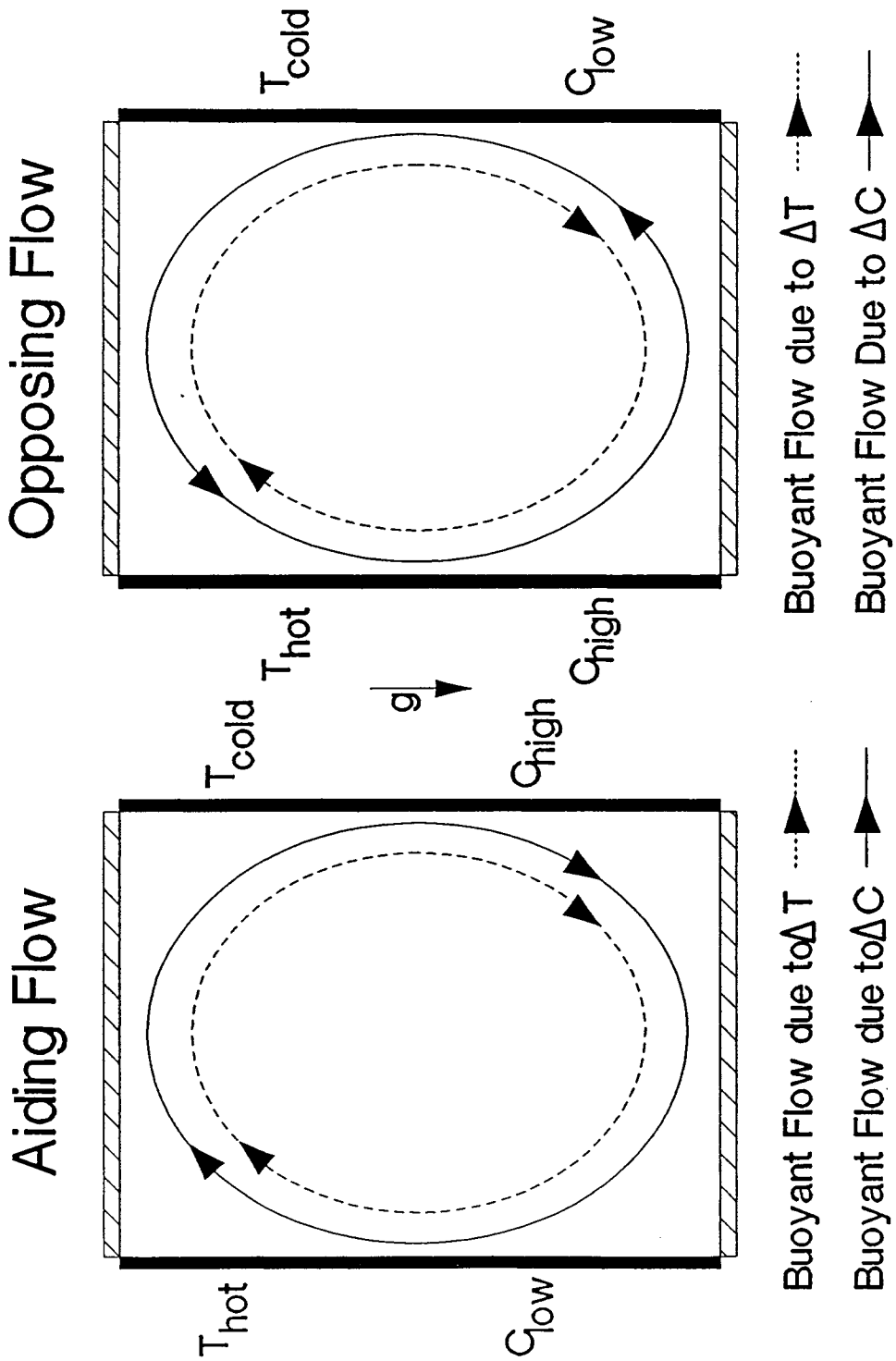

Figure 1.3 Effect of Concentration and Temperature Gradients on Buoyant Flow

1.7 System Parameters

Dimensional analysis shows that six main parameters exist for a closed annulus in axi-symmetric coordinates. These include geometric parameters such as the aspect ratio, Ar (ratio of the enclosure height to the radii difference) and the enclosure curvature ratio, K (ratio of the outer and inner radii of the enclosure). Fluid property parameters include the Prandtl number, Pr (ratio of the kinematic viscosity and the thermal diffusivity) and the Lewis number, Le (ratio of the thermal diffusivity and the mass species diffusivity). The thermal Rayleigh number is the measure of intensity of the temperature difference on the density gradient. The buoyancy ratio, n, is the ratio of the buoyancy forces due to the imposed concentration and temperature differences. If the buoyancy ratio is multiplied by the thermal Rayleigh number and the Lewis number, the mass species Rayleigh number can be obtained. Derivation of the governing equations and implementation of the boundary conditions for double-diffusive natural convection will be discussed in Chapter 3. Figure 1.4 is adapted from Han [4] and demonstrates the general flow regions and transport conditions as a function of the Lewis number (Le) and buoyancy ratio (n). As n approaches $\pm\infty$ the flow will resemble that of pure mass transfer, whereas if $n = 0$ pure heat transfer will result. At $Le = 1$ the mass species and thermal diffusivities are equal such that the net buoyancy force is the sum of the component buoyancy forces (refer to the simple additive flow region in fig. 1.4). The region bounded by the four "U" shaped boundaries ($Le = 1$, $n = 0, \pm\infty$) can be approximated by single-diffusive natural convection. A special case occurs at $Le = 1$ and $n = -1$ where a no flow condition results due

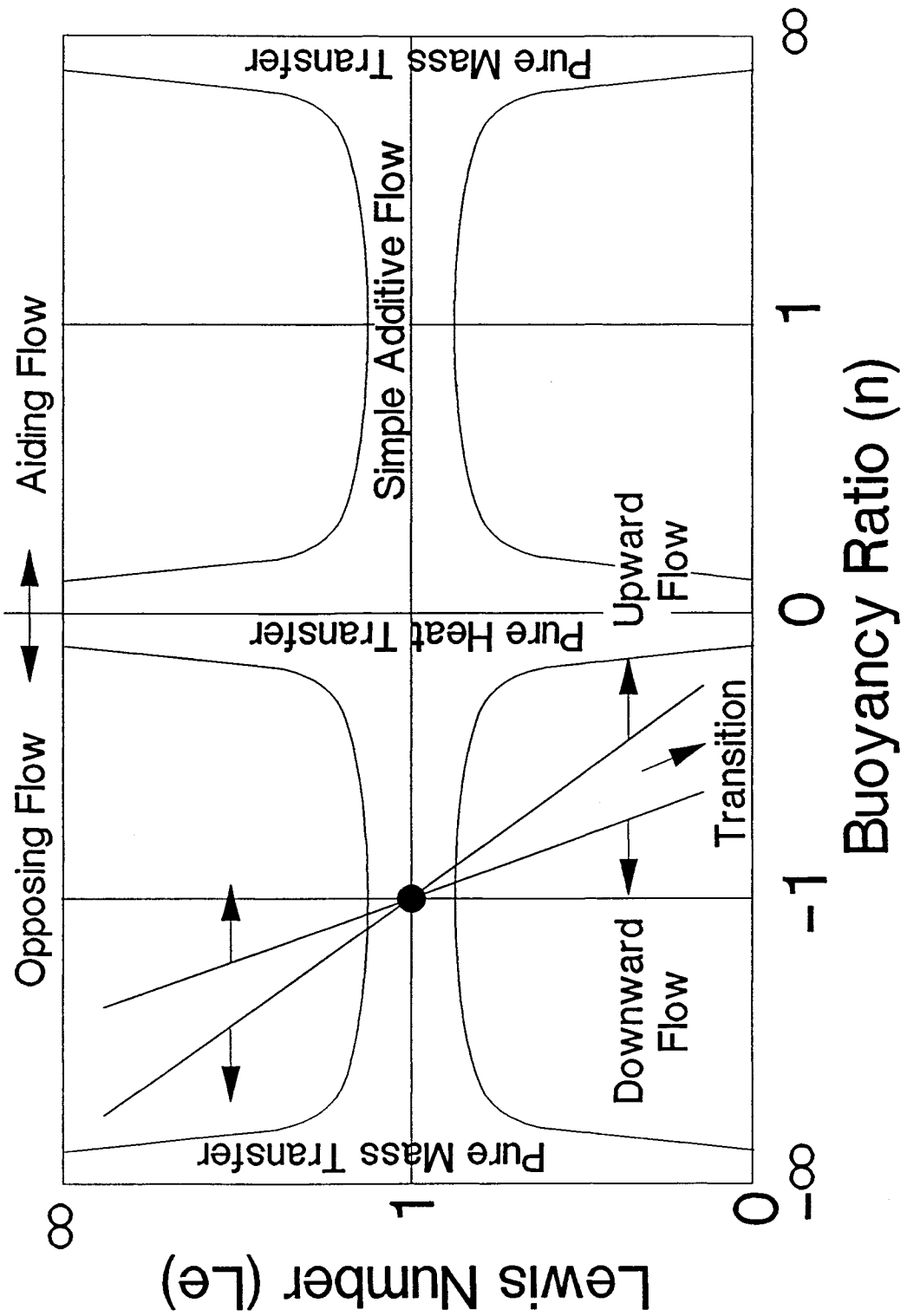

Figure 1.4 General double-diffusive flow regimes as a function of Lewis Lewis number (Le) and buoyancy ratio (n)

to the non-existent net buoyancy force (at this point the component buoyancy forces cancel each other). For $n > -1$ upward flow will result (assuming the surface is heated not cooled), whereas for $n < -1$ downward flow will result. If Le is greater than unity and n is less than negative unity a transition zone from downward to upward flow may develop. Consequently, $n > -1$ for transition to occur for the case of Le less than unity. Basically for transition to occur the buoyancy force of the less diffusive constituent must be greater than the buoyancy force of the more diffusive component.

1.8 Objectives

The objectives of this study are to examine laminar double-diffusive natural convection due to lateral temperature and concentration gradients for a closed annulus with an aspect ratio of one. The vertical walls are maintained at different uniform temperatures and concentrations such that both aiding and opposing buoyancy effects can be investigated. The top and bottom walls are considered to be adiabatic and impermeable to mass transfer. The study is limited to an enclosure curvature ratio of 2, and the fluid modeled is a water based solution with a Prandtl number of 7.

Numerically, the governing equations are solved using the finite volume SIMPLER algorithm developed by Patankar [7] in which the power law approach for discretization is applied across the control volume boundaries. The governing equations along with the boundary conditions are derived for laminar steady state equations of mass, momentum, thermal energy and mass species in axi-symmetric coordinates.

System parameters are extended over a wide range for the present study. The effects of the buoyancy ratio for a given thermal Rayleigh number and Lewis number are examined in detail. The hydrodynamic, temperature and concentration fields along with the overall heat and mass transfer rates from the vertical surfaces are also investigated.

The conditions for flow reversal are examined by varying the buoyancy ratio for various thermal Rayleigh numbers and Lewis numbers under opposing flow conditions. The influential parameters are identified for this phenomenon, where the flow structures and the overall Nusselt and Sherwood numbers (dimensionless temperature and concentration gradients) are closely inspected. The thermal Rayleigh number and the Lewis number are investigated for their effect on the critical buoyancy ratio. Finally, recommendations for further studies are made.

CHAPTER TWO

LITERATURE SURVEY ON DOUBLE-DIFFUSIVE NATURAL CONVECTION

2.1 Initial Studies

One of the first studies of double-diffusive natural convection came in the study of oceanography where the process is called *thermohaline* convection. Much work has been done on the study of salt fountains and fingers where convection is due to opposing thermal and salinity gradients aligned with the gravity vector (Turner [1] presents a good discussion of these effects). Stommel, Arons and Blanchard [8] provided the initial idea for the development of double-diffusive flow. Consider, if a long vertical metal tube is inserted vertically in the ocean where warm salty water is at the surface, and cooler less saline water is at the bottom of the pipe. If the water were to be initially pumped up through the pipe and allowed to reach thermal equilibrium with its surroundings at the same level (the metal tube is assumed to conduct heat but is impermeable to salt) it would be lighter than the surrounding water due to its low salinity content. This in effect would cause an upward buoyancy force resulting in a *salt fountain* if the externally applied pressure difference were to be removed (see figure 2.1a) [1]. If the flow were started downward, it would also continue to flow due to the more saline water cooling and becoming more dense than the surrounding less saline water.

The opposite case can also happen where warm salt water lies underneath colder fresher lighter water. Assume that a portion of the warm salt water is enclosed in an elastic heat conducting shell (figure 2.1b) and is displaced upwards. As this parcel of fluid rises it will lose heat but not salt, resulting in a denser fluid. The buoyancy force will drive it back down beyond its initial position thus producing an oscillating flow. In fact these oscillations can grow provided the dampening effect of the surrounding fluid is not too large. There would also be a time lag between the temperature of the fluid within the shell and the surroundings which further enforces the oscillations. Both salt fountains and oscillations can be demonstrated in the laboratory [9]. Stern [10] points out that shells or solid boundaries are not necessary for the previous examples. Similar motions can occur in the interior of the fluid due to the slower transfer of mass in relation to the transfer of heat ensured by the lower mass to thermal diffusivity of the salt water. *Salt fingers* are similar to salt fountains where rapid salt convection occurs in the form of tall thin columns of fluid alternately ascending and descending due to the stabilizing effect of the thermal gradient being overcome by the lateral diffusion of heat. The upper part of the fluid being more saline than the lower part (heavier fluid above lighter) provides the main driving force for this phenomenon.

2.2 Analytical Studies

The majority of analytical double-diffusive natural convection studies have been performed on simple configurations, usually a vertical

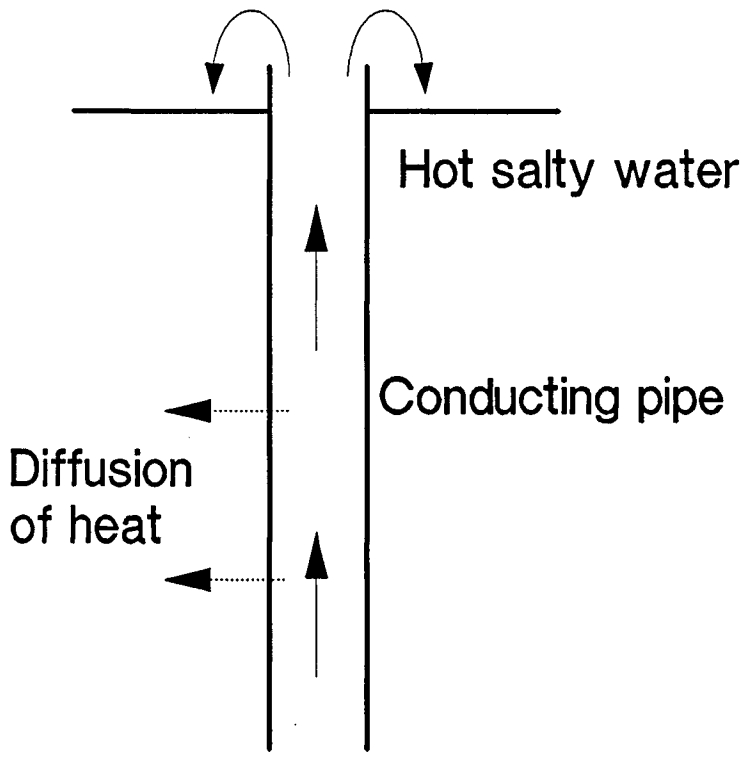

a) Salt Fountain

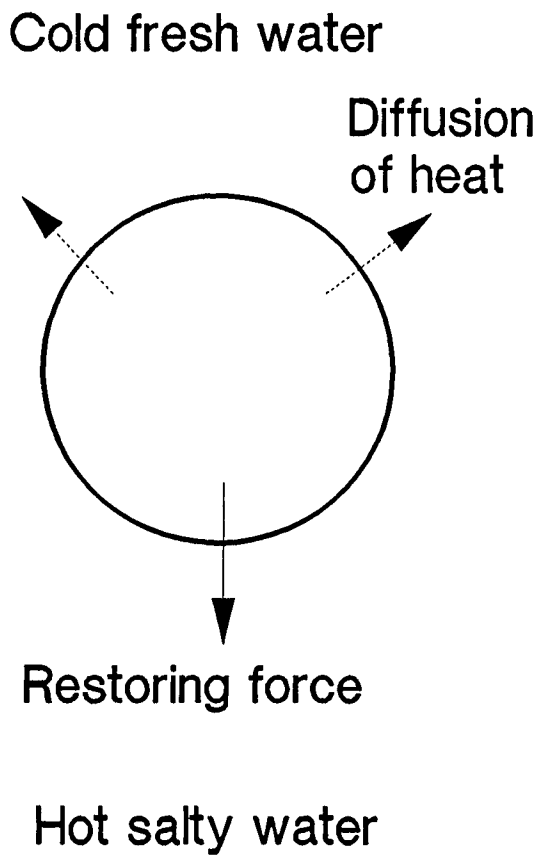

b) Oscillating Element

Figure 2.1 Two Kinds of Motion due to Opposing Vertical Gradients of Heat and Salt

flat plate, where boundary layer analysis has been extended from pure heat transfer analysis to include the additional effect of mass transfer.

One of the first studies into the analytical examination of double-diffusive natural convection was performed by Somers [11], where he considered the effects of thermal and mass transfer from a vertical flat plate. Evaporation and condensation effects were modeled from a wetted isothermal plate using an integral approach. A correlation of the average Nusselt and Sherwood numbers was determined for aiding flow where the Schmidt Prandtl ratio (Lewis number) is near unity. Somers concluded that the effect of the mass species Grashof number on the solution was modified by the square root of the Lewis number.

Wilcox [12] used an integral approach to find solutions for zero wall velocity and for mass transfer velocities for a vertical plate. The plate was either insulated or held at a uniform temperature. Results were determined for a range of Prandtl numbers from 0.01 to 1000 using arbitrary assigned velocity, temperature and concentration distributions. As with Somers, Wilcox reasoned that the square root of the Lewis number was a good approximation for modifying the mass species diffusive component of the aiding buoyancy force, especially when the Lewis number approaches 1. Transport conditions were compared with exact results for pure thermal diffusion driven flows, where differences were notable such that solutions were reasonable only for a small range of Prandtl numbers. Consequently the comparison does not validate the use of the simple integral approach for aiding double-diffusive free convection for a wide range of Prandtl numbers.

Gill, Del Casal and Dale [13] studied the effects of individual and various combinations of variations in species enthalpy, thermal conductivity, viscosity and density with concentration on free convection along a vertical plate for a binary gas system. Exact solutions for the nonlinear system of three coupled equations were obtained by integrating and numerically solving these equations by a method developed by the authors. Solutions were presented for systems where air was the ambient gas (Pr = 0.72, Sc = 0.25) and H_2, He, $H_2O_{(vap)}$, and CO_2 were introduced at the plate surface. The wall/ambient temperature ratio was 1.1 where all properties were evaluated at 200° F. Numerical results were obtained to demonstrate the relative importance of the various effects.

Taunton, Lightfoot and Stewart [14] examined the flow transport over a flat vertical two dimensional plate numerically; aiding and opposing flow effects were considered and an approximate procedure for predicting the onset of flow separation was offered. However, results for countercurrent flow were not offered (flow occurs in opposite directions beyond the point of separation). Results were determined for Prandtl numbers of 0.7, 7 and 1000, with Lewis numbers ranging from 1 to 1000. Taunton *et al.* determined that mildly opposing buoyant forces (small negative values of n) give similar results as aiding buoyant forces (flow occurs in same direction), but the fluid near the wall is slowed down. At the critical buoyancy ratio for Le ≠ 1 the velocity gradient at the wall will vanish resulting in the zero streamline separating from the wall surface. A further decrease in n will result in countercurrent flow and eventually to a second separation limit where

the flow occurs in the opposite direction. For the special case of Le = 1 at n = -1 the authors determined that no flow would occur, thus no countercurrent flow or separation can occur for Pr = Sc. Double-diffusive natural convection results were also presented for three dimensional objects including spheres, vertical cones, cylinders and fins.

Gebhart and Pera [15] argued that previous studies of flows and transport arising from multiple buoyancy causing agencies derived from integral method analysis were at variance with experimental and more exact analytical results. The primary reason for this variance resulted from arbitrary assumptions and formulations which are only reasonable when the Prandtl and Schmidt numbers are near each other (*ie.* Le $\simeq$ 1). Gebhart and Pera examined vertical flows adjacent to surfaces and in plumes for various Prandtl and Schmidt numbers ($0.1 \leq Sc \leq 10$ for Pr = 0.7 and $7 \leq Sc \leq 500$ for Pr = 7) under aiding and opposing conditions; interfacial mass velocities were neglected due to low concentration levels. Gebhart and Pera found for certain conditions of opposing flow (Pr = 0.7, Sc = 0.5, n = -0.5), countercurrent flow occurred within the hydrodynamic boundary layer. For small values of Sc and negative n, the authors postulated that the negative flow in the outer boundary region was due the thicker mass species diffusion layer, whereas the positive inner flow boundary region was a result of the thinner but higher thermal buoyancy component dominated thermal diffusion layer. This result particularly led Gebhart and Pera to believe that earlier studies were inappropriate for complicated combined buoyancy mechanisms due to

the fact that the boundary layer approximation was based on the similarity solution for single-diffusive buoyancy flows.

Schenk, Altmann and de Wit [16] repeated Gebhart and Pera's calculations for heat and mass transfer about an isothermal vertical flat plate in air. Their study only considered aiding flow for a Schmidt number range of 0.1 to 10 for a Prandtl number of 0.71. The authors confirmed that heat and mass transfer are mutually influenced, except for Sc = Pr. However the two effects can be approximated as mutually independent (within 2%) for $0.6 < Sc < 0.9$ (or $0.85 < Le < 1.25$). These limits are considered to be technologically important since they apply to water vapor and carbon dioxide in air.

Nilson's studies [17,18] revealed that a double-diffusive counterbuoyant boundary layer may possess the classical self-similar structure first investigated by Gebhart and Pera [15] only within two distinct and disconnected subdomains of the physical parameter space (buoyancy ratio and Lewis number in this case). In the outer dominated subdomain, it is the more diffusive of the buoyancy mechanisms which controls the primary direction of the flow. Conversely, the less diffusive component controls the primary direction of the flow within the inner dominated subdomain. Between these two domains there exists a third domain of counterflow, in which Nilson determined that self-similar solutions were inadmissible. Nilson examined this regime of bidirectional flows by using a procedure based on the method of matched asymptotic expansions, under the restriction that the Prandtl and Lewis numbers must both be large (*ie.* very small mass diffusion coefficient). The borderlines between the flow regimes along a vertical

flat plate were mapped out and may be used as a possible guideline for other configurations:

(i) unidirection downflow occurs when $n \leq -Le$ (inner dominated)

(ii) unidirection upflow occurs when $n \geq -Le^{1/3}$ (outer dominated)

(iii) bidirection counterflow occurs when $-Le \geq n \geq -Le^{1/3}$

These guidelines are based on the assumptions that the surface in question has a higher temperature and a high concentration than the surroundings, if this is not the case the flow directions are simply reversed. If the Lewis number is less than unity the conditions for (i) and (ii) are reversed, and finally if $Le = 1$ then counterflow will not occur.

Chen and Yuh [19] examined the combined heat and mass transfer in natural convection over an inclined plate. Similarity solutions were obtained and numerical results were presented for water and air over a range of Schmidt numbers (0.2 to 10 for $Pr = 0.7$ and 7 to 500 for $Pr = 7$). Uniform wall temperature and concentration cases along with uniform heat and mass flux cases were examined for buoyancy ratio ranges of $-1 \leq n \leq 2$ and $-2 \leq n \leq 2$ respectively. Solutions were found for decreasing buoyancy ratio to the point of flow separation, however there was no discussion of the latter, an important aspect of double-diffusive natural convection. The authors determined that surface heat and mass transfer diminishes as the angle of inclination from the vertical axis is increased. Furthermore, uniform heat and mass flux conditions provide larger Nusselt and Sherwood numbers than the corresponding uniform wall temperature and concentration conditions.

Similar studies have been applied to geometries other than the flat plate. An analytical study on flow transport along a vertical cylinder was examined also by Chen and Yuh [20], who investigated the effect of cylinder curvature on heat and mass transfer rates under aiding and opposing flow conditions. This was one of the first studies using axi-symmetric coordinates for natural convection due to double-diffusion; the authors attributed the lack of study on this problem to the rather difficult mathematical and numerical procedures involved in dealing with nonsimilar boundary layers. Solutions were found for a practical range of Schmidt numbers for species diffusion in air and water where the range of the buoyancy ratio was limited to $-0.5 \leq n \leq 1$, therefore neglecting to examine flow separation and mass species dominated opposing flow. The authors found that their analysis was in good agreement with the experimental study of Bottemanne [21], furthermore they determined that an increase in curvature results in the increase of both the local Nusselt and Sherwood numbers.

Hasan and Mujumdar [22] examined the free flow around a horizontal cylinder using local similarity and local nonsimilarity approaches for both aiding and opposing flow conditions. Solutions were found for Schmidt numbers of 0.63 and 2.57 representing water vapor and naphthalene diffusing in air, for a buoyancy ratios of -0.5, 0.5 and 2. Unfortunately, flow separation and counterflows were not considered in this study. The authors concluded that the local similarity approach provides reasonably accurate solutions compared to other convention approaches, however they found that the local nonsimilarity approach generates results that are inaccurate and inconsistent.

Trevisan and Bejan [23] developed analytical solutions for simultaneous heat and mass transfer in a two dimensional enclosure based on the Oseen-linearized solution for natural convection due to temperature variations in the fluid alone [24]. In the configuration the left and right walls had uniform distributions of heat flux and mass flux imposed on them, whereas the top and bottom walls were considered to be adiabatic and impermeable to mass transfer. The features of the boundary layer regime were based on four assumptions:

(i) The boundary layers have a constant thickness (altitude independent)

(ii) The core region is motionless and stratified.

(iii) The side wall temperatures and concentrations increase linearly with altitude at the same rate as the core temperatures and concentrations.

(iv) The fluid has a Prandtl number greater than one (eliminating the inertia terms of the momentum equation)

Solutions for the overall Sherwood and Nusselt numbers were determined for three simple cases. First, the Lewis number number was held at unity for an arbitrary buoyancy ratio, which in this case can be modeled as additive flow. Similarity solutions were used to determine the results for $Le \gg 1$ and $|n| \ll 1$ (heat transfer driven flow) and $Le \ll 1$ and $|n| \gg 1$ (mass transfer driven flow). In these two cases the concentration boundary layer (for the former) and the thermal concentration boundary layer (for the latter case) are considered to be very small due to the extremity of the Lewis number such that the flow can be considered to be driven by a single buoyancy force. The results

from these three test cases are not really a major improvement over the solutions from single diffusive natural convection in an enclosure except for the fact that both the diffusive components flux rates were determined and validated against numerical solutions from the same study. Nevertheless, it is the first logical step for an analytical solution for double-diffusive natural convection in an enclosure.

2.3 Experimental Studies

Many experimental studies have been performed on simultaneous heat and mass transfer in enclosures along with free surfaces. Evaporation and condensation have been studied in air, whereas electrochemistry has been used to stimulate mass transfer in liquids. The first experimental studies in double-diffusive natural convection were performed in conjunction with the first analytical studies in which free convection was studied along vertical surfaces.

Adams and McFadden [25] measured the local heat and mass transfer coefficients for subliming p-dichlorobenzene (Pr = 2.23) from a heated vertical surface into air. The buoyancy forces were opposed and approximately the same. The results were compared to the analytical solutions of Somers [11] and Wilcox [12] and were found to be between 10 and 15% lower. This discrepancy was somewhat expected since the analytical results were based on a near unity Lewis number and were limited to aiding, not opposing flow situations.

An electrochemical method was used by De Leeuw Den Bouter, De Munnik and Heerties [26] to study simultaneous thermal and chemical species diffusion in a $CuSO_4$-H_2SO_4-H_2O solution (Pr $\simeq$ 10 and Sc $\simeq$ 2000). A copper cathode was maintained at a constant temperature for aiding and

opposing buoyancy cases, in which upward, downward and oscillitory flows were observed. Mass and heat transfer parameters were correlated with analytical solutions using the $(Le)^{1/2}$ modifier, which gave good agreement for the aiding buoyancy cases. However, for opposing flow effects there was a significant disagreement of 30% and beyond, confirming that simple analytical solutions are inappropriate in these circumstances.

Bottemanne [21] felt that the vertical edge effects that occur with flat plates in experimental studies were large enough such that an alternative was warranted. His measurements for the evaporation of water into air were carried out on a vertical cylinder where the diameter was large enough so that only a small correction was needed to compare his results with theoretical solutions of flat plates. Only aiding flow cases were carried out due to experimental measurement difficulties encountered with opposing buoyancy forces. Furthermore, Bottemanne did hint that they may be difficulties with the validity of boundary layer approximation for these cases. The results from pure and simultaneous heat and mass transfer were within 2% of a previous analytical study made by Bottemanne [27] such that he concluded that the classical boundary layer theory was sufficient for predicting simultaneous mass and heat transfer in free convection for problems with $Sc = 0.63$, $Pr = 0.71$.

The first experimental studies of double-diffusive natural convection in enclosures examined the effects of temperature gradients on vertically stratified salt solutions. These laboratory experiments were attempting to model the vertical temperature and concentration

gradients found in oceans possibly due to the phenomenon of salt fingers. If a vertical wall is heated or cooled in the presence of a vertical stable salinity gradient, a definite layered structure of long thin cells of uniform concentration will develop adjacent to the wall. Furthermore the salinity of the solution will increase in a step wise fashion with depth. Mendenhall and Mason [28] offer an explanation for this phenomenon for a cooled wall: suppose that the temperature of one side of a container is lowered such that there is a uniform temperature difference across the container. If a sufficient density gradient is present in the liquid, a portion of the liquid near the cooler wall becomes denser than the average such that it descends. As it falls the negative buoyancy force decreases in intensity due the relative increasing density of the surrounding fluid. When the fluid portion reaches its density equilibrium with the surrounding fluid the downward flow will cease and the momentum will carry it into the interior of the fluid. This equilibrium depth acts as a boundary for this cell layer where local convection is established, mixing the fluid such that the concentration becomes nearly uniform within the interior of this layer. Below this boundary a similar cell will develop with the density almost uniform but more than that of the above cell, and in this manner the entire volume of liquid is divided into layers.

Thorpe, Hutt and Soulsby [29] examined the growth of cells from the top and bottom of a salt stratified container where the vertical walls were subjected to heating. The authors found that under certain conditions (supercritical thermal Rayleigh number), the convection cells or rolls would spring up simultaneously along the vertical wall, and

would grow laterally to reach the opposite wall of the container. Thorpe *et al.* suggested that these simultaneous intermediate layers were the result of a difference in the diffusivities of heat and salinity and the presence of horizontal gradients of temperature and salinity near the vertical wall. Near the wall the fluid will warm and rise, but its salinity will not change very much due to its small mass diffusivity thus creating a horizontal salinity gradient along with lateral temperature gradients leading to a physical instability with a layered structure. To support this theory, the authors performed a linear stability analysis for a case of stable stratified fluid confined between two parallel plates. The plates sustained horizontal linear gradients in temperature and concentration such that the horizontal density gradient is zero. For the onset of instability their solution yielded a relationship between the thermal Rayleigh number based on the lateral temperature gradient and the solute Rayleigh number based on the vertical salinity gradient. The stability limit was confirmed by their qualitative experimental results in slots.

Chen, Briggs and Wirtz [30,31] expanded on the Thorpe *et al.* study [29], in which they further examined the initiation of instability induced by the lateral heating of a stably stratified fluid. At subcritical Rayleigh numbers, the fluid rose almost imperceptibly parallel to the heated plate and the lateral transport of heat was entirely by conduction. The authors indicated that layers are induced by two mechanisms. One is the successive formation of layers due to the presence of top and bottom boundaries. The other is due to a critical Rayleigh number, which if exceeded, cells of approximately equal size

will appear simultaneously along all of the heated wall. The critical Raleigh number is based on the temperature difference, buoyancy ratio and vertical salinity gradient and was found to be 15 000 ± 2500. The authors also confirmed Mendenhall and Mason's observations [28] in which once the layers are established the fluid in each layer is well mixed and of fairly constant density with large gradients in temperature and salinity at the layer interface.

Natural convection in enclosures in which the thermal and concentration gradients are vertically aligned in a Bénard configuration was studied by Bergman, Incropera and Viskanta [32]. Bergman *et al.* examined the single mixed layer growth due to the heating of a salt stratified system from below, where an unstable temperature gradient will develop just above the heated surface. This gradient may induce local thermal instabilities and convective motion which, unlike single diffusive fluids, is restricted to the lower part of the enclosure by the stabilizing salt distribution. As heat is further supplied to the system, this mixed convective layer will expand, entraining fluid from the overlying stable region through an interfacial layer separating the two regions. This mixed layer height is a function of time, the bottom heat flux, the initial salinity profile and the thermophysical properties of the saline solution. The authors obtained data for this double-diffusive phenomenon and attempted to correlate the results ultimately using this correlation in a mathematical model for prediction mixed layer heights, temperatures and salt concentrations. Use of the mixed layer growth correlation for the model was in good agreement with the authors experimental data, however it is limited to water based

solutions and does not account for delays in the onset of convection. In a subsequent paper Bergman and Ungan [33] focused on the formation and growth of the lower convective regimes. They determined that the development of convective conditions is characterized by an interaction between Bénard type convection and longitudinal convective rolls possibly formed by horizontal temperature gradients which may provide clues for explaining the mechanisms by which mixed convective layers expand.

Little attention was paid to combined horizontal temperature and concentration gradients within an enclosure until recently due to the increased interest in crystal growth. In some horizontal growth techniques, such as the horizontal Bridgman, the fluid phase is subjected to simultaneous horizontal and temperature gradients. The lack of experimental studies on this specific configuration of the diffusive components inspired Kamotani, Wang, Ostrach and Jiang [34] to experimentally study double-diffusive convection in a low aspect ratio rectangular enclosure for both aiding and opposing flow conditions. The authors used a copper sulphate solution (Pr = 7, Sc = 2100) with an aspect ratio range of 0.13-0.55 for the investigation. Kamotani *et al.* determined that if the buoyancy ratio is greater than 6 for aiding flow, a three layer/cell structure will appear. If $n < 6$ for the same aiding flow conditions the flow will have a unicellular pattern with secondary cells at the vertical walls. The authors concluded that these secondary cells had been a double-diffusive effect, not shear, since they had not appeared when the enclosure was subjected to temperature gradients alone. For opposing flow situations, if n was less than -10, the flow

was three layered with secondary cells in the middle. For flows with a buoyancy ratio greater than -10, the flow was unicellular with secondary cells at the wall. On a point of interest, counterflow was observed at the vertical walls for opposing flow cases, where at the hot anode the flow within the solute boundary layer was downward, however less concentrated fluid in the thermal boundary layer outside the solute boundary layer rose. Complete flow reversal was not investigated, most likely due to the very high buoyancy ratios required by the large Lewis number (Le = 300).

Han [4] performed a similar study to Kamotani *et al.* for higher aspect ratios of 1 and 4 (Pr = 7, Sc = 2300-2600) in which he found similar flow patterns. Han decreased the buoyancy ratio for the opposing flow conditions and found that the number of cells increased. As the solutal buoyancy force is large compared to the thermal force, the fluid tends to be more stratified thus creating cell layers. For the aiding buoyancy condition, no appreciable difference in flow structure was observed from an opposing case with the same value of $|n|$. Han also performed a numerical simulation for a similar configuration and found that the results agreed with his experiments.

Other experimental investigations have included more diverse subject matter. Some have included complex geometries such as Lee, Parikh, Acrivos and Bershader [35] who have examined natural convection in a vertical channel with opposing buoyancy forces with porous and solid walls. Others have examined additional forces, such as Roušar and Cezner [36], who examined the effect of an electrical field of the flow of ions on a vertical flat plate. So far, there has been no

experimental study on record that examines double-diffusive natural convection with a vertical closed annulus.

2.4 Numerical Studies

Most of the numerical studies examining double-diffusive convection have been performed on enclosures with stabilizing vertical concentration gradients with destabilizing horizontal or vertical temperature gradients or enclosures with horizontal temperature and concentration gradients.

Wirtz [37] continued his studies on heat transfer across an enclosure in the presence of a stable solute gradient by complementing his and his colleagues experimental examinations [30,31] with a numerical investigation. In this study Wirtz was interested in how the lateral heat transfer due to a uniform temperature difference is affected by the presence of solute stratifications, furthermore, under what conditions will the interface separating convecting layers become unstable resulting in merging? The problems of this type are considered to be transient, since a steady state solution will eventually lead to layer merging with a uniform enclosure concentration. In order to simulate a thermohaline system, all calculations were made for Le = 100 and Pr = 6.7 with a buoyancy ratio varied between 0 and -10. Wirtz found that the major effect of solute layering was a reduction in the heat transfer across the enclosure. For $n < -1$ the flow would develop into layered convection cells with the Nusselt number slowly increasing as the salinity difference between the regions was diminished through vertical diffusion across the interface. However, for the flow field where $n > -1$ the interface separating the convecting regions became

unstable where flow penetrated the diffusive interface at the side walls and resulted in a rapid mixing of the layers.

There have been several numerical papers written on the Bénard problem, some have been written in conjunction with experimental studies such as Bergman and Ungan [33]. Others have studied more specific problems related to the Bénard problem such as stability, convection for infinite Prandtl number, or bifurcations and flow transitions to chaos.

The stability of salinity stratified layers with a vertical temperature gradient was investigated by Hassab, Tag and Kamal [38] using linear analysis to gain some insight into the mechanism of instability. Three separate conditions were considered: strong stabilizing salinity gradient opposed by a destabilizing temperature gradient, a weak destabilizing salinity gradient combined with a destabilizing temperature gradient, and a weak destabilizing salinity gradient counteracted by a stabilizing temperature gradient. Hassab *et al.* plotted the stability curves for various thermal and concentration Rayleigh numbers and vertical disturbances for the limiting case of a salt solution of Pr = 3.35 and Sc = 175. Hansen and Yuen [3] examined subcritical convection at an infinite Prandtl number to simulate flows applicable to geophysical flows in magma chambers. They established a relationship between the Lewis number and the buoyancy ratio for the onset of steady double-diffusive convection. For large aspect ratios, the authors established a bifurcation pattern for increasing Le with the sequence of: no steady states, three different steady state flows and then to a single elongated cell. A more in depth examination of bifurcation and chaos was performed by Moore, Toomre, Knolch and Weiss

[39] for a finite Prandtl number which revealed a transition from periodic oscillations to chaos through a sequence of period-doubling bifurcations, within the chaotic region there are narrow periodic windows.

The influence of Soret-induced solutal buoyancy forces on the hydrodynamics and heat transfer rates associated with the natural convection of an initially uniform concentration fluid in an enclosure with a lateral temperature gradient was examined by Bergman and Srinivasan [40]. The Soret effect can be described as the effect temperature gradients within a fluid have on the concentration profiles (a temperature gradient will induce a concentration gradient). Bergman and Srinivasan stated that most numerical double-diffusive studies tend to ignore this effect for the following various reasons. The time scale associated with the establishment of Soret effects is large compared to the thermal time scale due to the large Lewis numbers of binary liquids; compositional differences established by Soret effects will be washed out once convection begins; Soret diffusion coefficients for liquid mixtures are difficult to predict and experimental data are relatively scarce. The first reason is not relevant to steady state situations, the second reason depends on the magnitude of the Soret effect relative to buoyancy forces and finally the authors argue that the third reason does not justify the absence of Soret phenomena in double-diffusive systems. Contrary to their expectations the authors determined that Soret diffusion does not always need to be included in analysis unless there are special conditions. It may be necessary to include Soret phenomena in the modeling of the freezing and melting of water based

binary solutions since the effect seems to manifest itself in the vicinity of the density inversion temperature. However if conditions are to be determined in the far field as opposed the solid/liquid interface the Soret effect can be ignored.

In the past few years, study of double-diffusive natural convection due to horizontal temperature and concentration gradients in enclosures has really opened up. One of the initial numerical studies on this aspect of double-diffusive convection was performed by Trevisan and Bejan [23] in which they studied the convection produced by lateral heat and mass fluxes for limited aiding and opposing buoyancy situations. The main purpose of this numerical investigation was to validate analytical results for a similar configuration in which only basic calculations were made. Simple additive flow was examined where the Lewis number was held at unity while the buoyancy ratio ranged from -11 to 9 (in this case the dimensionless concentration and temperature profiles are identical due to the equivalent diffusivities). The authors determined that both the Sherwood and Nusselt numbers increase with the absolute buoyancy ratio. Furthermore, they also established that flow reversal will occur at $n = -1$. The Lewis number was only examined for the effect on the mass transfer rate alone, by equating the buoyancy ratio to zero enabling the flow to be independent of mass effects. The authors determined that an increase in the Lewis number will increase the Sherwood number and decrease the thickness of the concentration boundary layer. Trevisan and Bejan also examined the effect of aspect ratio and Prandtl number on the Nusselt and Sherwood numbers. They determined that an increase in the Prandtl number will

result in only a marginal increase, whereas the results for the aspect ratio indicated independence.

Lai and Ramsey [41] examined natural convection for two and three dimensional rectangular enclosures due to differential temperature and water vapor gradients for aiding flow conditions only. The authors determined that a combined Grashof number that combines the effects of both thermal and concentration gradients can be incorporated since the Lewis number for an air and vapor system is near unity and aiding flow is inherent for this specific mixture. The authors used Patankar's SIMPLER algorithm for Grashof numbers up to 10^6, however, for Grashof numbers beyond this range the algorithm would fail to converge and a direct solution technique was applied. When the combined Grashof number exceeded 5.0×10^4, a change from a basically unicellular circulation to a distinct boundary layer flow on the vertical walls with a stagnant interior was observed. Finally the authors determined that the differences between the two dimensional square and three dimension cubic enclosures for similar boundary conditions ranged in a 3% to 9% reduction in the average Nusselt number for the cubic enclosure. The authors concluded that a two dimensional approximation provided a good estimate avoiding the large computational time required for a simple three dimensional enclosure.

Ranganathan and Viskanta [42] examined the effects of combined lateral temperature and concentration gradients on natural convection in a two dimensional square cavity filled with a binary gas. The numerical study was limited to simple additive flow where the Schmidt number equaled the Prandtl number and the buoyancy ratio included aiding and

opposing buoyancy forces with n ranging from -5 to 5. The authors decided to include the velocity of material normal to the vertical walls in order to better model the transit of species across the cavity. Furthermore, they wanted to examine the effect of including this boundary condition in the overall solutions of the flow, temperature and concentration fields. It was determined that the normal velocities at the walls have a negligible effect on these fields inside the cavity (the vertical velocities near the vertical walls were two orders of magnitude higher than these normal velocities). The effect of the normal velocities on the Nusselt and Sherwood numbers were also negligible provided that the species in the enclosure is dilute.

Han [4,43] performed a numerical study to complement his experimental studies on double-diffusive convection due to lateral temperature and concentration gradients. Han studied various effects on the flow fields along with the heat and mass transfer characteristics for an enclosure encompassing a wider range of buoyancy ratios, Rayleigh numbers and Lewis numbers than previous studies. The effect of the buoyancy ratio, for given Rayleigh numbers, on the overall Nusselt and Sherwood numbers was examined and were found to be minimal around $n \simeq -1$ or the flow reversal area. It was determined that an increase in the thermal Rayleigh number, for a given buoyancy ratio, would result in an increase in the Nusselt and Sherwood numbers. This was not surprising since an increased flow rate would result at the walls thus increasing the mass and heat transfer rates. The flow structure was examined near the critical condition for flow reversal and revealed that more than one solution may exist for a given set of flow conditions. In fact, Han

determined that the solutions are based on the choice for the initial flow conditions, however, outside the critical buoyancy range unique solutions exist. The effect of the Lewis number on the critical buoyancy ratio range was investigated where the range of the critical buoyancy ratio was found to increase with the Lewis number. However, Han determined that increasing the Lewis number decreases the point of actual flow reversal. Similar results were found in the studies of Taunton *et al.* [14] and Nilson [17] for vertical flat plates. Han further studied the flow structures for tall enclosures in which he determined that multiple cells develop during flow reversal. However, as the buoyancy ratio was further decreased the multiple cell structure would disappear and unicell flow would develop with a stagnant core. Interestingly, Han also found that multiple cells develop for a small range of buoyancy ratios for aiding flow conditions during the transition from thermal dominated flow to concentration dominated flow.

An examination of double-diffusive flow in enclosures with a low aspect ratio (0.5) was performed by Benard, Gobin and Thevenin [44] for aiding thermal and solutal buoyancy forces only. Only the Lewis number and the buoyancy ratio were varied ($1 \leq Le \leq 10$ and $0.1 \leq n \leq 10$) to determine their effect on the mass and heat transfer in the enclosure. It was found that, when the buoyancy ratio was less than unity, an increase in the Lewis number (the Schmidt number would increase since the Prandtl number was held constant in this case) would result in an increase the Sherwood number while the Nusselt number would remain virtually unchanged. However for $n \geq 1$ the solutal buoyancy force is greater or equal to the thermal buoyancy force. Consequently an

increase in the Lewis number would result in a decrease in the Nusselt number especially for large buoyancy ratios. This is due to the thinning of the solutal buoyancy layer due to the decrease in the mass diffusivity, which has the effect of decreasing the boundary layer velocities which the heating or cooling efficiency depends on.

Krishnan [45] concentrated his study on varying the thermal Rayleigh number for a square cavity with a buoyancy ratio of -1 for a single Lewis number of 3.162. He determined that the transition from the conductive to a steady convective regime occurs around a Rayleigh number of 4.65×10^3, and that a transition from steady state flow to transient convection with oscillatory motions occurs at $Ra \simeq 6.25 \times 10^4$. Krishnan also confirmed Han's finding that two unique solutions may be obtained for a certain range of Rayleigh number, with the solution depending on the initial conditions.

CHAPTER THREE

MATHEMATICAL FORMULATION

The derivation of the governing equations for laminar, nearly incompressible flow in axi-symmetric coordinates is presented. Assumptions and approximations for the solution model are discussed. The boundary conditions for both aiding and opposing flow are imposed and the non-dimensional system parameters are derived.

3.1 Assumptions and Approximations

All the equations formulated for the flow, thermal and mass species fields are regarded to be steady and laminar. The fluid is considered to be incompressible and Newtonian in behavior with negligible viscous dissipation. The Boussinesq linear approximation is utilized to model the effect of the density change on the buoyancy force due to the temperature and concentration gradients. All other properties are considered to be independent of temperature, concentration and pressure effects. Both Soret and Dufour effects are neglected, as heat transfer is independent of the concentration gradient and mass transfer is independent of temperature gradients. Dufour effects are considerably weaker than Soret phenomena which in turn, according to Bergman and Srinivasan [40], can be neglected provided that the fluid is not in the vicinity of the density inversion temperature (see Chapter 2). Of course, the results for the Boussinesq fluid

considered here may not be applicable to this situation since the Boussinesq density/temperature/concentration relationship is assumed to be linear. However for real systems, these assumptions are only valid when the solution is dilute, the temperature differences are small and the average fluid temperature is significantly higher than the freezing point. In order for the system to be considered laminar and steady the thermal and species Rayleigh numbers should not exceed 10^6. This is a conservative limit since it is generally well known that the laminar limit of the Rayleigh number is around 10^9. Furthermore, as discussed in chapter two, Krishnan determined that transition to transient convection will occur at a much lower Rayleigh number [45]. Finally it should be said that this investigation of a simple model of double-diffusive natural convection is intended to demonstrate the basic phenomena for an axi-symmetric system.

3.2 Governing Equations

By exercising the above assumptions into the conservation of mass, momentum, energy and mass species using primitive variables, one can obtain the governing equations for an axi-symmetric coordinate system.

Continuity:

$$\frac{\partial(r\,u)}{r\,\partial r} + \frac{\partial v}{\partial z} = 0 \tag{3.1}$$

Radial Momentum:

$$u\frac{\partial u}{\partial r} + v\frac{\partial u}{\partial z} = \nu\left[\frac{\partial}{r\,\partial r}\left(r\frac{\partial u}{\partial r}\right) - \frac{u}{r^2} + \frac{\partial^2 u}{\partial z^2}\right] - \frac{\partial P}{\rho_r\,\partial r} \tag{3.2}$$

Axial Momentum:

$$u\frac{\partial v}{\partial r} + v\frac{\partial v}{\partial z} = \nu\left[\frac{\partial}{r\,\partial r}\left(r\frac{\partial v}{\partial r}\right) + \frac{\partial^2 v}{\partial z^2}\right] - \frac{\partial P}{\rho_r\,\partial z} + \frac{\rho_r - \rho}{\rho_r}\,g \qquad (3.3)$$

Thermal Energy:

$$u\frac{\partial T}{\partial r} + v\frac{\partial T}{\partial z} = \alpha\left[\frac{\partial}{r\,\partial r}\left(r\frac{\partial T}{\partial r}\right) + \frac{\partial^2 T}{\partial z^2}\right] \qquad (3.4)$$

Mass Species:

$$u\frac{\partial C}{\partial r} + v\frac{\partial C}{\partial z} = D\left[\frac{\partial}{r\,\partial r}\left(r\frac{\partial C}{\partial r}\right) + \frac{\partial^2 C}{\partial z^2}\right] \qquad (3.5)$$

The density for the fluid is a function of both temperature and concentration. Using the first order Boussinesq approximation, the density can be expressed as,

$$\rho = \rho_r\left[1 - \beta_T\,(T - T_r) - \beta_C\,(C - C_r)\right] \qquad (3.6)$$

The subscript " r " refers to a reference state. The coefficients β_T and β_C are the volumetric expansion coefficients at the reference temperature and concentration respectively,

$$\beta_T = -\frac{1}{\rho_r}\left(\frac{\partial \rho}{\partial T}\right)_r, \qquad \beta_C = -\frac{1}{\rho_r}\left(\frac{\partial \rho}{\partial C}\right)_r \qquad (3.7)$$

Note: for water based solutions β_T is usually positive and β_C is usually negative.

3.3 Dimensionless Variables and Governing Equations

The governing equations can be made dimensionless by using the radii difference as the reference length, $R = r_o - r_i$, where

$$r^* = r/R, \qquad z^* = z/R \tag{3.8}$$

$$u^* = \frac{u\,R}{\alpha}, \qquad v^* = \frac{v\,R}{\alpha} \tag{3.9}$$

$$P^* = \frac{P\,R^2}{\rho_r \alpha^2} \tag{3.10}$$

$$T^* = \frac{T - T_r}{T_i - T_o}, \qquad C^* = \frac{C - C_r}{C_i - C_o} \tag{3.11}$$

The subscripts "i" and "o" refer to the inner and outer radii respectively. Substituting the Boussinesq approximation for the buoyancy force term in equation (3.3), and inserting the dimensionless variables,

Continuity:

$$\frac{\partial(r^* u^*)}{r^* \partial r^*} + \frac{\partial v^*}{\partial z^*} = 0 \tag{3.12}$$

Radial Momentum:

$$u^* \frac{\partial u^*}{\partial r^*} + v^* \frac{\partial u^*}{\partial z^*} = Pr \left[\frac{\partial}{r^* \partial r^*} \left(r^* \frac{\partial u^*}{\partial r^*} \right) - \frac{u^*}{r^{*2}} + \frac{\partial^2 u^*}{\partial z^{*2}} \right] - \frac{\partial P^*}{\partial r^*} \tag{3.13}$$

Axial Momentum:

$$u^* \frac{\partial v^*}{\partial r^*} + v^* \frac{\partial v^*}{\partial z^*} = Pr \left[\frac{\partial}{r^* \partial r^*} \left(r^* \frac{\partial v^*}{\partial r^*} \right) + \frac{\partial^2 v^*}{\partial z^{*2}} \right] - \frac{\partial P^*}{\partial z^*} + Ra_T\, Pr \left[T^* + n\, C^* \right] \tag{3.14}$$

Thermal Energy:

$$u^* \frac{\partial T^*}{\partial r^*} + v^* \frac{\partial T^*}{\partial z^*} = \frac{\partial}{r^* \partial r^*} \left(r^* \frac{\partial T^*}{\partial r^*} \right) + \frac{\partial^2 T^*}{\partial z^{*2}} \tag{3.15}$$

Mass Species:

$$u^* \frac{\partial C^*}{\partial r^*} + v^* \frac{\partial C^*}{\partial z^*} = \frac{1}{Le} \left[\frac{\partial}{r^* \partial r^*} \left(r^* \frac{\partial C^*}{\partial r^*} \right) + \frac{\partial^2 C^*}{\partial z^{*2}} \right] \tag{3.16}$$

where the fluid system parameters are,

$$Pr = \frac{\nu}{\alpha}, \qquad Le = \frac{\alpha}{D} \tag{3.17}$$

$$Ra_T = \frac{g \beta_T (T_i - T_o) R^3}{\alpha \nu} \tag{3.18}$$

$$n = \frac{\beta_C (C_i - C_o)}{\beta_T (T_i - T_o)} = \frac{Gr_C}{Gr_T} = \frac{Ra_C}{Ra_T} Le \tag{3.19}$$

3.4 Enclosure Geometry

The geometry for the present study is illustrated in figure 3.1 in axi-symmetric coordinates. The physical model consists of two concentric cylinders closed off at the top and bottom. The inner cylinder radius is specified as r_i and the outer radius is defined as r_o. The aspect ratio is measured as the ratio of the annulus height (H) and the radii difference (R). The curvature ratio (K) is determined by the ratio of the outer and inner radii. (Note, as K approaches unity, the configuration can be considered to be two dimensional in cartesian

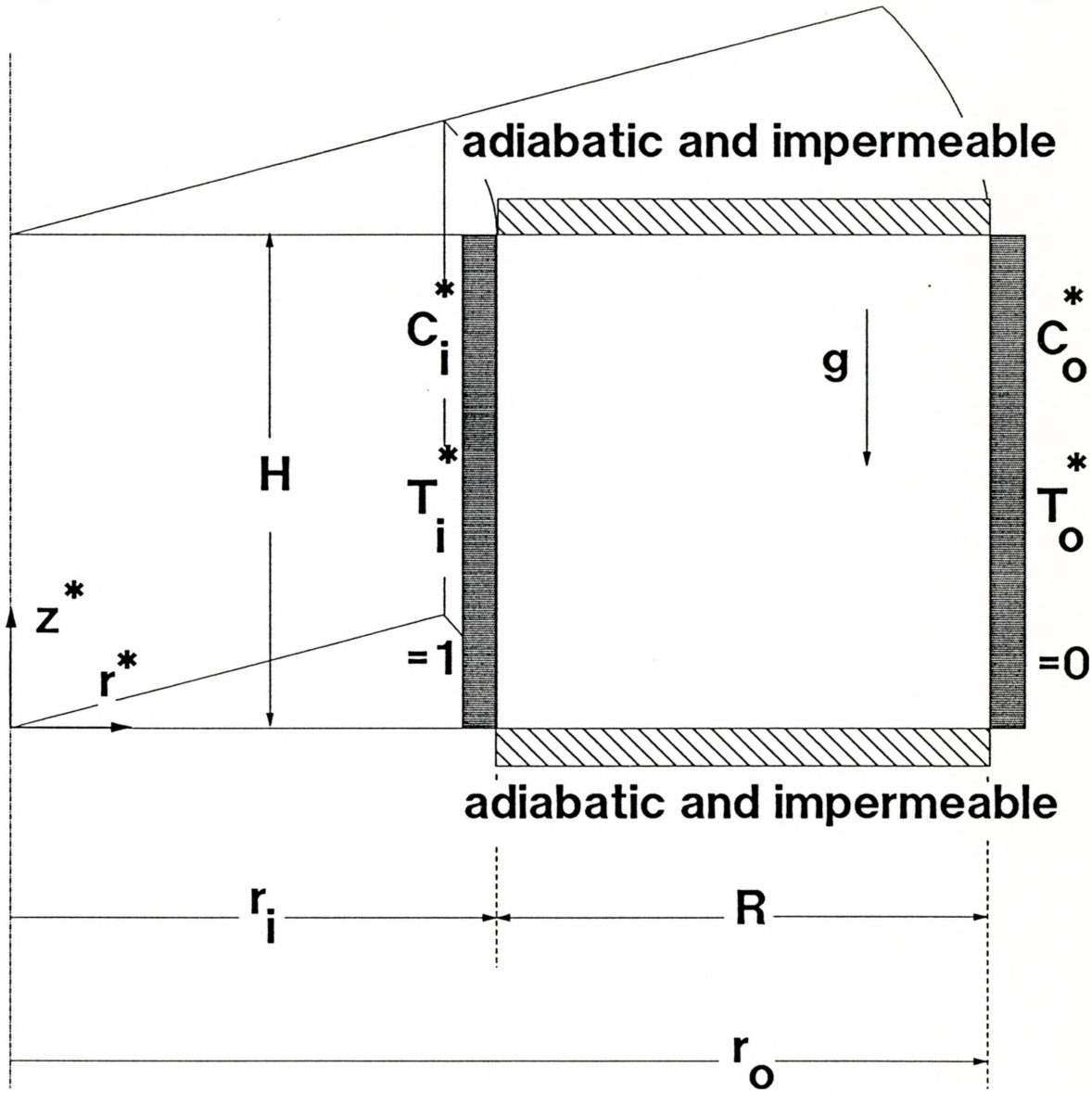

Figure 3.1 Schematic of Enclosure

coordinates as opposed to axis-symmetric.) The geometric system parameters, aspect ratio and curvature ratio as defined above are,

$$Ar = \frac{H}{R} \qquad K = \frac{r_o}{r_i} \tag{3.20}$$

3.5 Boundary Conditions

The boundaries of the enclosure consist of four walls; where the top and bottom walls are considered to be adiabatic and impermeable to mass transfer, and the inner and outer vertical radial walls are maintained at uniform temperatures and uniform concentration. Other boundary conditions can be easily applied to the vertical walls, such as uniform heat and mass fluxes, however it is not the intention to study this at the present time. Non slip velocity conditions are applied to all four of the enclosure walls. There are also no normal velocity boundary conditions applied to the walls, consequently no fluid enters or exits the cavity.

The dimensionless radii of the inner and outer enclosure walls depend on the value of the curvature ratio constant, where

$$K = \frac{r_o}{r_i}, \qquad r_i^* = \frac{r_i}{r_o - r_i}, \qquad r_o^* = \frac{r_o}{r_o - r_i}$$

therefore,

$$r_i^* = \frac{1}{K - 1}, \qquad r_o^* = \frac{K}{K - 1} \tag{3.21}$$

For purposes of this study the curvature ratio is limited to two, thus

$$r_i^* = 1, \qquad r_o^* = 2 \tag{3.22}$$

The reference condition is taken at the outer wall for all flow situations,

$$T_r = T_o, \qquad C_r = C_o$$

thus at the inner radial wall,

$$T_i^* = \frac{T_i - T_o}{T_i - T_o} = C_i^* = \frac{C_i - C_o}{C_i - C_o} = 1 \tag{3.23}$$

and at the outer radial wall,

$$T_o^* = \frac{T_o - T_o}{T_i - T_o} = C_o^* = \frac{C_o - C_o}{C_i - C_o} = 0 \tag{3.24}$$

At the bottom and top wall:

$$\frac{\partial T^*}{\partial z^*} = \frac{\partial C^*}{\partial z^*} = 0 \tag{3.25}$$

The velocity boundary conditions are defined as follows,

$$u^* = 0, \quad v^* = 0 \qquad \text{for } (r^* = r_i^*, r_o^*) \text{ or } (z^* = 0, Ar) \tag{3.26}$$

3.6 Buoyancy Ratio for Aiding and Opposing Buoyancy Forces

By virtue of the their definitions, the *dimensionless* temperatures and concentrations at the inner and outer walls will always equal 1 and 0 respectively, except when $T_i = T_o$, or $C_i = C_o$, which results in a singularity. Aiding and opposing flow conditions are determined by the sign of the buoyancy ratio. If we impose the thermal condition that $T_i > T_o$, then for aiding flow: $C_o > C_i$, and for opposing flow: $C_i > C_o$. If one examines the definition of the buoyancy ratio (equ. 3.19),

$$n = \frac{\beta_C (C_i - C_o)}{\beta_T (T_i - T_o)}$$

then for aiding flow, $(C_i - C_o)$ is negative, $(T_i - T_o)$ is positive, while the expansion coefficients, β_T and β_C are positive and negative respectively. This results in a positive buoyancy ratio for aiding flow. For opposing flow, the terms retain their signs except for the now positive $(C_i - C_o)$, resulting in a negative buoyancy ratio.

CHAPTER FOUR

NUMERICAL SOLUTION

4.1 Control Volumes and Staggered Grid

The governing equations are numerically solved using a finite volume approach. The variables are determined at discrete points on a staggered grid in which Patankar's SIMPLER [7,46] (*S*emi-*I*mplicit *M*ethod for *P*ressure *L*inked *E*quations-*R*evised) algorithm is adopted. This algorithm is applied to discretize the equations by integrating the differential equations over the control volumes and then solving for the variables. A brief description of the SIMPLER algorithm for the discretization of the axi-symmetric differential equations, along with the general solution procedure are presented in Appendix B. The staggered grid can be examined in figure 4.1. To avoid a checkerboard pressure pattern [7, p.116] the radial and axial velocity (u and v, respectively) components are offset from the pressure, temperature and concentration grid points. This staggered approach has the effect of reducing the complexity of the solution by directly calculating the mass flow into the pressure/temperature/concentration control volume at the control volume boundaries. Another advantage is that the pressure difference between two *adjacent* grid points becomes the driving force for the velocity component between these two points, thus complex non-linear interpolation is avoided if all the variables are to be

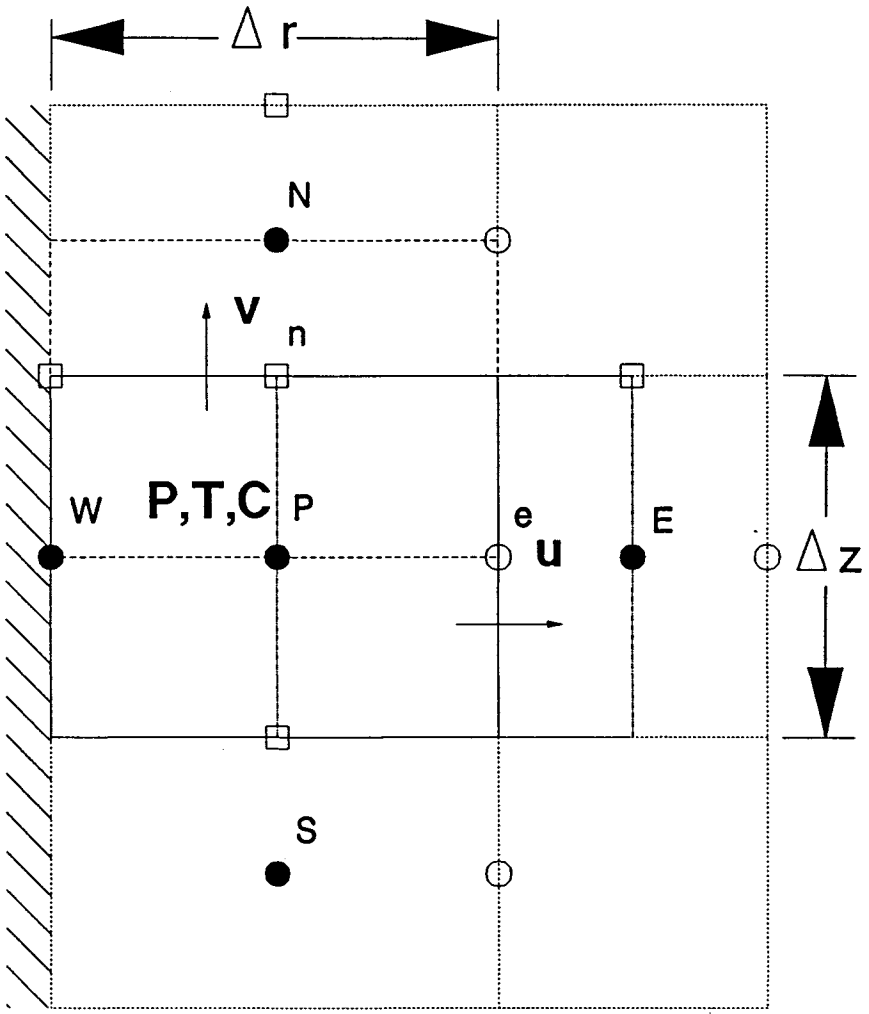

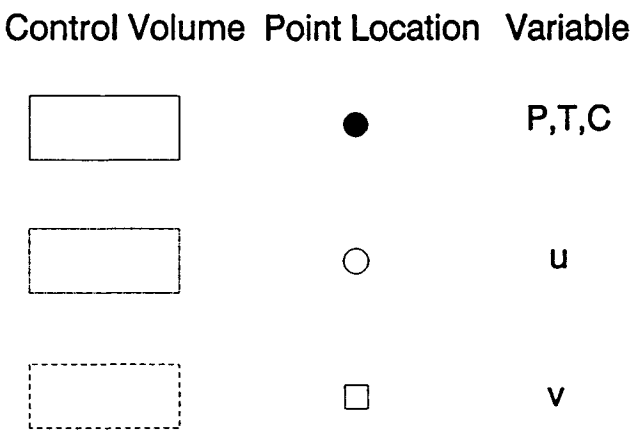

Figure 4.1 Staggered Control Volumes for the SIMPLER Algorithm

calculated on the same point. Treatment of wall conditions can also be examined in figure 4.1; the wall is treated as control volume with zero width, such that if the wall variable is unknown, it can be solved implicitly with the interior control volumes. However, if the variable is a boundary condition (*ie* fixed), the control volume can be easily dropped from the solution.

4.2 Generalized Equation

The governing equations, apart from continuity, can simply be expressed as a simple general conservation equation with a dependent variable, a diffusion constant, and a source term.

$$\frac{\partial \phi}{\partial t} + u^* \frac{\partial \phi}{\partial r^*} + v^* \frac{\partial \phi}{\partial z^*} = \Gamma \left[\frac{\partial}{r^* \partial r^*} \left(r^* \frac{\partial \phi}{\partial r^*} \right) + \frac{\partial^2 \phi}{\partial z^{*2}} \right] + S \tag{4.1}$$

The first term on the left hand side can be neglected since it is time dependant and we are only concerned with the steady state solution. The other terms on the left hand side represent convection. On the right hand side the terms in the square brackets represent the radial and axial diffusion respectively. The final term represents the source term. Depending on the dependent variable, ϕ, the diffusion coefficient, Γ, and the source term, S, the general governing equation can take on specific meanings. These are demonstrated in table 4.1 for the conservation of momentum, energy and mass species in axi-symmetric coordinates. The mass continuity equation can be examined in Chapter Three (eqs 3.1 and 3.12). A unique feature of this generalized equation is that it can easily be converted to two dimensional cartesian coordinates by substituting the enclosure width for R and equating r^*

(but not ∂r^*) to unity. Of course the radial velocity source term would have to be dropped in the radial momentum equation.

Table 4.1 Variables, Coefficients and Source Terms for eq.(4.1)

Equation	ϕ	Γ	S
Radial Momentum	u^*	Pr	$-Pr\ \frac{u^*}{r^{*2}} - \frac{\partial P^*}{\partial r^*}$
Axial Momentum	v^*	Pr	$-\frac{\partial P^*}{\partial z^*} + Ra_T\ Pr\ (T^* + n\ C^*)$
Energy	T^*	1	0
Mass Species	C^*	$\frac{1}{Le}$	0

4.3 Differencing Schemes for Convective Terms

There is a choice of profile schemes in which the variable can be determined at a control volume interface. One of the more accurate schemes is the exponential scheme based on the exact solution for a one-dimensional convection-diffusion problem with constant properties and zero source terms. However, this approach involves ample computer time to determine the exponentials. There are two approximations for this scheme: the power law differencing scheme by Patankar [7, pp. 90-95], and a slightly different scheme by Raithby [47, p.253], both of which involve less computational time. These differencing schemes along with the upwind and hybrid differencing schemes can be examined in figure 4.2. The variable ϕ_P is centered between two points (W and E)

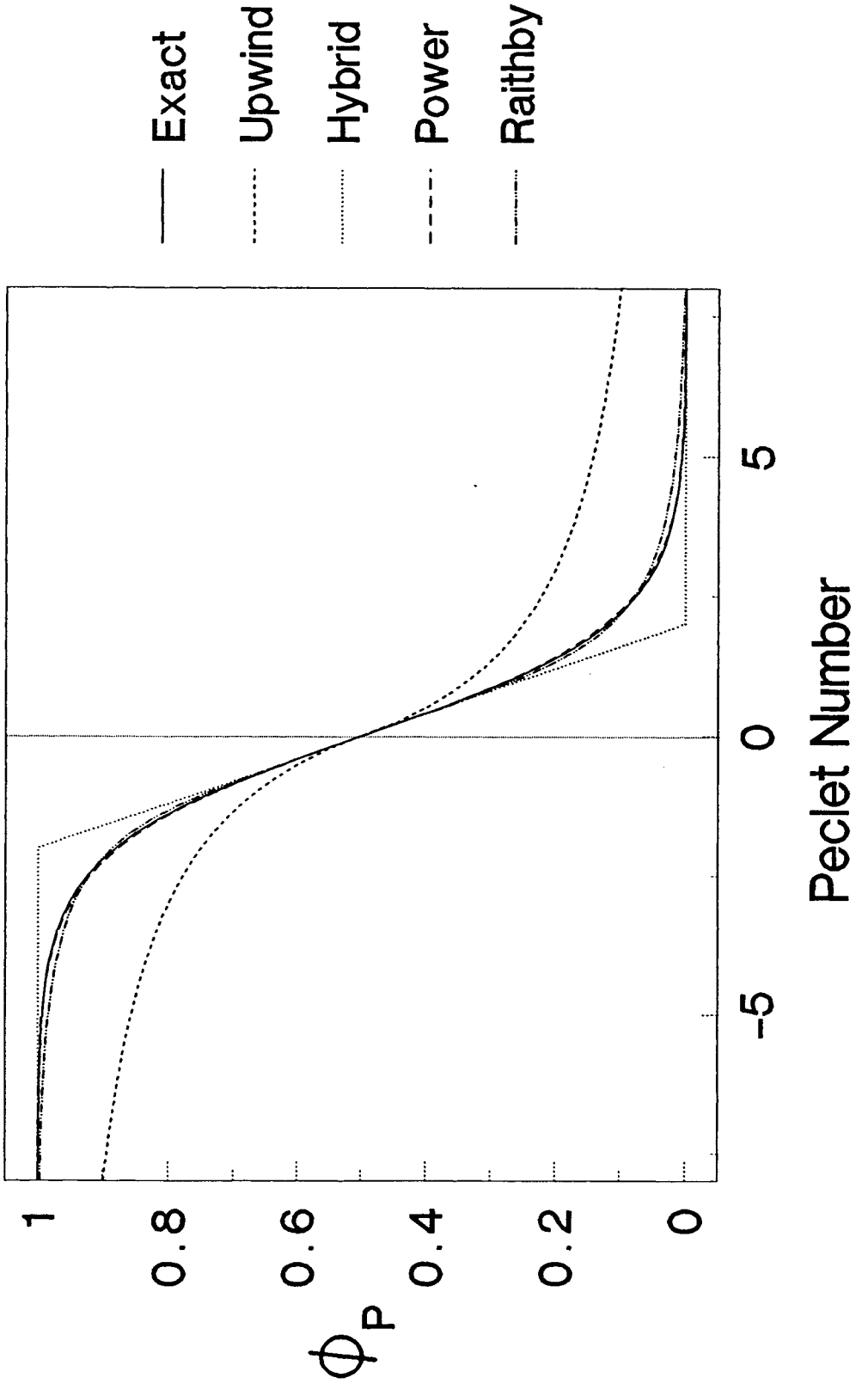

Figure 4.2 Comparison of Differencing Schemes with Respect to Pe

with values of 0 and 1, respectively. The Peclet number (Pe) is the ratio of convection and diffusion across a control volume,

$$Pe = \frac{u\,\Delta r}{\Gamma} \tag{4.3}$$

If there is no convection (*ie*. Pe = 0), then $\phi_P = 0.5$. For |Pe| > 6, the exact solution seems to be the value of the upstream point ($\phi_P = \phi_W = 0$, for Pe > 6; $\phi_P = \phi_E = 1$, for Pe < -6). The differences between the exact, power and Raithby's solutions are minimal, however Raithby's differencing scheme is more complicated than Patankar's, thus the power law differencing scheme, for reasons of computational efficiency, is chosen for the present study.

4.4 Solution of a General Field Equation

Due to the nature of the cross linked equations (concentration and temperature fields are dependent on the flow fields, but the buoyancy force in the axial momentum equation is determined by the concentration and temperature fields) the solution is iterative. It is determined that only one local iteration is required for the solution of a general field equation (axial momentum, pressure *etc.*) since all the equations are interlinked (note: a local iteration refers to a solution of a general field equation, whereas a global iteration signifies one complete cycle through the SIMPLER procedure). A converged solution of a field equation after many local iterations is unnecessary, if not wasteful, since the field conditions will change for the next global iteration. Certain variables may be underrelaxed in order for convergence, specifically it is found that the axial and radial

velocities must be relaxed the most. Underrelaxation may be expressed as follows, where ϕ is an arbitrary variable

$$\phi = \omega \, \phi_{new} + (1-\omega) \, \phi_{old}$$

Values of ω may be found for each governing equation in table 4.2. The general field equation is numerically solved by use of a combined alternating direction tridiagonal matrix algorithm (TDMA) enhanced with overrelaxation. In the solution procedure one local iteration actually consists of four sweeps of the numerical grid: one line sweep from the bottom to the top, then a line sweep from the left to right, followed by top to bottom and then finally right to left. The TDMA is a widely known algorithm and is presented in Appendix C, however the TDMA enhancement is less well known and is presented below.

4.4.1 Enhancement of the Tridiagonal Matrix Algorithm

The TDMA is enhanced by use of overrelaxation in which the changes in variables ahead of the present line are predicted and incorporated into the solution for the present line [47, p.262]. For the standard TDMA the value $\phi_{I,J+1}^{m-1}$ is required for the present "J" line sweep, but this value is lagged (m-1) at its best estimate value at this stage (m) of the sweep application. A revised estimate can be given by

$$\phi_{I,J+1} = \phi_{I,J+1}^{m-1} + (\eta - 1) \left(\phi_{I,J+1}^{m} - \phi_{I,J+1}^{m-1} \right) \qquad (4.4)$$

Generally, $\phi_{I,J+1}^{m}$ is not known, however a reasonable estimate of the *change*, $\phi_{I,J+1}^{m} - \phi_{I,J+1}^{m-1}$, can be obtained. This estimate is determined

by approximating the change at (I,J+1) by the change at (I,J) which is currently being calculated, thus

$$\phi_{I,J+1} \simeq \phi_{I,J+1}^{m-1} + (\eta - 1)\left(\phi_{I,J}^{m} - \phi_{I,J}^{m-1}\right) \tag{4.5}$$

A similar approach is applied for "I" line sweeps. The optimum values for the TDMA overrelaxation factor can be found in table 4.2.

Table 4.2 Underrelaxation and TDMA Overrelaxation Factors

Equation	r-Momentum	z-Momentum	Pressure	Energy	Mass Spec.
ω	0.5	0.5	1	1	1
η	1.2	1.2	1.85	1.8	1.8

4.5 Convergence Criteria

The convergence criteria is based on the equation residuals as opposed to solution changes. Convergence based on solution changes is particularly dangerous in some cases since convergence may become so slow that it appears converged when in fact it may be far from it. This problem is inherent when heavy underrelaxation is used. Equation residuals basically test how well the discretization equations are satisfied by the current values of the dependent variables. The general discretization equation for a control volume is usually written as

$$a_P\phi_P = \sum a_{nb}\phi_{nb} + b \tag{4.6}$$

(For more details of the discretization equation, see Appendix B) The residual for the control volume may be calculated as

$$R = \sum a_{nb}\phi_{nb} + b - a_P\phi_P \tag{4.7}$$

where, R, represents the residual. If the discretization equation is satisfied, R will be zero. However, it is sufficient to set the value of $|R|$ to be less than a small number. The major indicator of convergence is the residual for the mass continuity equation since this equation is influenced by all the other variables. The convergence limits for each governing equation are presented in table 4.3, where every control volume residual must satisfy this criteria in order for the solution to be considered converged. For certain cases with high thermal Rayleigh numbers the convergence level for the momentum equations is reduced to 10^{-4} since these equations converge to the tighter level only in double precision (which requires extra computational time). However, the mass equation convergence residual limit is still satisfied. Figure 4.3 illustrates the convergence of the maximum control volume equation residuals against the number of global iterations for an arbitrary trial. Notice that after 950 global iterations the momentum equations have reached a residual level of 10^{-4} while the mass continuity residual has reached 10^{-7}.

Table 4.3 Maximum Equation Residuals for Convergence

Mass	r-Momentum	z-Momentum	Pressure	Energy	Mass Spec.
10^{-6}	$5.\times 10^{-5}$	$5.\times 10^{-5}$	10^{-6}	10^{-5}	10^{-5}

4.6 Calculation of Nusselt, Sherwood Numbers and Streamfunctions

The Nusselt and Sherwood numbers are calculated at the inner wall after convergence has been obtained. The local Nusselt number at

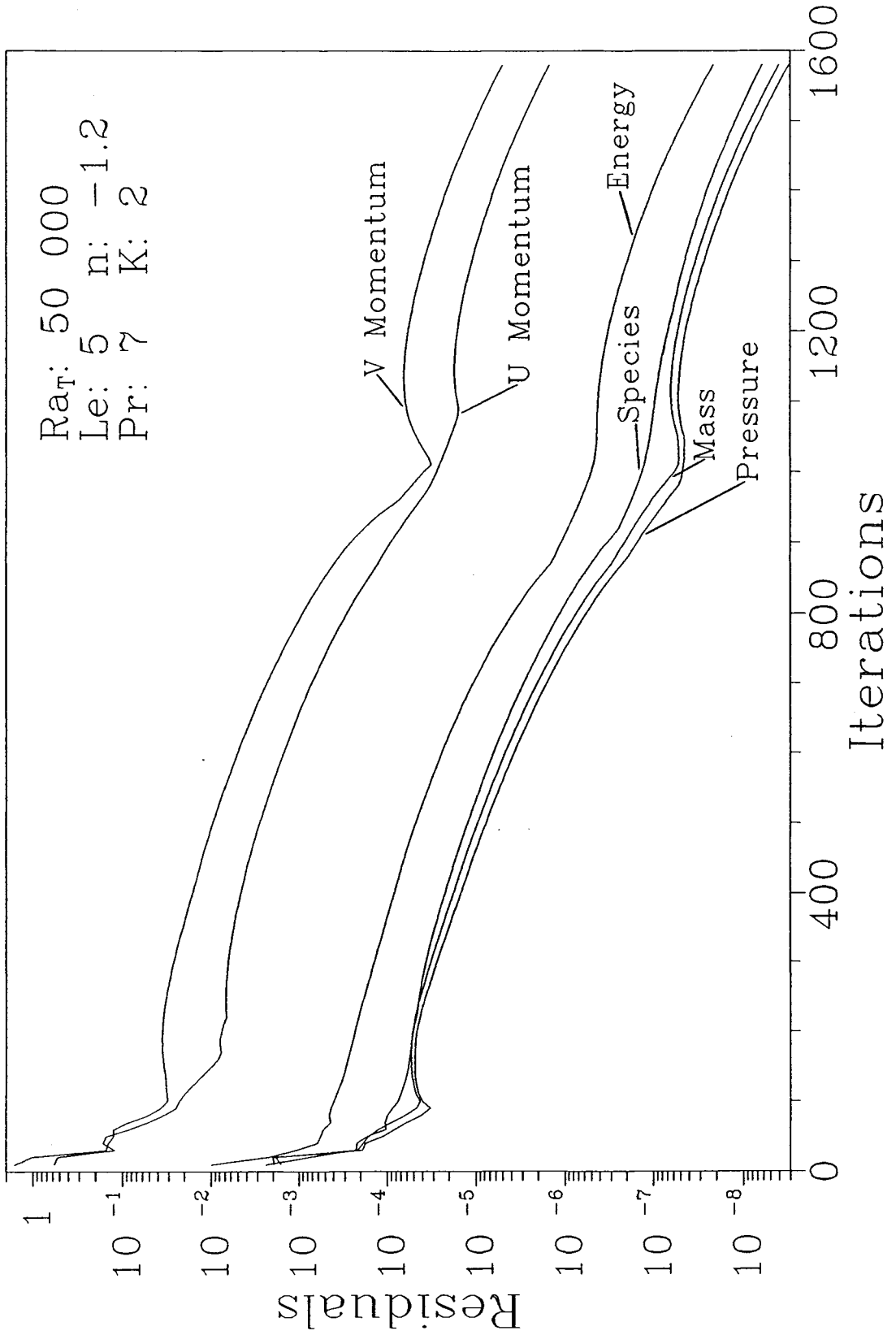

Figure 4.3 Convergence of the Maximum Equation Residuals

the wall is defined as the non-dimensional temperature gradient,

$$Nu_{i(z)} = - \left. \frac{\partial T^*}{\partial r^*} \right|_{r^* = r_i^*} \tag{4.8}$$

The Nusselt number in dimensional coordinates is easy to determine

$$Nu_{i(z)} = - \left. \frac{\partial T^*}{\partial r^*} \right|_{r^* = r_i^*} = - \frac{R}{T_i - T_o} \left. \frac{\partial T}{\partial r} \right|_{r = r_i} \tag{4.9}$$

but

$$q_i'' = -k \left. \frac{\partial T}{\partial r} \right|_{r = r_i} \qquad q_i'' = h_{i(z)} (T_i - T_o) \tag{4.10}$$

Combining the two equations above (4.10) and substituting into equ. 4.9

$$Nu_{i(z)} = \frac{h_{i(z)} R}{k} \qquad \text{at the inner wall} \tag{4.11}$$

The local Sherwood number at the inner wall can be determined in a similar fashion

$$Sh_{i(z)} = - \left. \frac{\partial C^*}{\partial r^*} \right|_{r^* = r_i^*} = \frac{h_{m_{i(z)}} R}{D} \qquad \text{at the inner wall} \tag{4.12}$$

The dimensionless gradient is calculated by approximating the linear profile at the wall. Higher order approximations can be used, however due to the nature of the discretized equations, source fluxes will produce linear variable distributions within the control volume near the boundary wall. Since the flux-variable distribution relationship is linear, unknown fluxes should be determined by linear variable distributions. The overall Nusselt and Sherwood numbers are determined by integrating the local Nusselt and Sherwood numbers along the inner wall.

$$\overline{Nu}_i = \int_0^{Ar} \left(\frac{\partial T^*}{\partial r^*} \right) \Bigg|_{r_i^*} dz^* \qquad \overline{Sh}_i = \int_0^{Ar} \left(\frac{\partial C^*}{\partial r^*} \right) \Bigg|_{r_i^*} dz^* \tag{4.13}$$

Due to the differences in radii it can be shown that the relationship between the inner and outer overall Nusselt number is

$$\overline{Nu}_o = \left(\frac{r_i}{r_o} \right) \overline{Nu}_i \tag{4.14}$$

Furthermore the relationship between the inner and outer Sherwood number can be similarly described

$$\overline{Sh}_o = \left(\frac{r_i}{r_o} \right) \overline{Sh}_i \tag{4.15}$$

Due to the curvature ratio being constant for this study the outer overall Nusselt and Sherwood numbers will be half of the overall inner Nusselt and Sherwood numbers respectively.

For purposes of plotting the flow field, streamline functions need to be defined. The streamfunctions are formulated in axi-symmetric coordinates, where the relationship between the streamfunction and velocity is

$$u^* = \frac{1}{r^*} \frac{\partial \psi^*}{\partial z^*}, \qquad v^* = - \frac{1}{r^*} \frac{\partial \psi^*}{\partial r^*} \tag{4.16}$$

Thus,

$$\psi_b^* = \psi_a^* + \int_a^b u^* \, r^* \, dz^*, \qquad \text{or} \qquad \psi_d^* = \psi_c^* - \int_c^d v^* \, r^* \, dr^* \tag{4.17}$$

where b and a refer to the axial location of the top and bottom boundaries of a control volume for a line of constant r^*. Similarly d and c refer to the radial location of the right and left boundaries of a

control volume for a line of constant z^*. Either equation will result in the same streamfunction field because of mass continuity. The enclosure boundary walls are arbitrary assigned a streamfunction value of zero.

4.7 Solution Grid and Grid Independence

A grid independence test is performed using various uniform, semi-uniform and non-uniform grid structures in order to obtain a suitable grid layout which the solutions are independent of. In general, fine grid spacings are required in the wall regions where there is high shear along with steep temperature and concentration gradients. This region is also important since the analysis of the problem significantly examines the Nusselt and Sherwood numbers in this region (in this study, the Nusselt number is examined for the indication of grid independence). The general theory behind grid independence is that as the number of grids are increased a certain point will be reached where the solution is independent of further grid refinement. An arbitrary test case is chosen with the following parameters: Ar = 1, K = 2, Pr = 1 , Le = 4, n = -1 and Ra_T = 20 000.

4.7.1 Uniform Grids

Initially a uniform grid structure is chosen with a range of 11 by 11 to 101 by 101 control volumes. Examining the circular data points on figures 4.4 and 4.5 indicates the solution's dependence on the grids with a uniform structure. From the uniform cell size of 0.0164 (61 by 61) to 0.0099 (101 by 101) the difference in the Nusselt number is only 0.002 or a 0.06% relative change. From this minimal change and the curved distribution in figures 4.4 and 4.5 it can be reasonably assumed

that grid independence has been achieved at the 61 by 61 uniform control volume grid. However solutions for a 61 by 61 grid (3721 control volumes or *cells*) are time consuming and solving for a 101 by 101 grid (10 201 cells) is simply unreasonable.

4.7.2 Non-Uniform Grids

To decrease the amount of grids, yet obtain accurate solutions for the wall heat and mass transfer, a non-uniform parabolic increment grid structure has been proposed. The cell sizes are increased at a predetermined percentage (i) from the boundary wall to the cell centre, where

$$(\text{cell size})_I = (\text{cell size})_{I+1} (1 + i/100) \qquad (4.18)$$

Grid structures ranging from 11 by 11 to 101 to 101 have been examined with cell size increases of 0 (uniform), 5, 10, 15, 20, and 30%. An example of this grid structure (11 by 11, i = 10; and 51 by 51, i = 20) can be examined in figure 4.6. Figure 4.4 represents the overall Nusselt numbers for various combinations of the above grid sizes and cell size increments plotted against the maximum cell size in the centre of the enclosure. The results prove to be unsuccessful in obtaining grid independence. (Note: the results also have been plotted against the minimal cell size, which also proves to be inconclusive.)

4.7.3 Semi-Uniform Grids

Hrymak [48] suggested the use of two or three different levels of uniform cells: uniform cells within the centre of the cavity and finer uniform boundary layers adjacent to the walls (see figure 4.7). A similar semi-uniform method was used by Trevisan and Bejan [23]. Because of their success in obtaining grid independence, this grid

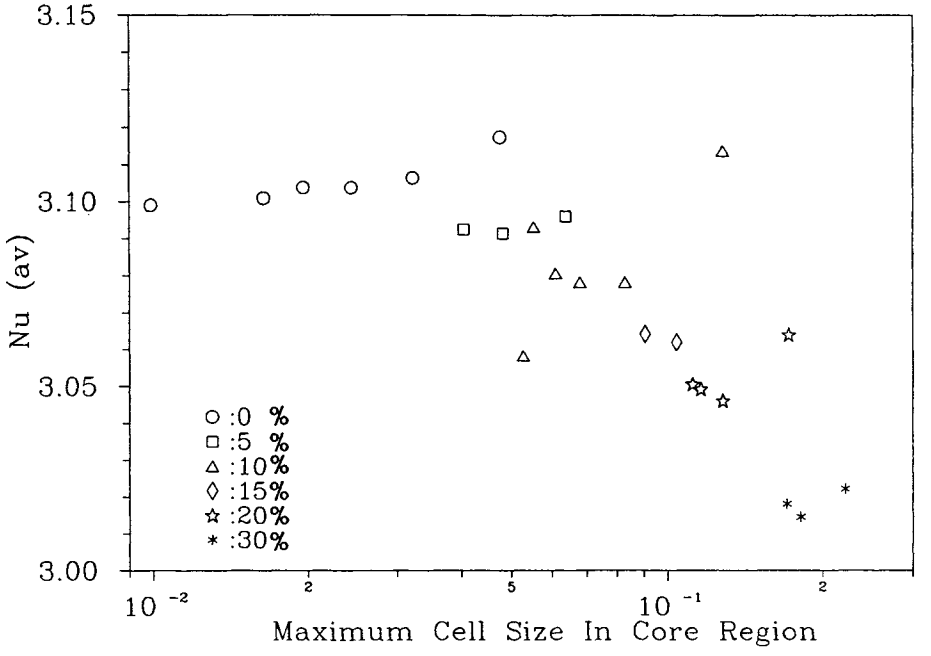

Figure 4.4 Grid Independence for Non-Uniform Grids

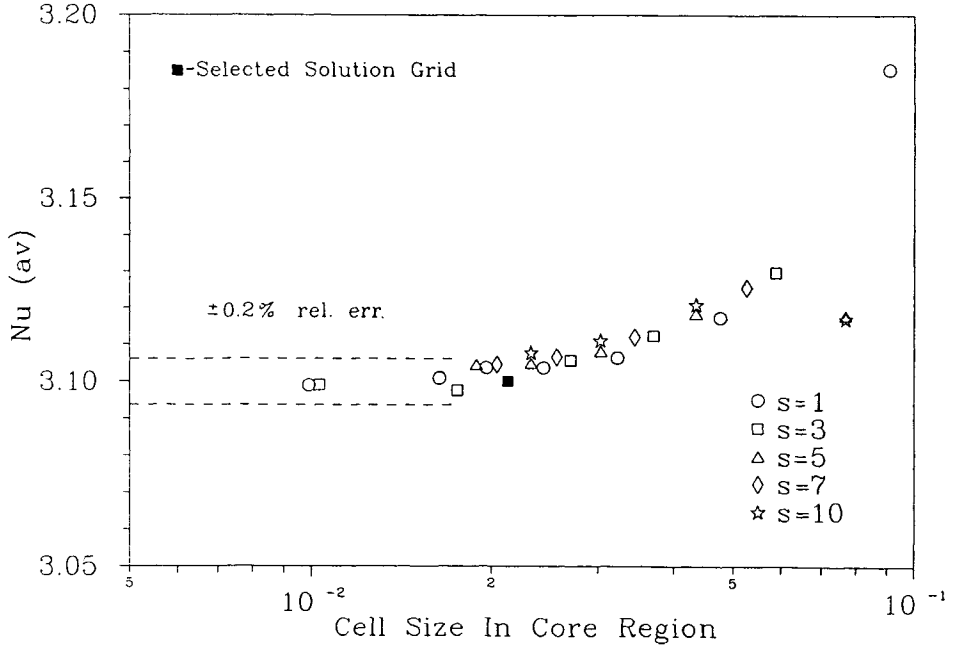

Figure 4.5 Grid Independence for Semi-Uniform Grids

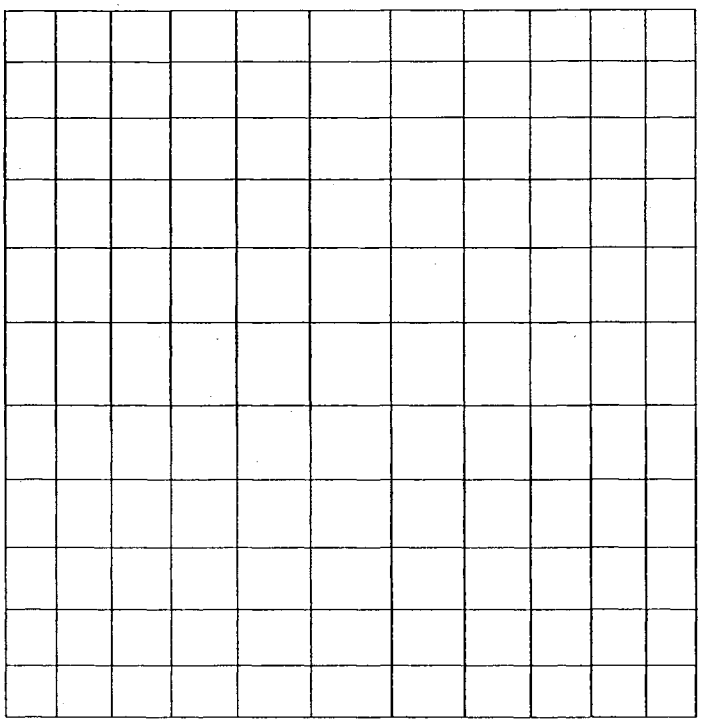

a) 11 by 11 Grid, i = 10%

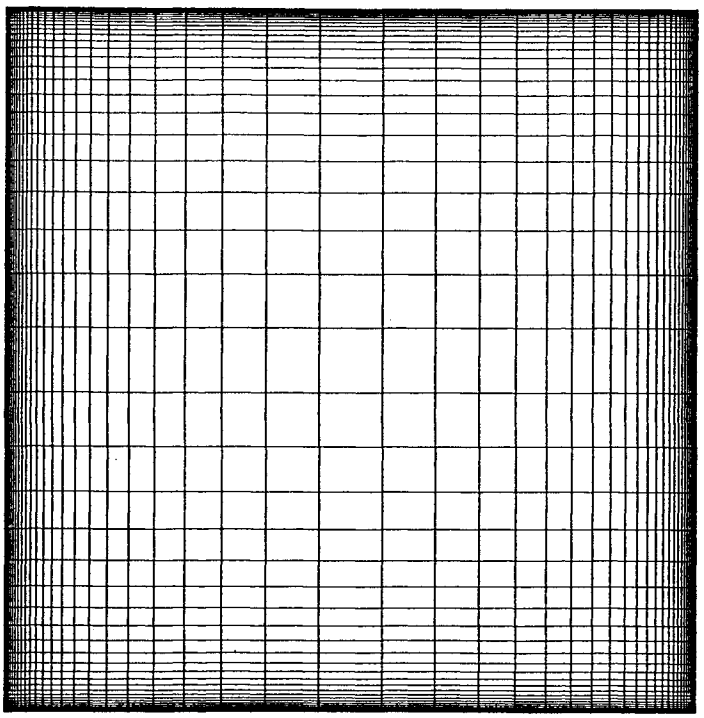

b) 51 by 51 Grid, i = 20%

Figure 4.6 Examples of Non-Uniform Grid Structure

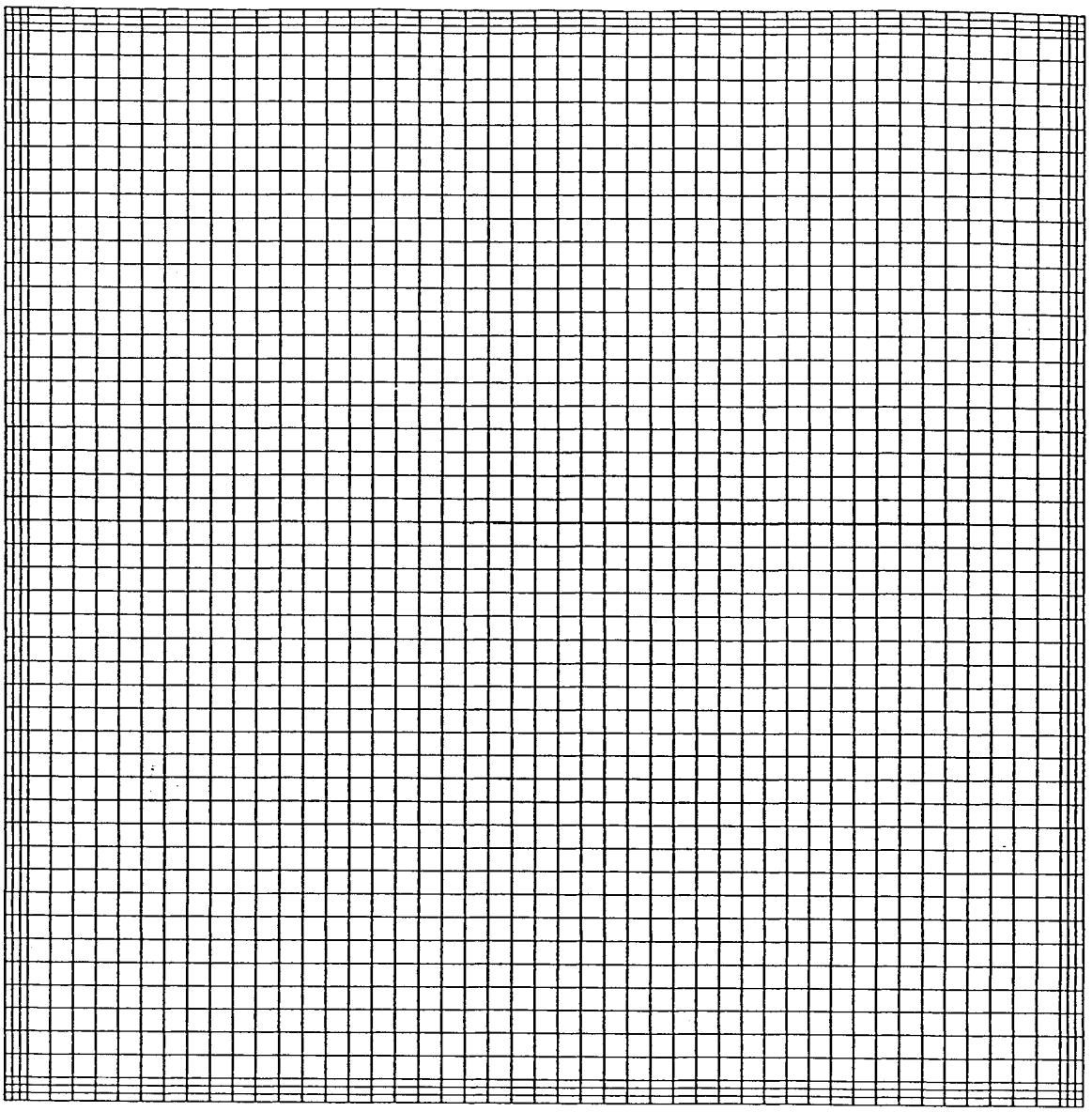

Figure 4.7 Semi-Uniform Grid Structure Chosen, $m = 51$, $s = 3$

structure has been adopted for the present study. The enclosure is divided into m by m control volumes where there are s thin cells normal and adjacent to the walls, with a thickness of $1/s$ of a core cell. This results in the core section having $(m - 2s)$ by $(m - 2s)$ cells (for fig. 4.7, $m = 51$, $s = 3$). Examination of figure 4.5 reveals a definite trend in convergence for a decrease in the cell size in the core region with approximately half the data points fitting in the 0.2% relative difference band (based around the uniform grid solution for 101 by 101 cells). Thus a grid size is chosen for the present study with $m = 51$ and $s = 3$, optimizing the number of boundary cell layers for determining accurate wall results, while minimizing the total number of cells (2601) for reduced computer solution time.

4.8 Numerical Error

The SIMPLER algorithm is susceptible to a numerical error commonly known as *false diffusion* or *numerical diffusion*. Maximum false diffusion occurs when flow is oblique to grid lines and when there is a high gradient of the dependent variable in the direction normal to the flow. For a rectangular grid structure, this error has the greatest effect when the flow is 45 degrees to the grid lines. Patankar [7, p.108] suggests that the following expression [49] approximately represents the false diffusion coefficient for two dimension situations

$$\Gamma_{false} = \frac{u^* \Delta x^* \Delta y^* \sin 2\theta}{4\,(\Delta x^* \sin^3\theta + \Delta y^* \cos^3\theta)} \qquad (4.19)$$

where Δx^* and Δy^* represent the control volume size and θ is the angle the flow makes with the x-axis (it is probable that this expression can

be extended to an axi-symmetric system with the error being of the same order). It should be stressed that the source of false diffusion is a local phenomenon, however diffusion will permeate most of the grid. The majority of flows adjacent to walls will not be significantly affected since the flow is parallel to the grid lines. Flows within the interior of the enclosure may be more influenced since the flow may be oblique to the grid lines at certain locations. However it is expected that false diffusion will be minimal since the velocities in this region are expected to be low along with the variable gradients since high gradients usually occur at the boundary walls. Schemes that significantly reduce false diffusion are available (*ie* Skewed Upwind Differencing, QUICK [47, pp 256-259]), however they are more complex and involve more neighbouring point values in the discretization equations thereby involving significantly more computational effort. Finally, it should be said that false diffusion can effectively be reduced by obtaining a grid independent solution.

CHAPTER FIVE

CODE VERIFICATION

Due to the lack of other numerical and experimental studies of double-diffusive natural convection in axi-symmetric coordinates in the literature, the computer code cannot be exhaustively validated. Instead, three separate verification tests are conducted. The first test is simply to verify the Nusselt and Sherwood numbers on the outer and inner radial walls under no flow or stagnant conditions. The second test is a complete double-diffusive natural convection comparison against Trevisan and Bejan's [23] two dimensional numerical study in a rectangular enclosure. The computer code has the optional ability to solve double-diffusive problems in cartesian coordinates, where the simple modifications are discussed in Chapter Four (section 4.2). Finally, to examine the axi-symmetric capabilities of the program, a comparison has been made with a numerical study performed by Thomas and de Vahl Davis [50] on heat transfer driven natural convection in annular cavities.

5.1 Stagnant Flow

The initial test is to examine the Nusselt and Sherwood numbers of conductive heat transfer and diffusive mass transfer under no flow conditions. It is also important to ensure that there is no flow when these conditions are applied. Examining the axial momentum equation

(eq. 3.14), a no flow condition will exist when the buoyancy source term,

$$\left[T^* + n\, C^*\right] = 0 \tag{5.1}$$

This can be achieved by equating the buoyancy ratio (n) to negative unity and limiting the Lewis number (Le) to unity, ensuring that the thermal and mass species diffusivities are equal in order to obtain similar dimensionless temperature and concentration distributions. An alternative for stagnant flow for Le ≠ 1 is to limit the thermal Rayleigh number to a low value ($Ra_T \leq 5000$, at low Rayleigh numbers the viscosity of the fluid acts as a stabilizer) while again equating the buoyancy ratio to negative unity. The initial conditions must be stagnant, otherwise an instability may induce convection.

The alternative condition is used to examine stagnant flow heat and mass transfer using the following arbitrary parameters: Ar = 1, Pr = 7, K = 2, n = -1, Le = 5. and $Ra_T = 5000$. The standard solution grid is used ($m = 51$, $s = 3$, see Chapter Four) resulting in an inner wall overall Nusselt and Sherwood number of 1.442634, where as the outer radial wall overall Nusselt and Sherwood number is calculated to be 0.721002. The ratio between these two values is 0.4998 which is extremely close to the value of 0.5 predicted by equations 4.14 and 4.15.

The exact solution for conductive heat and diffusive mass transfer in axi-symmetric coordinates can be derived from the conservation of the energy and mass species equations. Dropping the advection terms in equation 3.15

$$\frac{\partial}{r^* \partial r^*}\left(r^* \frac{\partial T^*}{\partial r^*} \right) + \frac{\partial^2 T^*}{\partial z^{*2}} = 0 \qquad (5.2)$$

Since the radial walls have uniform temperatures and the top and bottom walls are adiabatic, the problem can be considered to be one dimensional such that the axial diffusion term can be dropped, therefore

$$\frac{\partial}{\partial r^*}\left(r^* \frac{\partial T^*}{\partial r^*} \right) = 0 \qquad (5.3)$$

Integrating equation 5.3 twice and solving for the boundary conditions of $T^* = 1, 0$ at r_i^*, r_o^* respectively

$$T^* = \frac{\ln\left(r^*/r_o^* \right)}{-\ln(K)} \qquad (5.4)$$

(The actual temperature distribution can be observed in figure 5.1) The Nusselt number is defined as the dimensionless temperature gradient, thus

$$Nu = \frac{1}{r^* \ln(K)} \qquad (5.5)$$

For $K = 2$,

$$Nu_i = 1.442695, \qquad Nu_o = 0.721348 \qquad (5.6)$$

The Sherwood numbers are equivalent to the above Nusselt numbers since the diffusion coefficient drops out in equation 5.2. The results from the stagnant flow conditions are considered to be extremely good, furthermore it demonstrates that 1st order Nusselt number approximation (Chapter Four, section 4.6) is sufficient.

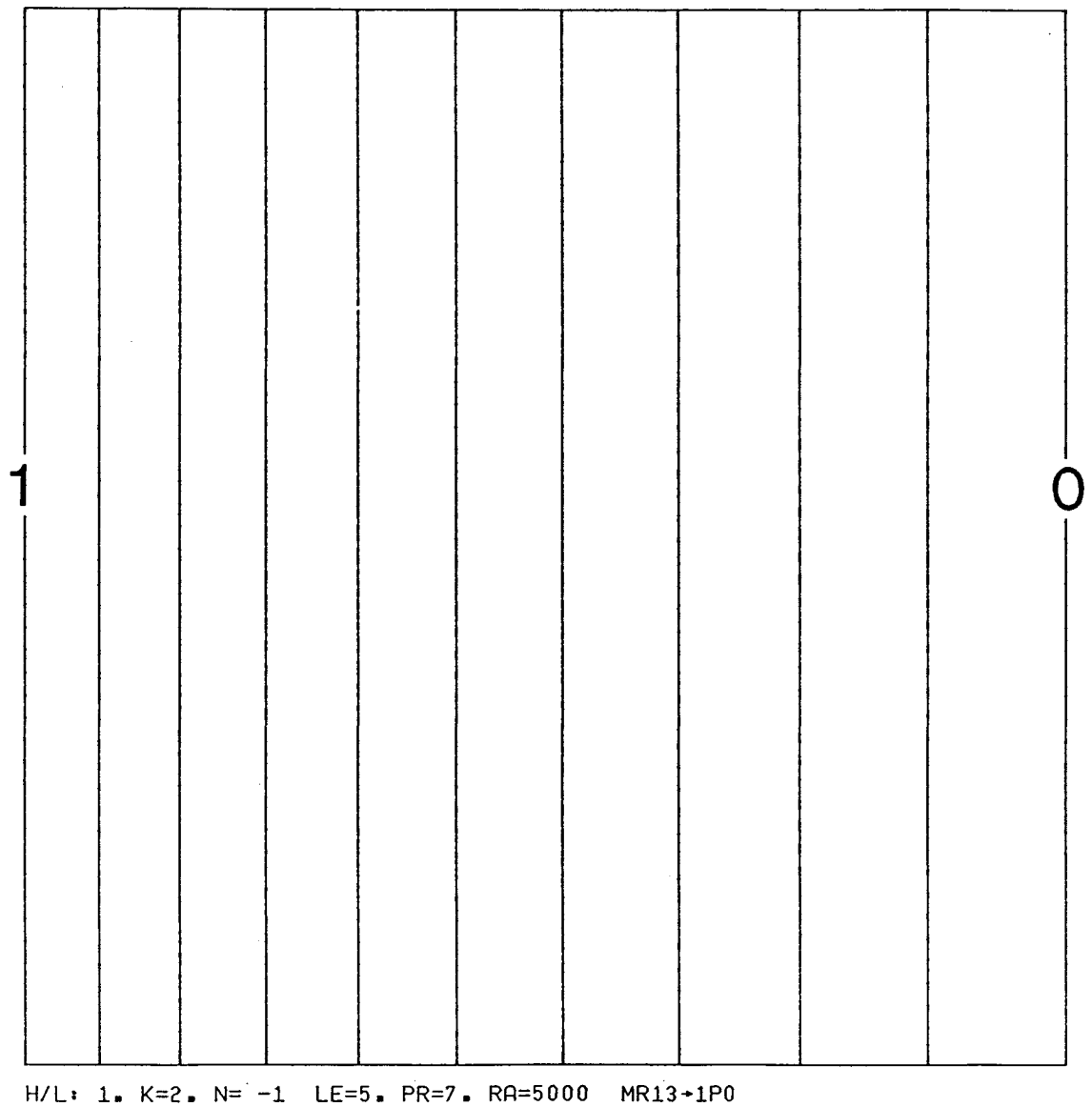

Figure 5.1 Dimensionless Thermal Distribution for Stagnant Conditions

5.2 Two Dimensional Double-Diffusive Test

The computer code is tested against a double-diffusive natural convection study in a two dimensional rectangular enclosure performed by Trevisan and Bejan [23]. At the time of code verification, this is one of the few simple double-diffusive studies known to the author without complicated flow dependent boundary conditions (*ie.* velocity normal to a wall due to mass species influx). The schematic for the two dimensional enclosure can be examined in figure 5.2; the enclosure is similar to the axi-symmetric enclosure used in the present study in two aspects: the aspect ratio is unity, and the top and bottom enclosure walls are adiabatic to heat transfer and impermeable to mass transfer. However the boundary conditions on the vertical walls are imposed with uniform heat and mass transfer as opposed to uniform temperature and concentration differences. These boundary conditions will slightly change the definitions of some of the dimensionless variables and system parameters, specifically the dimensionless temperature and concentration, the thermal Rayleigh number and the buoyancy ratio. Therefore

$$T' = \frac{k(T - T_r)}{q'' L}, \qquad C' = \frac{D \rho_r (C - C_r)}{j'' L} \tag{5.7}$$

and

$$Ra_T' = \frac{g \beta_T q'' L^4}{\alpha \nu k}, \qquad n' = \frac{\beta_C k j''}{\beta_T D \rho_r q''} \tag{5.8}$$

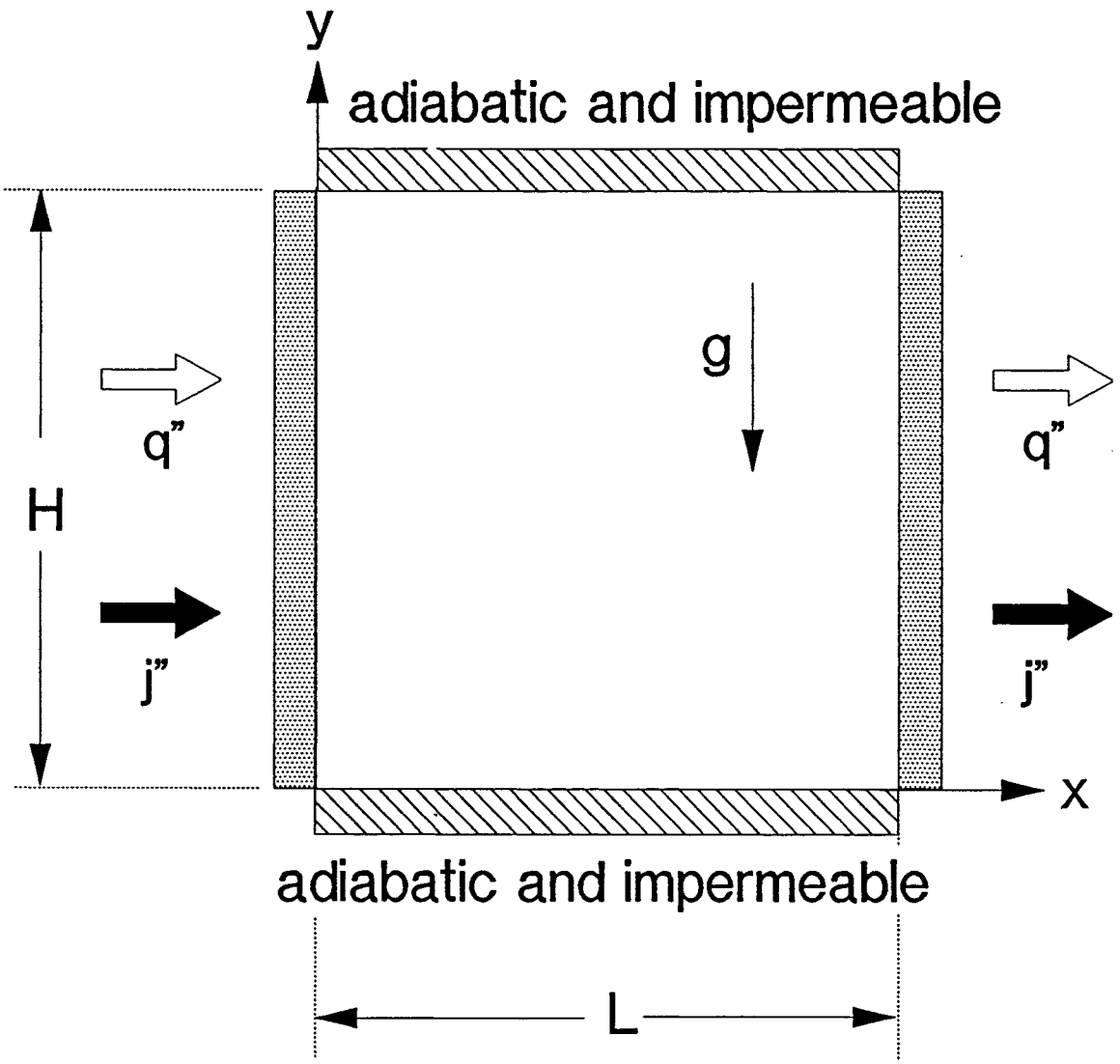

q": Heat Flux

j": Species Mass Flux

Ar=H/L=1

Figure 5.2 Schematic For Two Dimensional Enclosure

The definition of the overall Nusselt and Sherwood numbers have also been modified for the heat and mass flux boundary conditions

$$\overline{Nu}' = \left(\int_0^1 \Delta T' dy^* \right)^{-1}, \qquad \overline{Sh}' = \left(\int_0^1 \Delta C' dy^* \right)^{-1} \tag{5.9}$$

where $\Delta T'$ and $\Delta C'$ represent the dimensionless temperature and concentration differences across the enclosure.

The Trevisan and Bejan study used Patankar's control volume approach [7,46] to discretize the governing equations. However as opposed to using primitive variables, the governing equations were set up for streamline and vorticity functions eliminating the pressure terms and solved using a Gauss-Seidel iterative routine. For the present configuration a thermal Rayleigh number of 3.5×10^5 was applied across the vertical walls, the Prandtl number corresponds to air and water (0.7 and 7), the Lewis number was ranged from 1 to 10, and the buoyancy ratio had a range of -1 to 9. A similar grid structure to the original study was used. A comparison of the results for Le = 1 may be found in table 5.1; for this case the Nusselt and Sherwood numbers will be equivalent.

Table 5.1 Comparison of Results for Double-Diffusive Natural Convection in a Two Dimensional Cavity with (Le = 1, Ar = 1, $Ra' = 3.5 \times 10^5$).

n'	Pr	Present Study		Trevisan and Bejan	
		$\overline{Nu}'$, $\overline{Sh}'$	Nu,Sh(y/H=.5)	$\overline{Nu}'$, $\overline{Sh}'$	Nu,Sh(y/H=.5)
-1	7	1.001	1.00079	1.04	1.05
	0.7	1.001	1.00079	1.04	1.05
0	7	4.89	5.77	4.83	5.88
	0.7	4.85	5.71	4.78	5.82
1	7	5.78	6.72	5.73	6.83
	0.7	5.73	6.68	5.72	6.87
3	7	6.81	7.78	6.88	8.05
	0.7	6.75	7.76	6.76	7.92
9	7	8.44	9.41	8.67	9.86
	0.7	8.37	9.43	8.44	9.55

The agreement between the present study and Trevisan and Bejan's results for Le = 1 is fairly good, with the largest Nusselt number difference around 4%. However, the case with n' = -1 should be examined closely; when Le = 1, the thermal diffusivity equals the mass species diffusivity resulting in identical thermal and concentration distributions within the enclosure. The result is a no flow situation, consequently for a two dimensional enclosure the Nusselt and Sherwood numbers should be equivalent and equal unity. For this case, Trevisan and Bejan's model predicts the average Nusselt number to be 1.04, whereas the present model predicts an overall Nusselt number of 1.001. This difference can be attributed to the fact that Trevisan and Bejan have used a convergence criteria based on the relative change in variables as opposed to a minimal equation residual. One may

hypothesize that Trevisan and Bejan's solutions have not fully converged which may explain the small difference in the Nusselt and Sherwood numbers between the present study and the Trevisan and Bejan study. Neglecting the no flow case for the comparison of the two solutions the largest relative difference between the Nusselt numbers is 2.7%.

Solutions for a buoyancy ratio of zero with the Lewis number as the main parameter are presented in table 5.2. Physically speaking, n' = 0 indicates that the concentration difference across the enclosure has a negligible effect on the density, thus there is no concentration effect on the flow structure. Consequently, natural convection is driven by temperature gradients alone. The Nusselt number for these trails is constant since only the diffusivity of the mass species is being changed. It should be noted that the Nusselt number for the Trevisan and Bejan case varies slightly, most likely for the same reasons as mentioned in the previous paragraph. Generally the Sherwood number results are in good agreement with the comparative study with the greatest relative difference being 3.6%.

Table 5.2 Comparison of Results with the Lewis Number as Main Parameter ($n' = 0$, $Ar = 1$, $Pr = 7$, $Ra'_T = 3.5 \times 10^5$)

	Present Study		Trevisan and Bejan	
Le	$\overline{Nu}'$	$\overline{Sh}'$	$\overline{Nu}'$	$\overline{Sh}'$
1	4.89	4.89	4.83	4.83
2	4.89	6.49	4.81	6.46
4	4.89	8.04	4.81	8.15
10	4.89	10.61	4.81	10.99

To further complement the comparison, concentration profiles are presented in figures 5.3 and 5.4. Figures 5.3a-b demonstrates the dimensionless concentration profile with system parameters of Pr = 7, Le = 1 and n' = 0, in this case the distributions are approximately the same. Under similar conditions, except for Le = 10, figures 5.4a-b are slightly different; the zero concentration contour from the Trevisan and Bejan study is a linear diagonal through the core of the cavity, however from the present study the same contour is wavy. This indicates that there are small eddies within the centre of the enclosure for the present study, whereas the original study had one square like eddy in the same location. The contour line for C' = .06 indicates that the distributions are slightly unmatched with the present study predicting high absolute concentrations at the vertical walls, assuming that the concentration profiles in the original study have constant increments.

In general the two studies are comparable with minor differences. The general flow patterns are similar and the overall Sherwood and Nusselt numbers for the two studies are close. Differences are probably due to the two different solution procedures along with the different variable forms of the governing equations and solution convergence criteria. This section verifies the code in two dimensional cartesian coordinates, however there is a need to know how well the code will perform in axi-symmetric coordinates.

5.3 Axi-Symmetric Heat Transfer Driven Comparison

Since there are no previous double-diffusive studies in a vertical closed annulus known to the author, the code has been verified against a thermal natural convection study by Thomas and de Vahl Davis

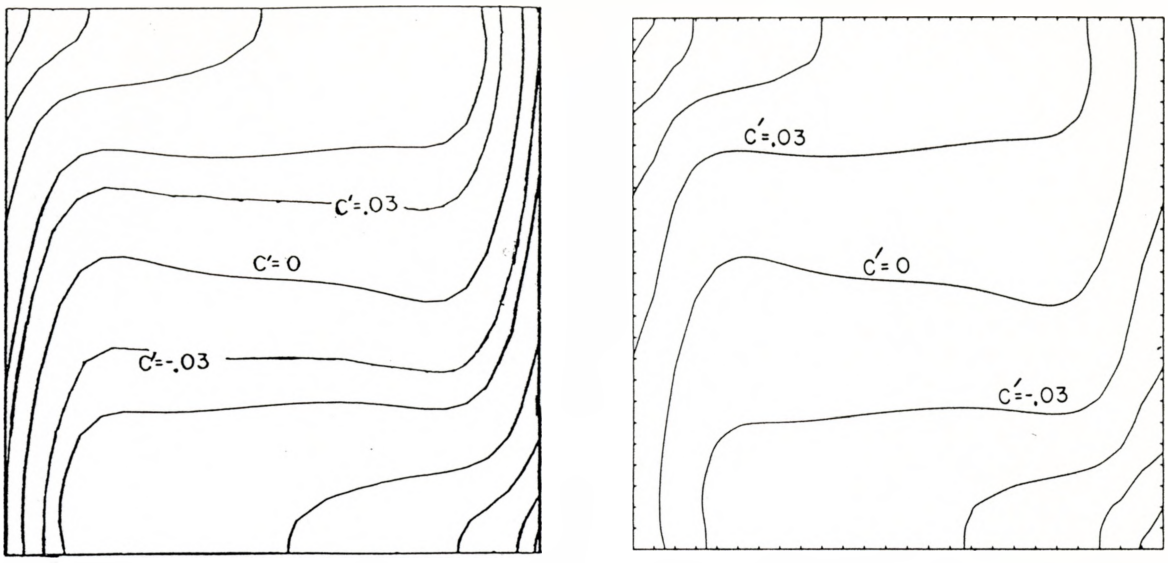

a) Present Study Le = 1 b) Trevisan and Bejan Le = 1

Figure 5.3 Dimensionless Concentration Contours for Two Dimensional Enclosure. (Ar = 1, $Ra'_T = 3.5 \times 10^5$, Pr = 7. and n' = 0)

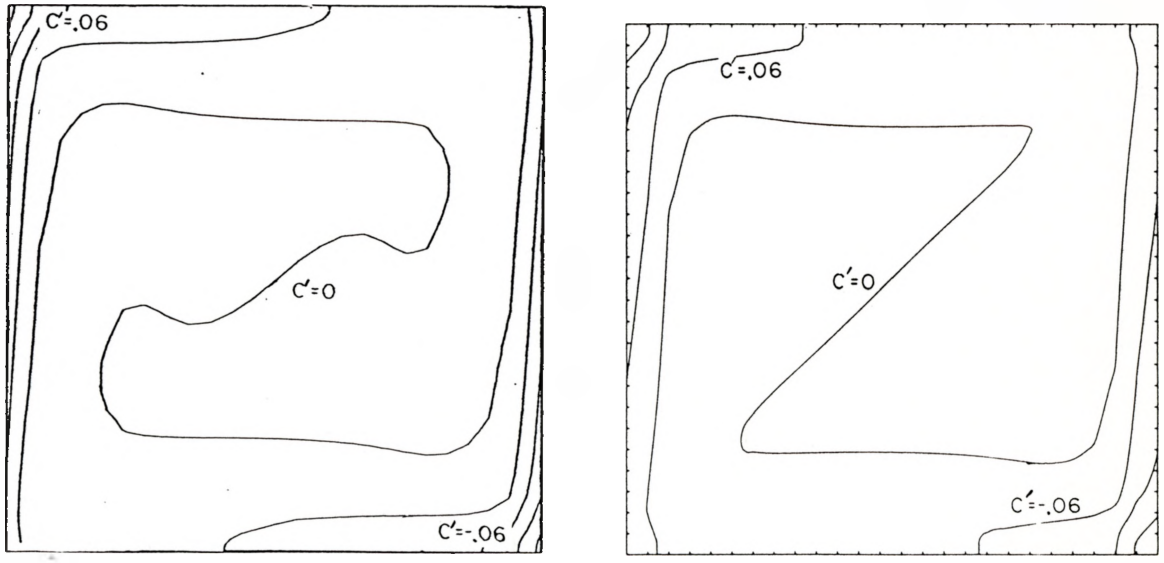

a) Present Study Le = 10 b) Trevisan and Bejan Le = 10

Figure 5.4 Dimensionless Concentration Contours for Two Dimensional Enclosure. (Ar = 1, $Ra'_T = 3.5 \times 10$, Pr = 7. and n' = 0)

[50] in order to check the performance of the code in axi-symmetric coordinates. The mass species equation is identical to the energy equation apart from the difference in the diffusivities, such that the separate verification of the mass species equation in axi-symmetric coordinates would be inconsequential since it has already been validated in the previous section. The axi-symmetric configuration under the present verification has an aspect ratio of ten with a curvature ratio of two where a single uniform temperature difference is laterally placed across the inner and outer walls (see fig. 5.5 for the schematic). The top and bottom enclosure walls are considered to be adiabatic. Thomas and de Vahl Davis have studied the problem for a Prandtl number of unity and for thermal Rayleigh numbers of 2000, 20 000 and 100 000. Since the natural convection is driven by heat transfer alone the buoyancy ratio for the present code is zero and the Lewis number does not have to be defined. The original solution used vorticity/streamfunction variables for the governing equations and was solved using an underrelaxed alternating direction iterative method.

A visual presentation of the streamfunctions and thermal contours for the original and present studies can be examined in figures 5.6 and 5.7. A comparison of the mid-radial and mid-axial velocity profiles can be examined in figures 5.8 and 5.9, while the overall Nusselt numbers are presented in table 5.3. Both the streamfunction and thermal contour plots are almost identical. For the velocity profiles, both the studies are in good agreement. The velocity distributions are almost identical and the error in relative magnitude seems to be within an acceptable 5%. The agreement for the overall Nusselt number is

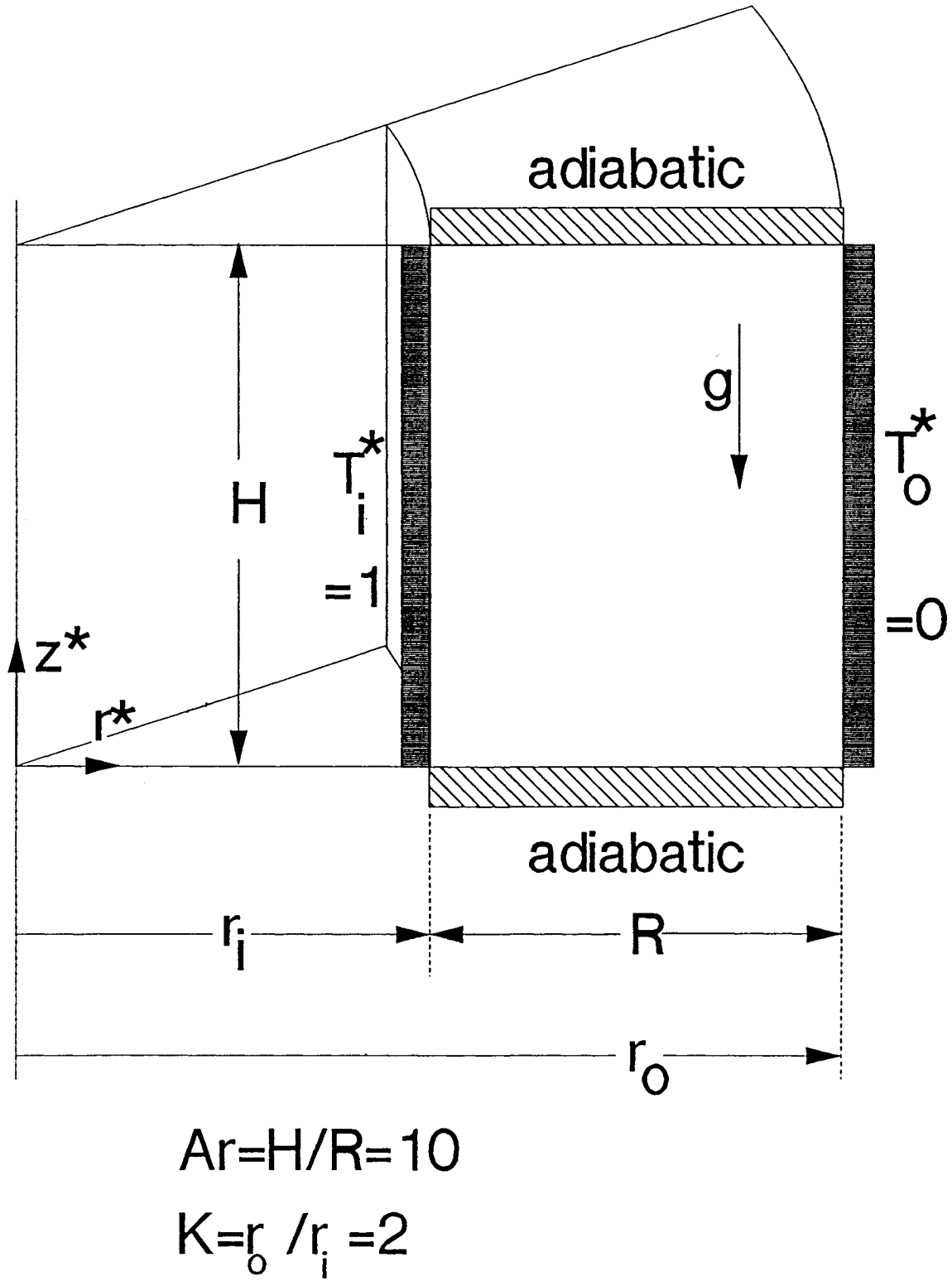

Figure 5.5 Schematic of Axi-Symmetric Single-Diffusive Enclosure

Present Study

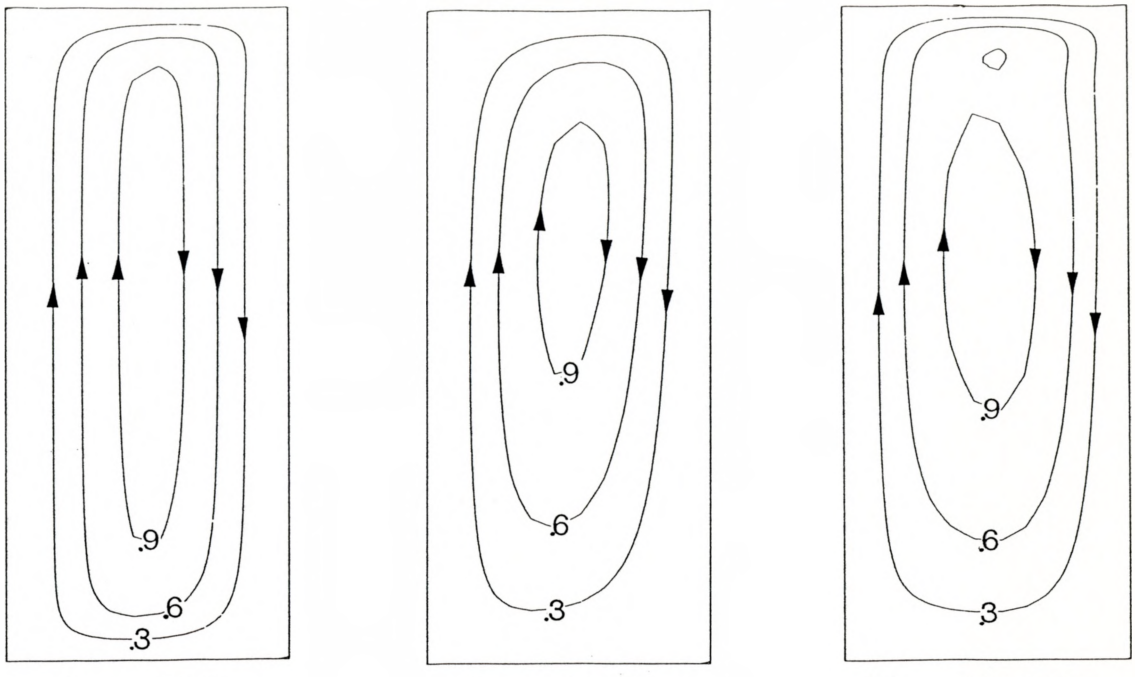

Ra_T = 2000 Ra_T = 20 000 Ra_T = 100 000

Thomas and de Vahl Davis

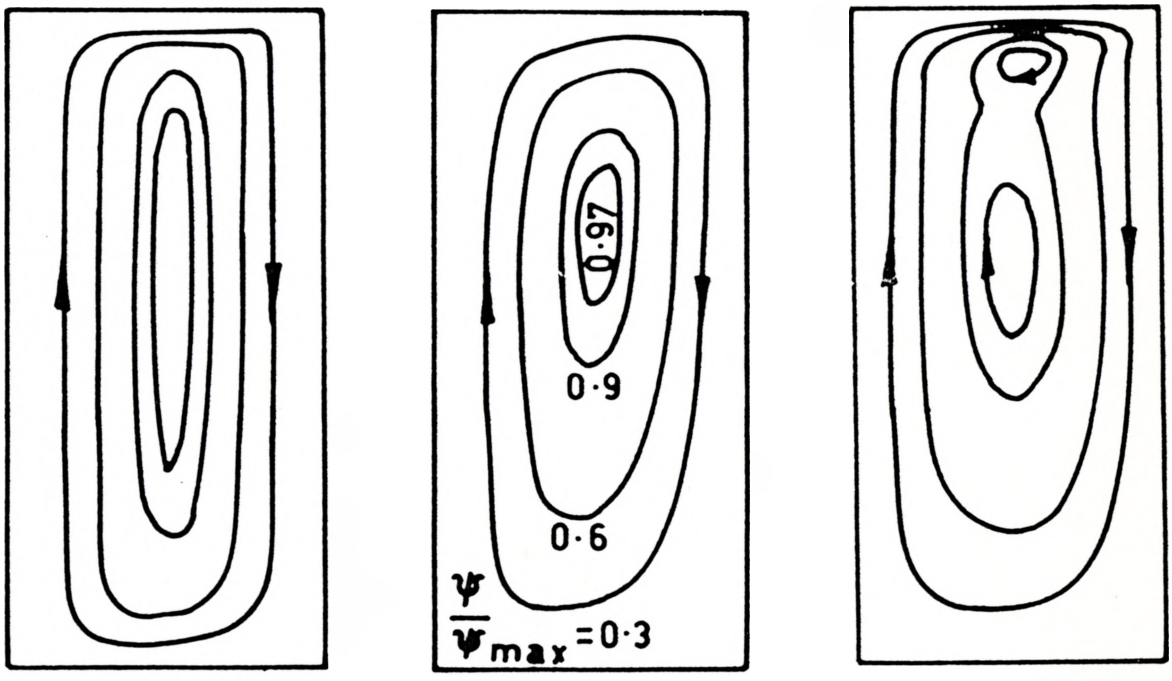

Ra_T = 2000 Ra_T = 20 000 Ra_T = 100 000

Figure 5.6 Streamfunctions for Single-Diffusive Case (Ar = 10, K = 2, Pr = 1, n = 0) Note: Enclosure Heights are Compressed.

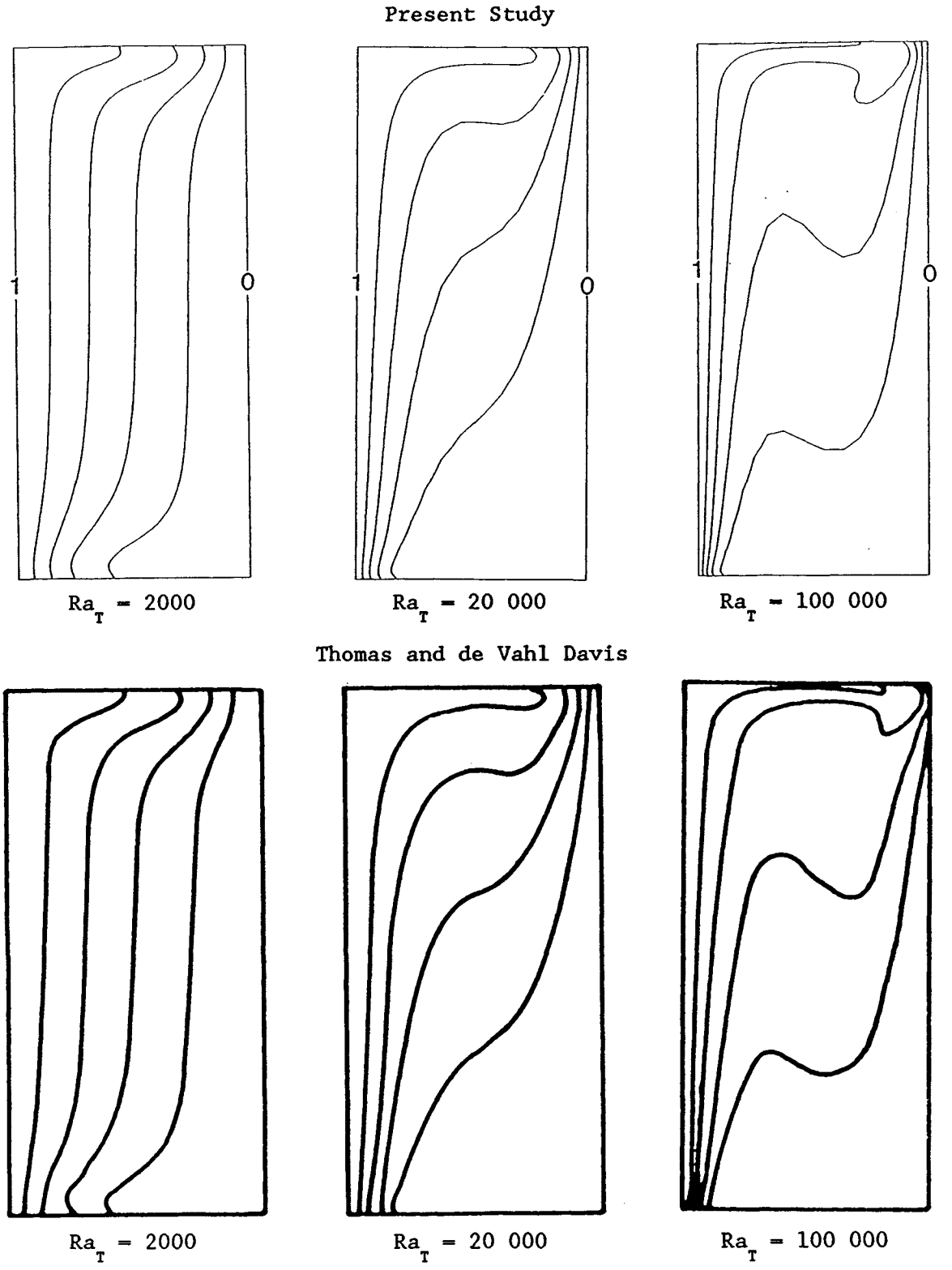

Figure 5.7 Thermal Distribution for Single-Diffusive Case (Ar = 10, K = 2, Pr = 1, n = 0) Note: Enclosure Heights are Compressed.

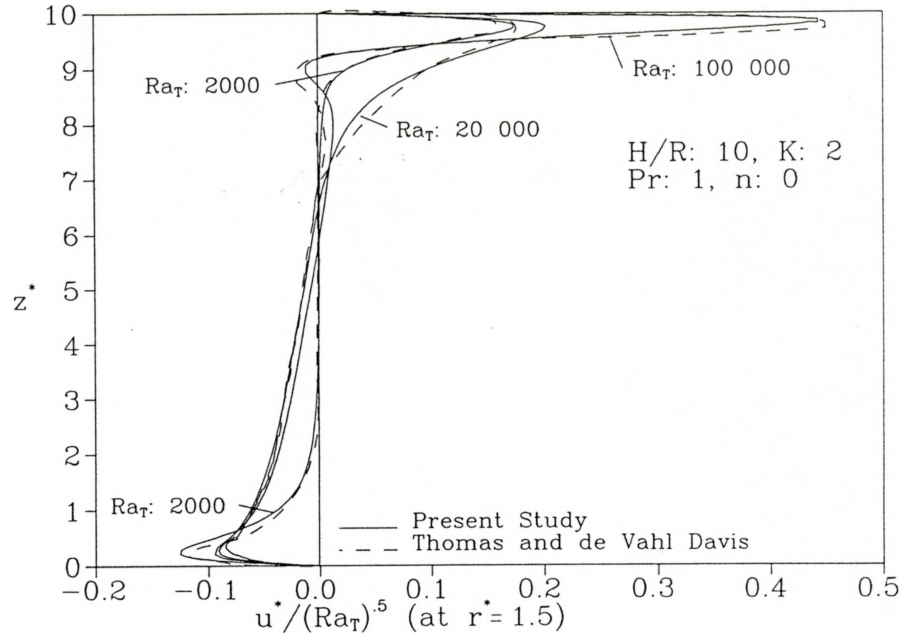

Figure 5.8 Comparison of Radial Velocities at $r^* = 1.5$

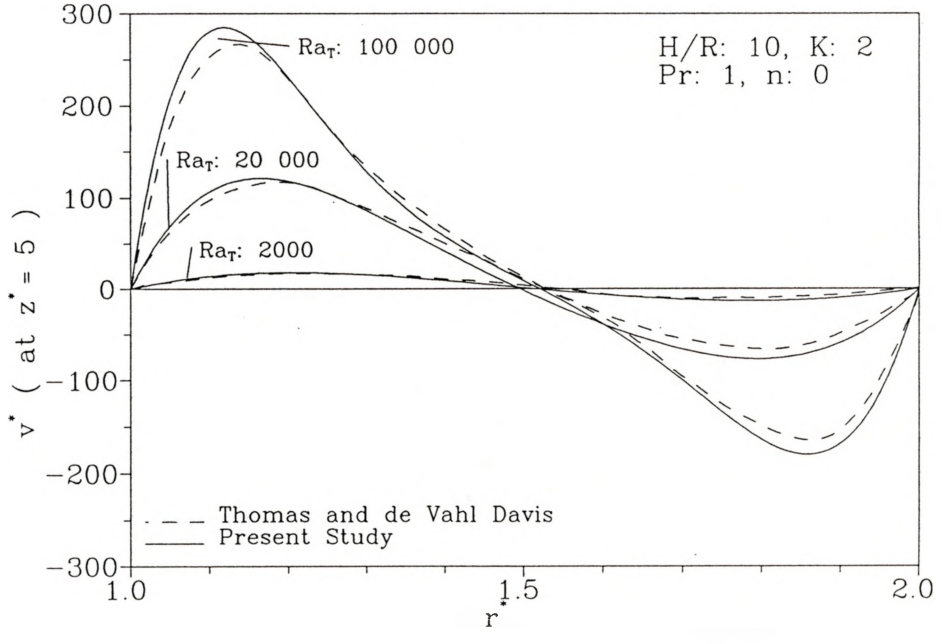

Figure 5.9 Comparison of Axial Velocities at $z^* = 5$.

excellent. Overall the agreement between the two studies is excellent, and differences due to the different solution techniques is minimal. Therefore as a result of the three comparisons the code can confidently be considered to be verified.

Table 5.3 Comparison of Overall Nusselt Numbers for Single-Diffusive Natural Convection in a Vertical Cylinder (Ar = 10, K= 2, n = 0, Pr = 1)

Ra_T	Present Study	Thomas & de Vahl Davis
2000	1.61	1.61
20 000	2.88	2.83
100 000	4.35	4.38

CHAPTER SIX

RESULTS AND DISCUSSION

6.1 Parameter Limitations

To examine the complete interdependence of all the parameters in this study would be such an enormous task that the examination of the effects of each parameter must be limited. Clearly, the top priority must be given to the parameters that have the most impact on convection. These parameters include the buoyancy ratio (n), the thermal Rayleigh number (Ra_T) and the Lewis number (Le). The other parameters also play a role in the convection, but for this study they have been limited. The fluid modeled is considered to be a water based solution such that the fluid Prandtl number is limited to 7. In fact, both Han [4, p.151] and Trevisan and Bejan [23] agree that the effect of the Prandtl number is minimal for values near and above unity. The final two parameters, the aspect ratio and the curvature ratio, are physical enclosure based parameters. For the present study these two parameters are limited to an enclosure with an aspect ratio of one and a curvature ratio of two. (Note: for the remainder of the text, Pr, Ar and K will remain constant at the values specified above.) Though the variation of these parameters are important, their effects on convection will have to be examined in a future study.

The range of the major parameters considered in the present study is $5000 \leq Ra_T \leq 100\ 000$, $1 \leq Le \leq 10$ and $-10 \leq n \leq 10$. For water based solutions the mass species diffusivity is usually less than the thermal diffusivity such that examination of the Lewis number below one is not required. The buoyancy ratios beyond the range specified do not need to be examined since the present extremes reflect strong mass species dominated buoyancy forces where the effect of the thermal induced buoyancy forces are minimal for the present Lewis number range. The range of the thermal Rayleigh number is determined by numerical code restrictions. Initially the thermal Rayleigh number has been varied from 1000 to 300 000. For thermal Rayleigh numbers less than 2000, no flow or stagnant conditions exist. For $Ra_T > 200\ 000$ the solution does not converge and there is a strong indication that the flow within the cavity may be periodic. This range agrees with the bifurcation studies of Moore *et al.* [39] for a two dimensional enclosure. For Ra_T between 100 000 and 200 000, convergence of the solution is possible but difficult to obtain without an excessive amount of iterations. As a result of these code restrictions the thermal Rayleigh numbers are limited to the range stated above.

To examine the effects of the three major parameters efficiently, a central case must necessarily be established in which the parameters can be varied singly. Furthermore, the effects of the variation of the Lewis number and thermal Rayleigh number should be examined under a comprehensive range of buoyancy ratios to fully establish their influence. Based on these two criteria, variations of the parameters are centered around the case of $Ra_T = 50\ 000$ and $Le = 5$,

where the results are examined for a range of buoyancy ratios ($-10 \leq n \leq 10$). The Lewis number or Ra_T is varied while the other parameter is held constant. If both these parameters are to be varied at the same time for a range of buoyancy ratios, the amount of data will be enormous and the presentation of the results for three independent variables will be difficult (for simultaneous presentation of the results, the plots would have to be four dimensional).

6.2 Effect of the Buoyancy Ratio on Convection

To establish the general effect of the buoyancy ratio on the hydrodynamic, temperature and concentration fields, the results are only presented for the central case (Ra_T = 50 000, Le = 5).

6.2.1 Streamfunction, Temperature and Concentration Profiles

One can examine the streamfunction, temperature and concentration profiles for the central case for $-10 \leq n \leq 10$ in figures 6.1 to 6.9. The left vertical wall represents the inner radius with a constant dimensionless temperature and concentration of one, while the right vertical wall represents the outer radial wall with a dimensionless temperature and concentration of zero. The isotherms and concentration contours have an increment of 0.1. The streamfunctions on the enclosure walls have an arbitrary value of zero, and the streamfunction values are indicated for each plot.

At n = -10 (fig. 6.1) the flow is clearly dominated by the mass species buoyancy force, indicative of the strong counter-clockwise flow. The hydrodynamic boundary layer on the radial walls is relatively thin, and the core section has a relatively low flow rate. The concentration contours are vertically stratified within the core and the concentration

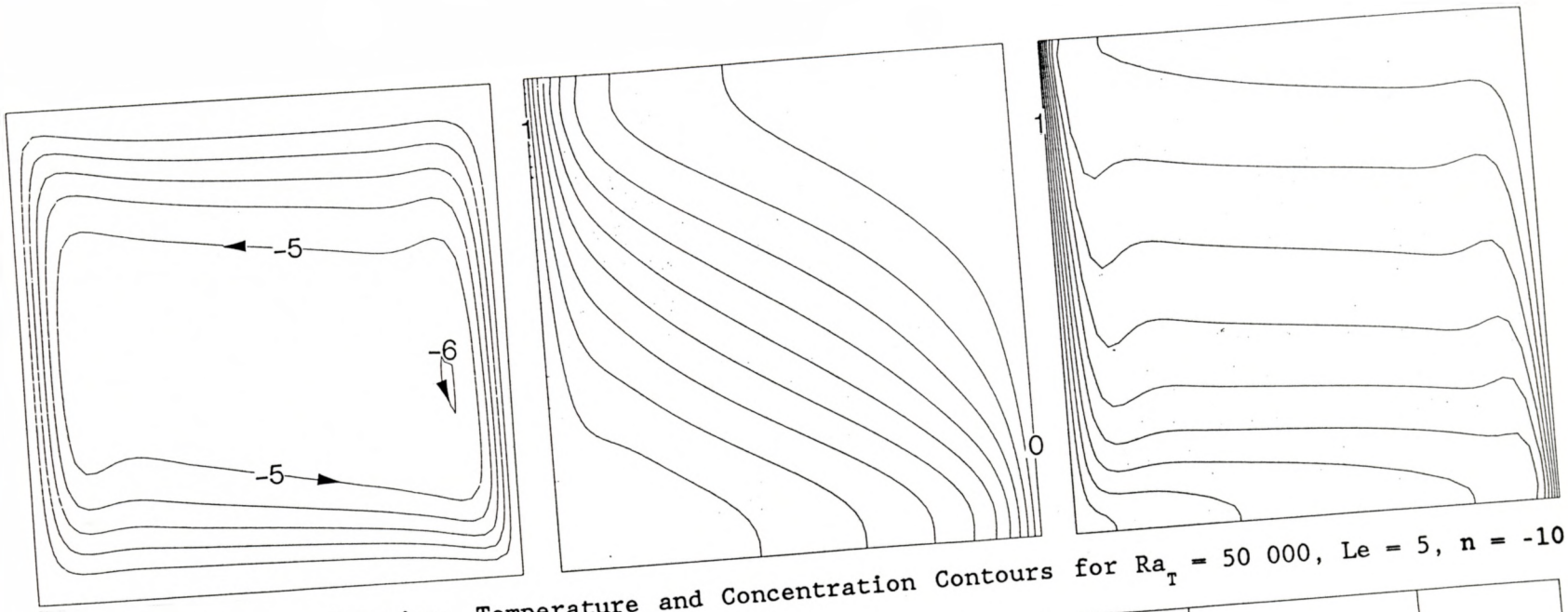

Figure 6.1 Streamfunction, Temperature and Concentration Contours for Ra_T = 50 000, Le = 5, n = -10

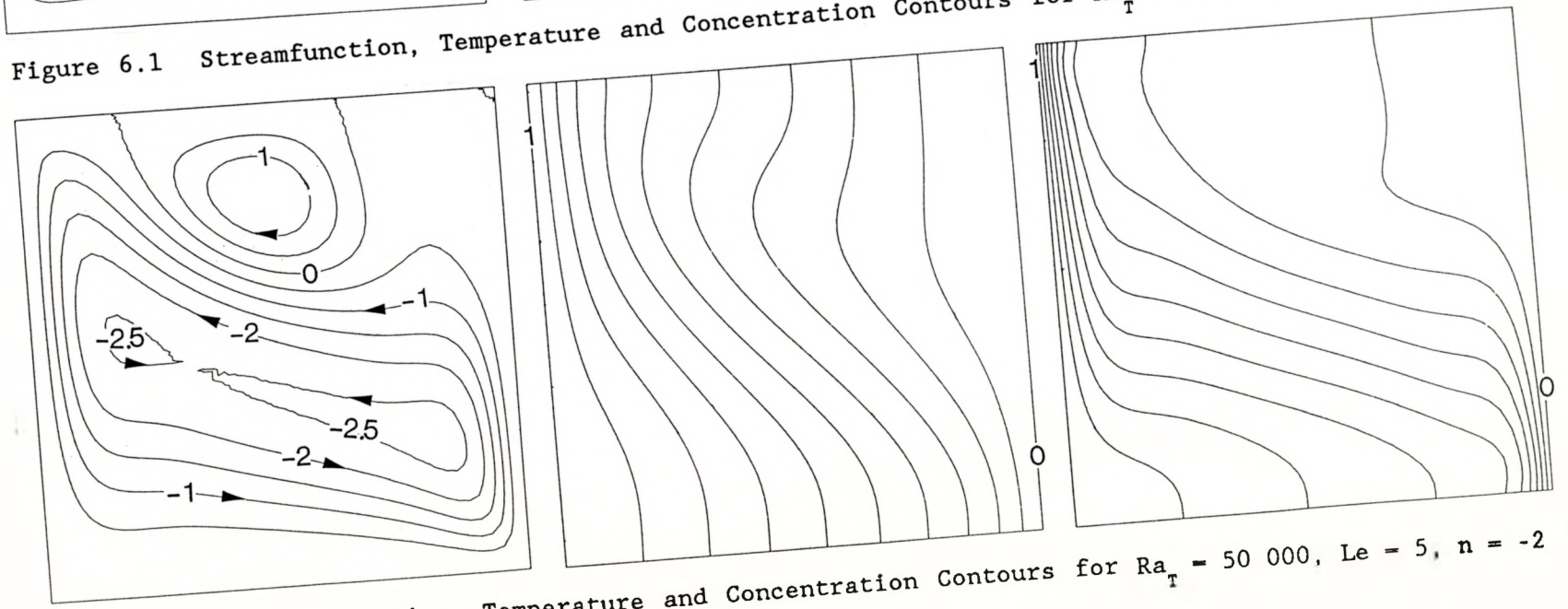

Figure 6.2 Streamfunction, Temperature and Concentration Contours for Ra_T = 50 000, Le = 5, n = -2

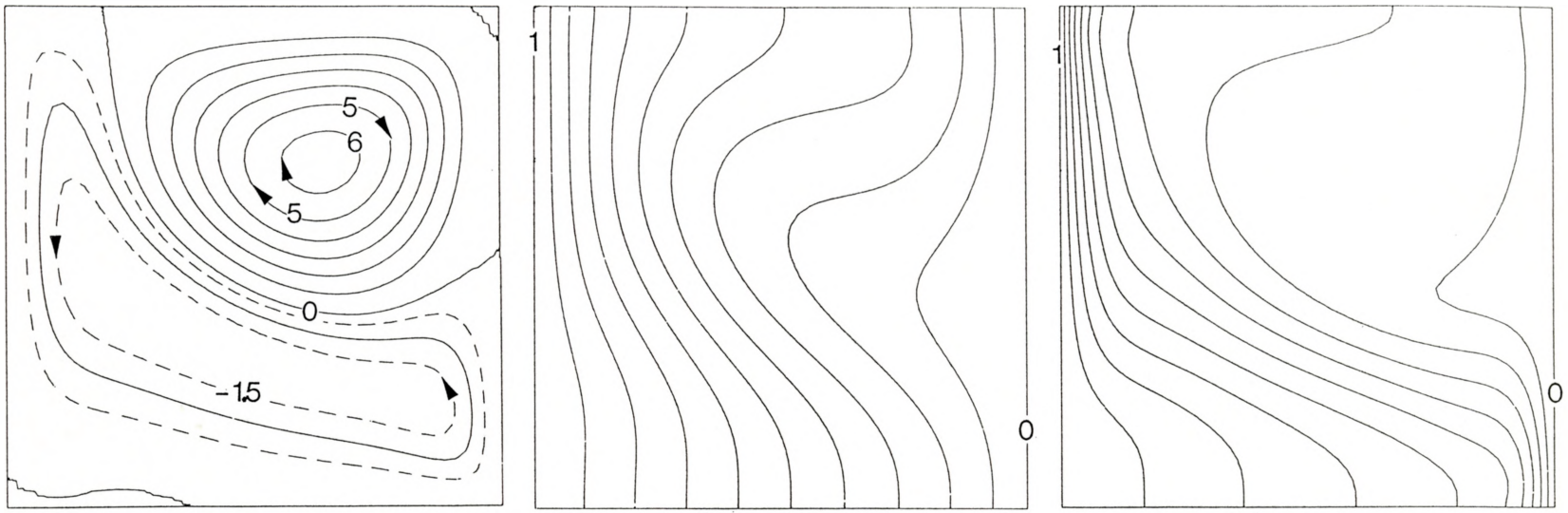

Figure 6.3 Streamfunction, Temperature and Concentration Contours for Ra_T = 50 000, Le = 5, n = -1.5

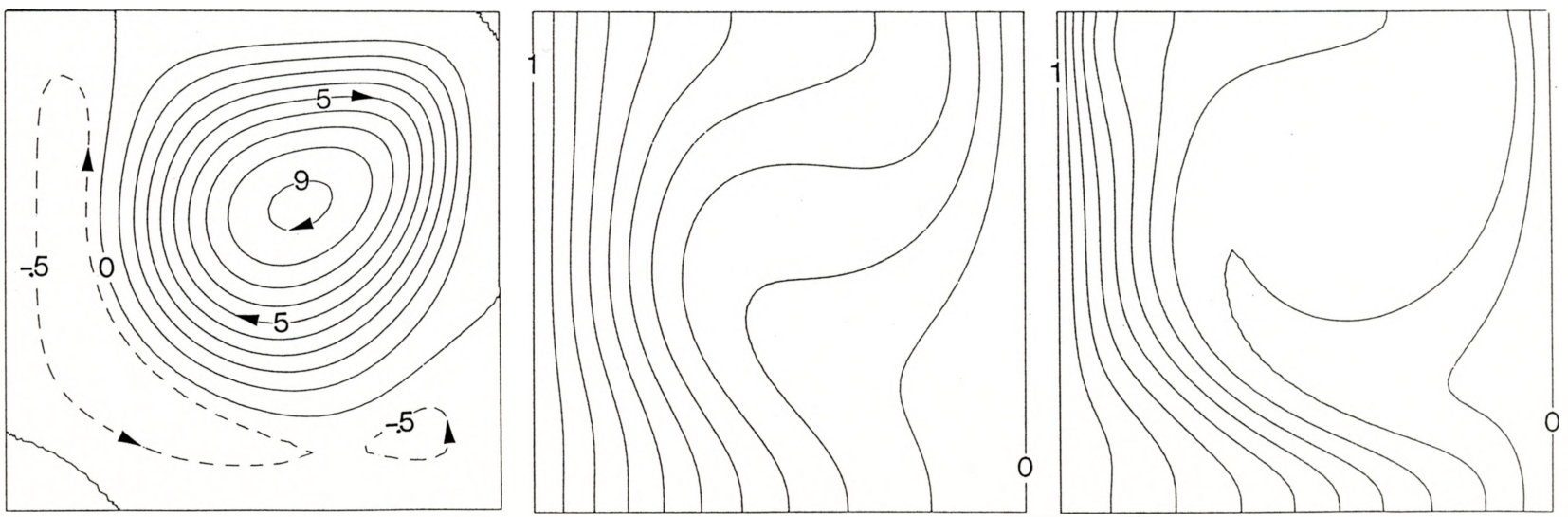

Figure 6.4 Streamfunction, Temperature and Concentration Contours for Ra_T = 50 000, Le = 5, n = -1.2 (transition from mass species to thermal dominated flow)

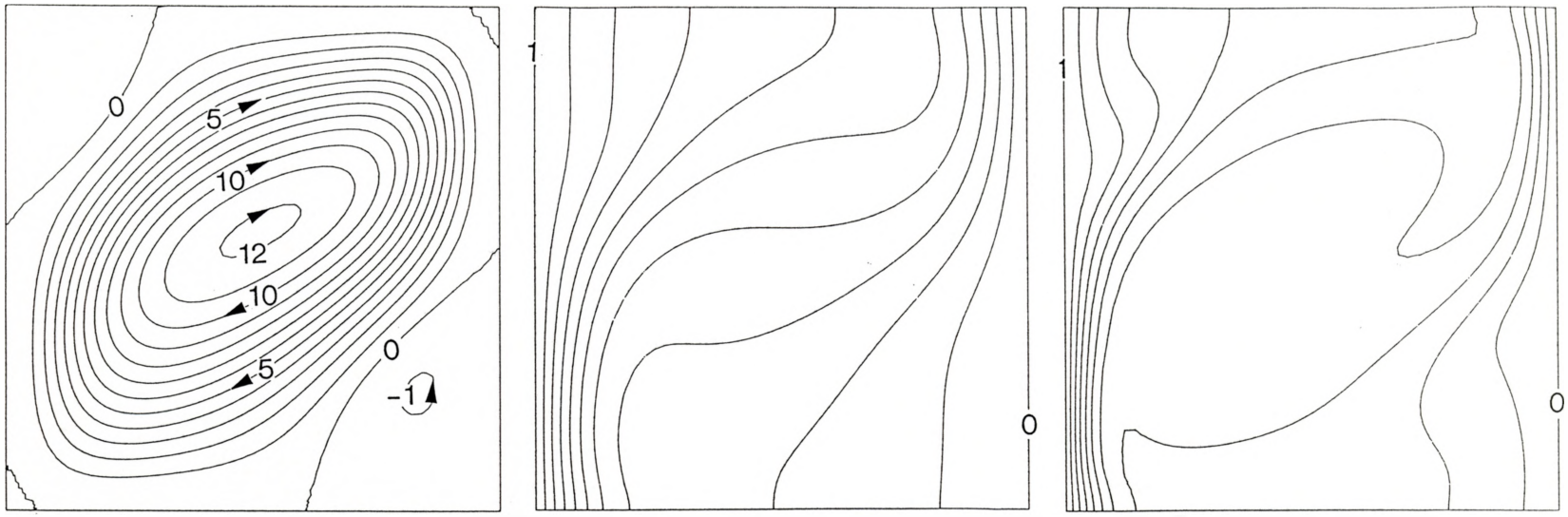

Figure 6.5 Streamfunction, Temperature and Concentration Contours for Ra_T = 50 000, Le = 5, n = -1.2 (thermal dominated flow)

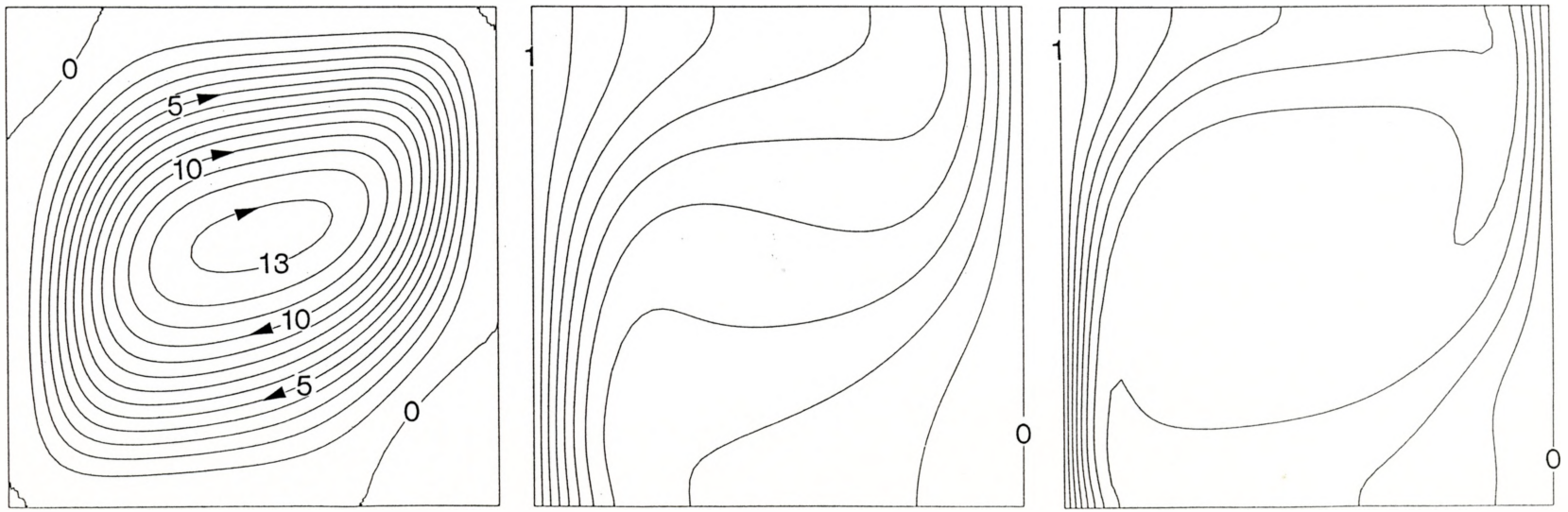

Figure 6.6 Streamfunction, Temperature and Concentration Contours for Ra_T = 50 000, Le = 5, n = -1

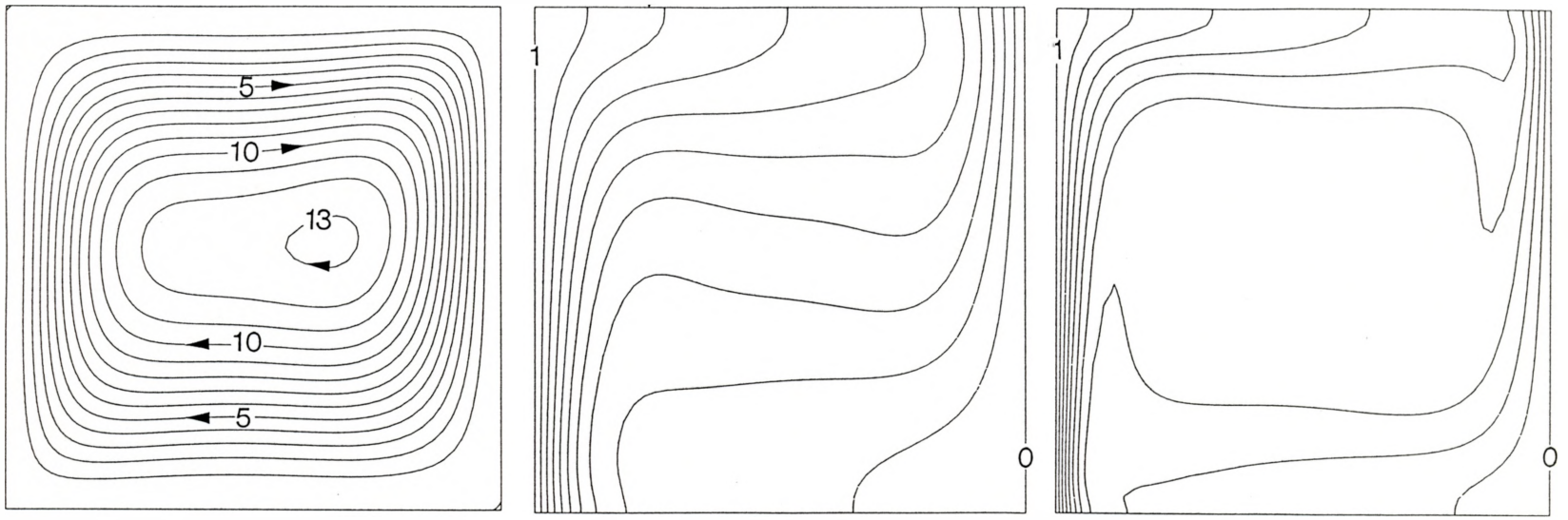

Figure 6.7 Streamfunction, Temperature and Concentration Contours for Ra_T = 50 000, Le = 5, n = 0

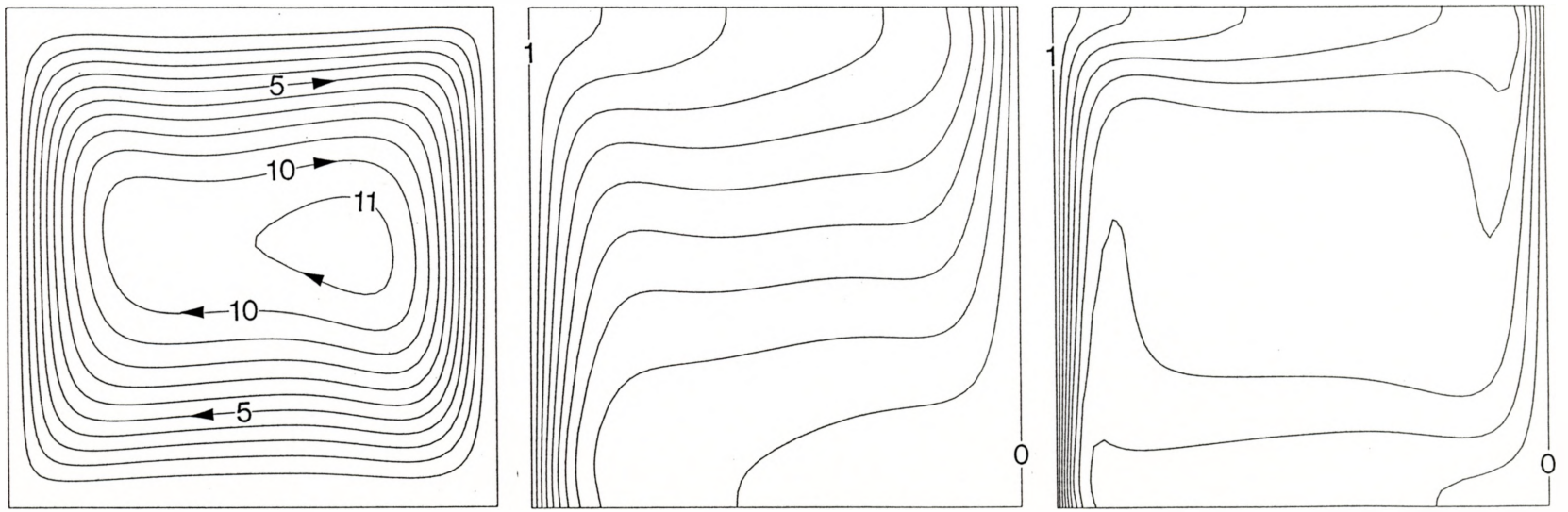

Figure 6.8 Streamfunction, Temperature and Concentration Contours for Ra_T = 50 000, Le = 5, n = 2

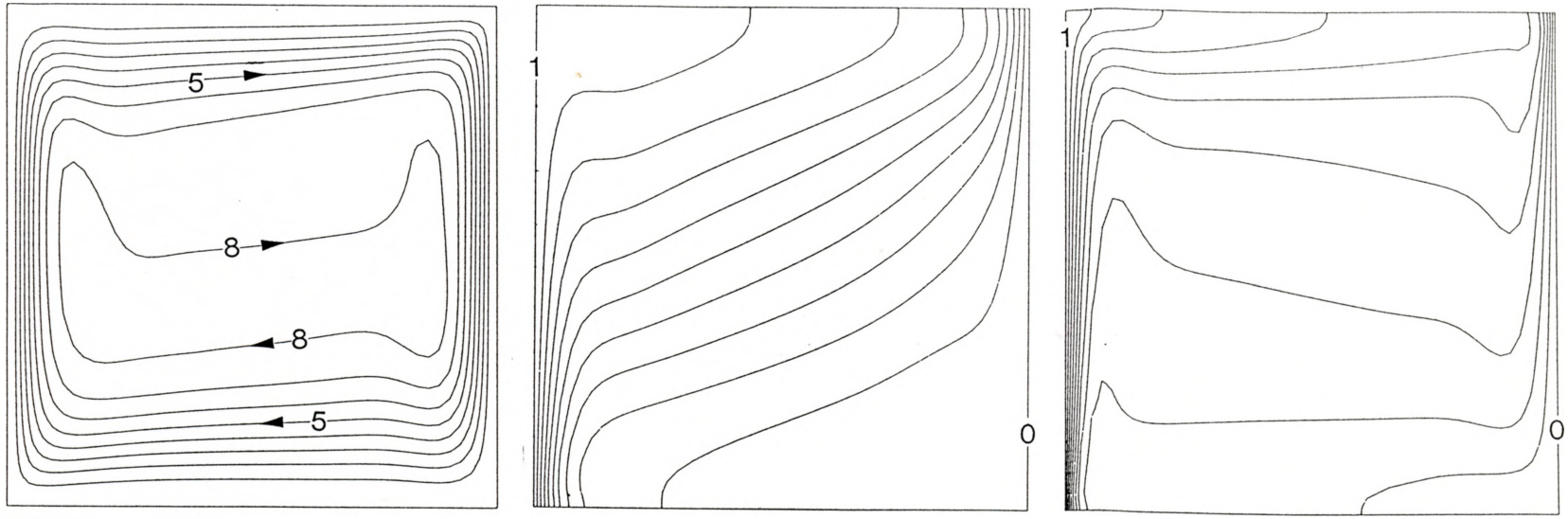

Figure 6.9 Streamfunction, Temperature and Concentration Contours for Ra_T = 50 000, Le = 5, n = 10

boundary layers are relatively thin. The steep concentration gradient at the top of the inner radius indicates a high mass transfer rate in this area. The isotherms are less affected by the flow than the concentration isopleths, as illustrated by a diagonal rather than a vertical distribution. This is due to the thermal diffusivity being five times the mass species diffusivity.

At n = -2 (fig. 6.2) the effect of the thermal buoyancy force is introduced by the clockwise vortex at the top centre of the enclosure. However, the opposing concentration buoyancy force still dominates the flow even though the hydrodynamic boundary layers are thicker and the flow is weaker. The isotherms are clearly becoming more vertical and the top centre distortion indicates a vorticity reversal. In the same area the concentration gradient is relatively low, while the lower isopleths are becoming more diagonal than stratified. The mass species boundary layers are thickening which is indicative of lower mass species transfer across the enclosure. This trend continues as n is increased to -1.5, as shown in figure 6.3.

As n is increased to -1.2 (fig. 6.4), the thermal buoyancy force is clearly dominating the flow with the opposing concentration buoyancy flow limited to the lower left of the annulus (dashed streamfunction). However, the flow along the majority of the inner wall and the lower half of the outer wall is still counterclockwise even though its intensity is much less than the thermal buoyancy dominated vortex. From the isotherms and mass species isopleths, it is clear that the mass species boundary conditions have little or no direct influence on the upper vortex by virtue of the fact that the temperature gradients in

this area are significantly higher than the concentration gradients. In the "L" shaped vortex region (dashed contour) the temperature and concentration gradients are within the same order, giving the concentration gradients the edge on the net buoyancy force due to the mass species dominated buoyancy ratio.

The flow structures shown from figures 6.2 to 6.4 are classified as *transitional* flow in which thermal and mass species buoyancy forces dominate separate circulations within the enclosure. The *onset* of transition is the buoyancy ratio at which flow separation occurs due to the intrusion of the thermal buoyancy force dominated vortex. Flows are considered transitional until a critical buoyancy ratio is reached at which the thermal dominated vortex completely spans the enclosure (see fig. 6.5). At this point the thermal dominated vortex dominates the majority of the enclosure.

If n is increased above -1.19, an interesting change occurs. The concentration governed "L" eddy vanishes and the thermal dominated clockwise vortex moves from the top centre to the centre of the core. At this point complete flow reversal has occurred where there is one major vortex extending from the outer top corner to the inner bottom corner. In the remaining two corners there are small eddies resulting from the bisection of the "L" eddy by the thermal governed vortex. When the buoyancy ratio is decreased, the flow field does not immediately revert to the previous solution for the same n (compare the two cases for n=-1.2, figures 6.4 and 6.5). Instead, the flow field tends to retain its characteristics until a lower critical buoyancy ratio is

reached. In this case, the thermal dominated vortex does not separate from the bottom inner corner until $n < -1.725$, letting the two minor eddies join into the "L" vortex.

At $n = -1$ (fig. 6.6) the effect of the temperature difference and concentration difference are evenly matched. If the thermal and mass species diffusivities are equal ($Le = 1$), a no flow situation would exist where the temperature and concentration distributions would emulate solid conduction and mass diffusion, respectively. However, since $Le = 5$ for this case, a clockwise thermal buoyancy force dominates the flow results. Examining the temperature and concentration distributions for this case, the mass species boundary layer at the inner and outer radial walls is thinner than the thermal boundary layers for the same regions. This leads to a much larger temperature gradient than concentration gradient within the annulus core resulting in a temperature dominating flow extending to the enclosure walls.

At $n = 0$ (fig. 6.7), the effect of concentration does not exist and the flow is completely governed by the imposed temperature difference. The corner eddies have completely disappeared, and the temperature profiles are stratified through the core region. When the buoyancy ratio is further increased above zero, the flow is considered to be aided with the mass species and thermal buoyancy forces acting in the same direction. Observing the hydrodynamic, temperature and concentration distributions for $n > 0$ ($n = 2$, fig. 6.8; $n = 10$, fig. 6.9), the streamfunctions indicate that the flow rate near the walls is increasing as well as the size on the stagnant fluid in the centre. The temperature and concentration boundary layers are thinning along the

vertical walls which further indicates an increasing wall velocity. For n = 10 (fig. 6.9), the core region has become stagnant due to stabilizing effect of the combined vertical temperature and concentration gradients in this area.

6.2.2 Velocity Distributions

The flow direction can be examined for the centreline ($z^* = 0.5$) vertical velocity distribution as shown in figure 6.10. For high mass species dominated flows in both aiding and opposing modes, the hydrodynamic boundary layer near the inner wall appears to be relatively thin with the flow confined to this region and the core remaining stagnant. For thermal dominated flows and transition flows, there tends to be an increased amount of flow within the core area, including a thicker boundary layer. The difference between thermal dominated flow and transitional flow (thermal to mass species dominated) for opposing buoyancy conditions is clearly marked with positive to negative velocity gradients at the inner wall. For n = -1.2 (transitional flow) the two buoyancy effects are distinguished by the mass species dominated downward flow near the inner wall, while the core region is still dominated by the thermal buoyancy force as demonstrated by the positive vertical flow on the warmer side of the centre core.

6.2.3 Horizontal Temperature and Concentration Profiles

Temperature and concentration distributions along the horizontal centreline may be examined in figs. 6.11 and 6.12. Generally, the mass species boundary layers are thinner than the thermal boundary layers due to the lower mass species diffusivity. For high mass species dominated flows (n = 10, -10), the temperature distribution is almost similar to

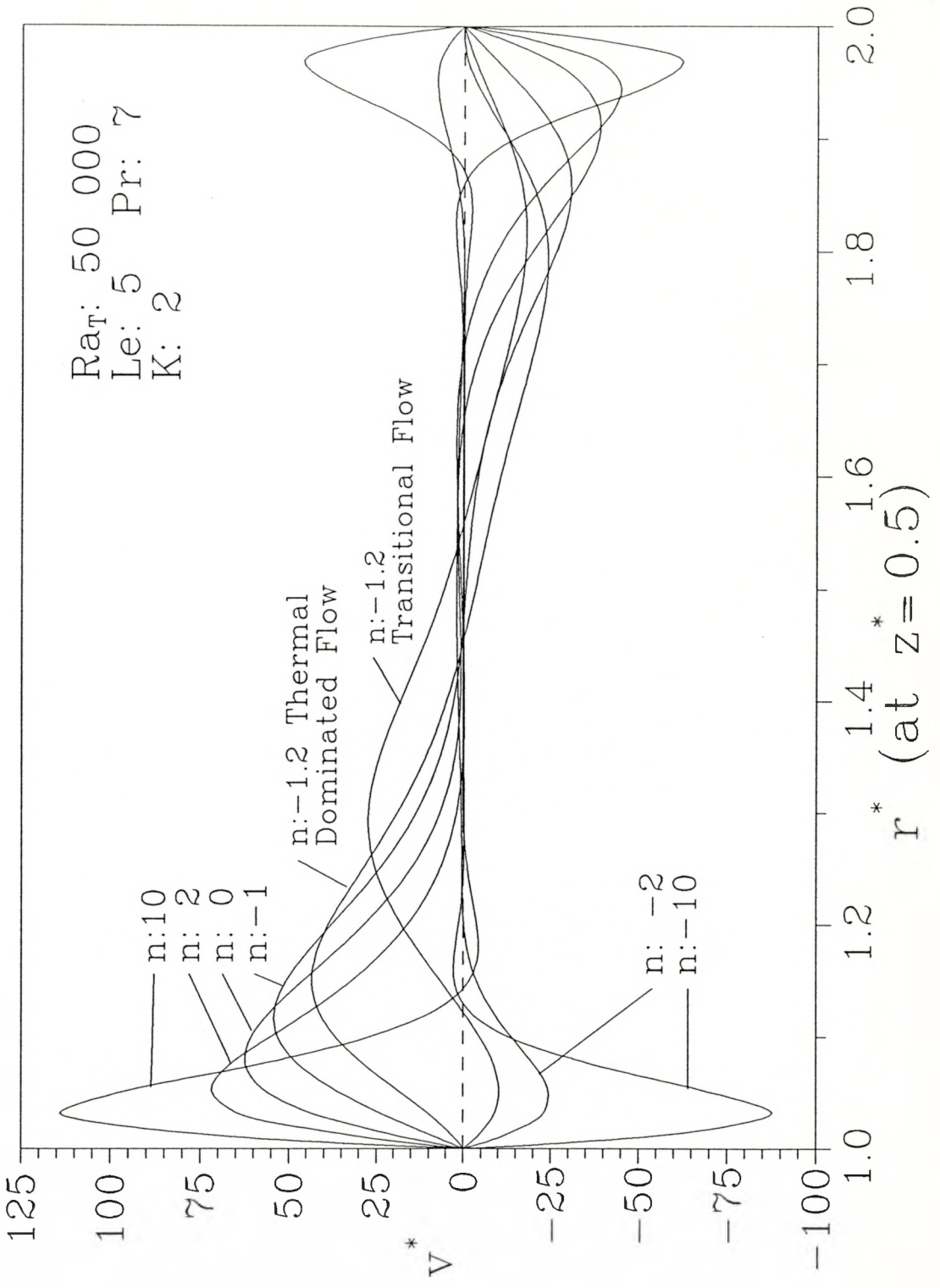

Figure 6.10 Vertical Velocity Distribution along the Horizontal Centreline

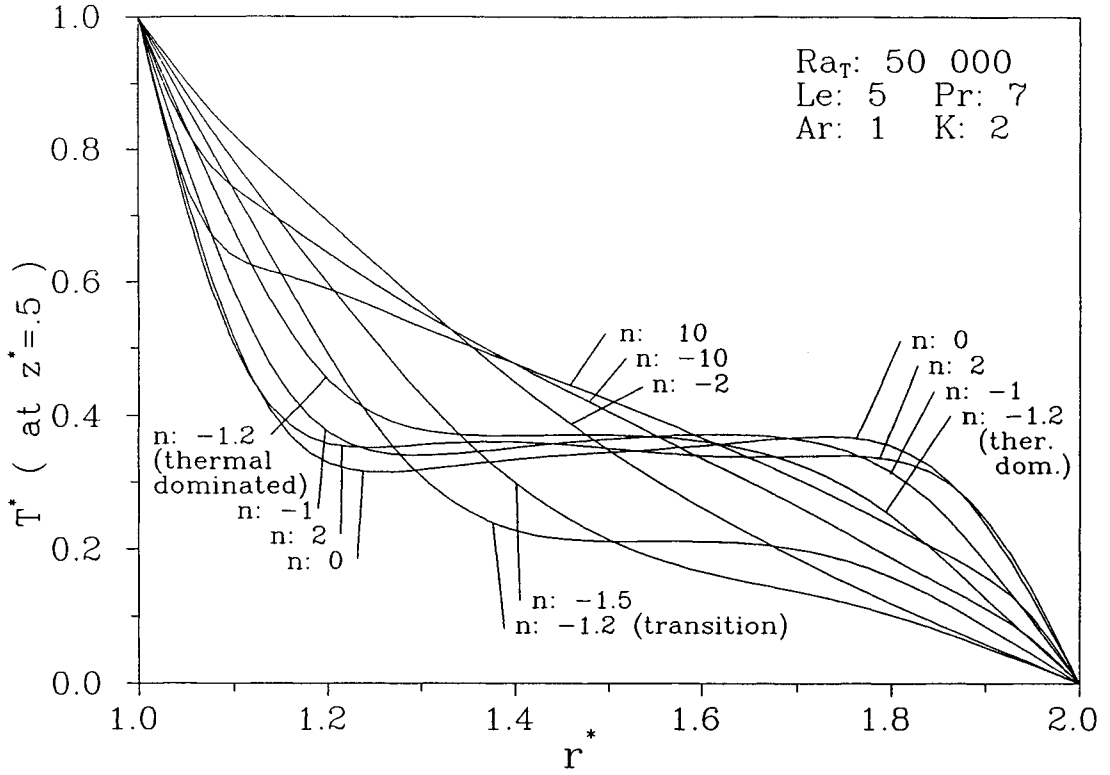

Figure 6.11 Temperature Distributions along the Horizontal Centreline

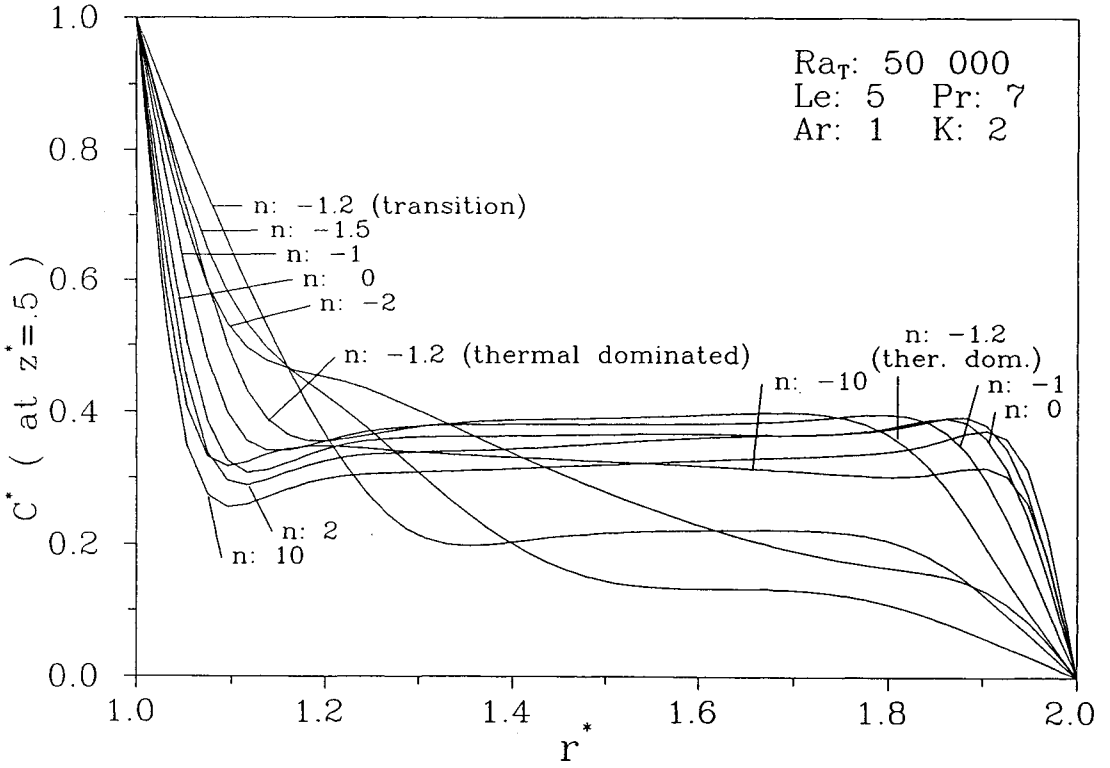

Figure 6.12 Concentration Distributions along the Horizontal Centreline

that of a pure conduction regime. This is due to the relatively stagnant core for this type of flow. For single major vortex regimes where the core is not stagnant (n = 2, 0, -1 and -1.2 (thermal dominated)), the horizontal centreline temperature seems to remain constant within the core region. The same can be said for the concentration distributions for the same buoyancy ratios as well as for the strong mass species dominated flows. The latter is due to the weaker mass species diffusivity in which the mass species gradients can not penetrate the stagnant core as far as thermal gradients.

6.3 Effect of the Thermal Rayleigh Number on Convection

The effect of Ra_T on convection is only demonstrated for a few specific buoyancy ratios to obtain a concise understanding of the relationship. In this case the thermal Rayleigh number is varied from 5000 to 100 000 with a range of buoyancy ratios specified at n = -2, -1.2, -1 and 2, which reflect conditions at mass species dominated opposing, transitional, unity buoyancy ratio, and mass species dominated aiding flows respectively. The Lewis number is held constant at 5.

The effect on convection for a buoyancy ratio of -2 can be examined in figures 6.13 to 6.16. At a low thermal Rayleigh number of 5000 (fig. 6.13), the flow regime is completely dominated by the mass species buoyancy force. However, as the thermal Rayleigh number is increased, the thermal buoyancy force increases its influence on the convection. At this point it should be restated that the counterpart mass species Rayleigh number is increased at the same rate as Ra_T since the buoyancy ratio remains constant. At Ra_T = 20 000, separation occurs at the top of the enclosure. For higher thermal Rayleigh numbers this

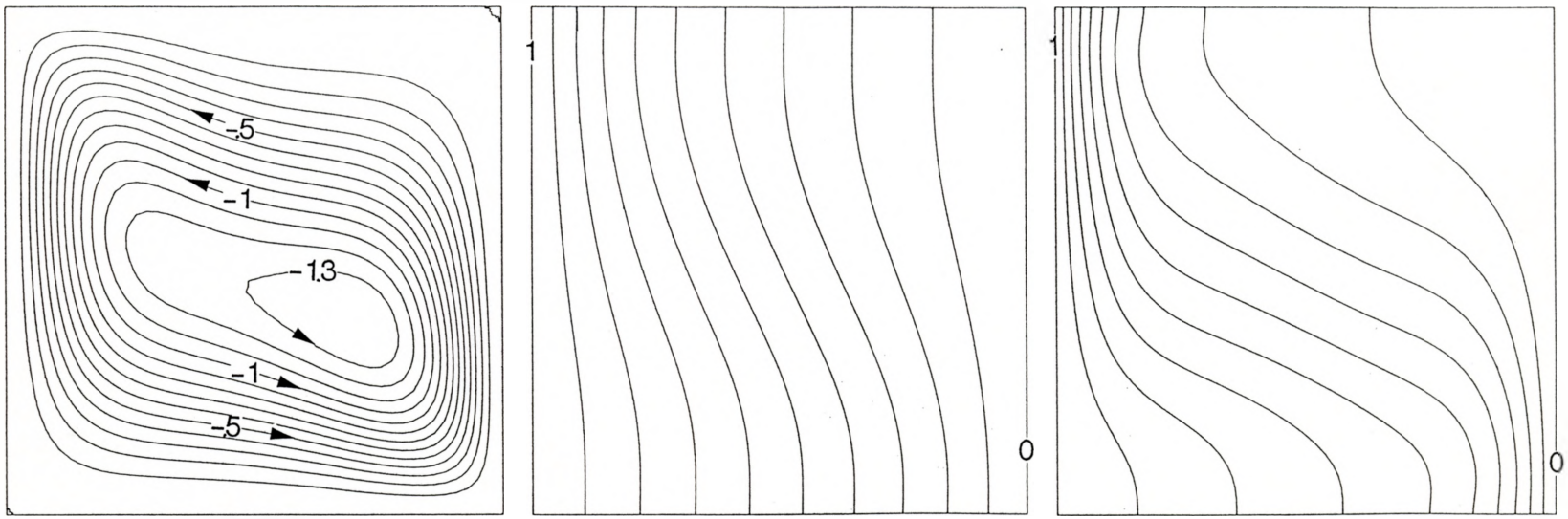

Figure 6.13 Streamfunction, Temperature and Concentration Contours for Ra_T = 5000, Le = 5, n = -2

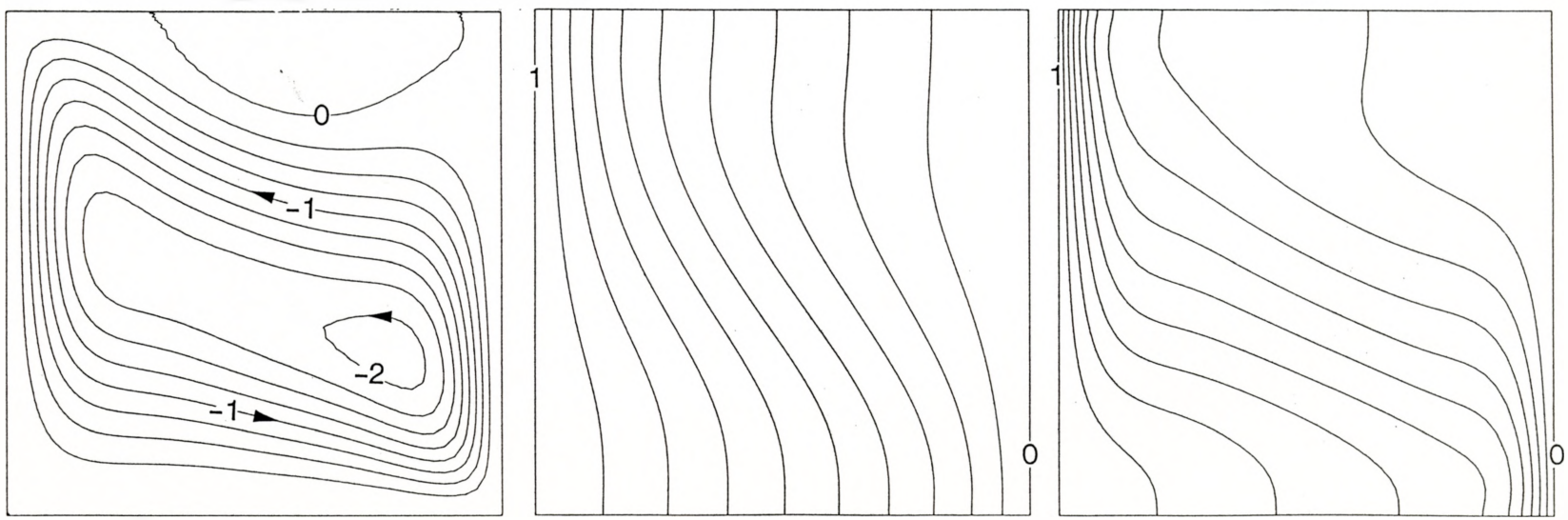

Figure 6.14 Streamfunction, Temperature and Concentration Contours for Ra_T = 20 000, Le = 5, n = -2

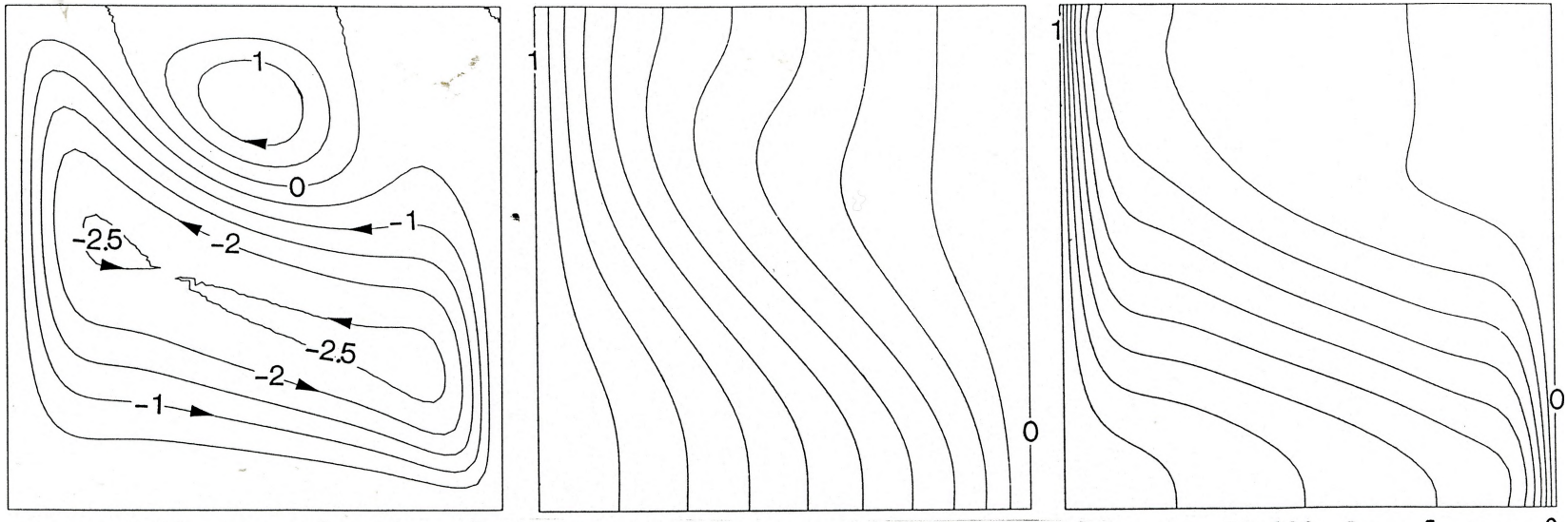

Figure 6.15 Streamfunction, Temperature and Concentration Contours for Ra_T = 50 000, Le = 5, n = -2

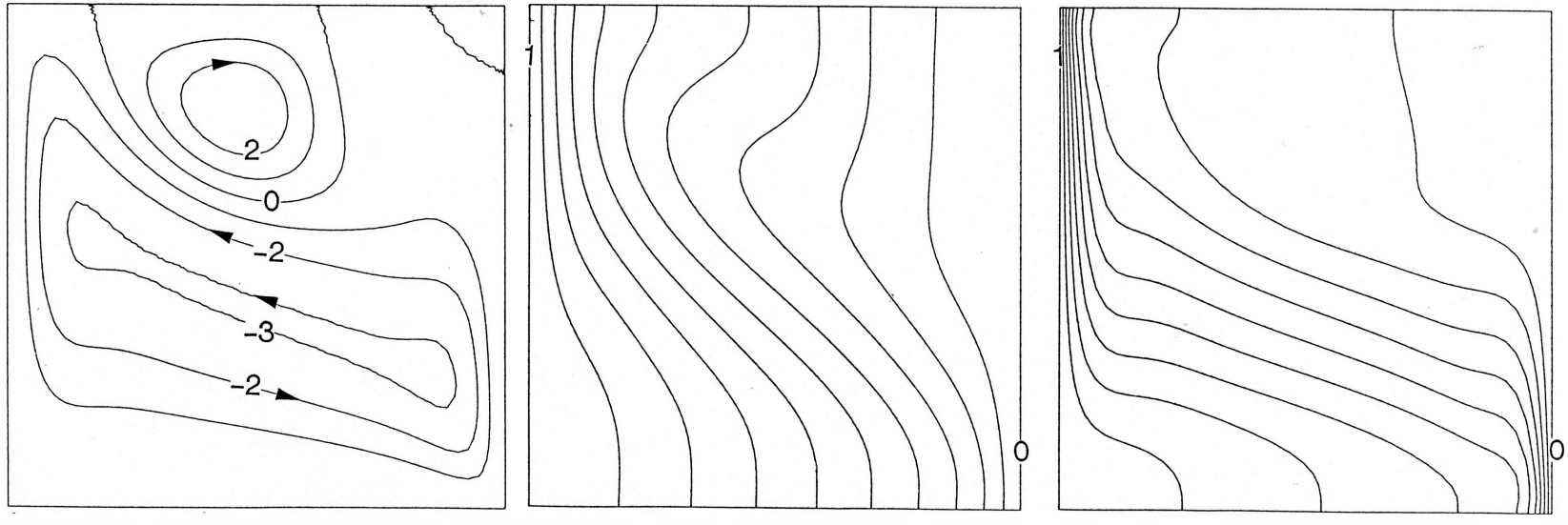

Figure 6.16 Streamfunction, Temperature and Concentration Contours for Ra_T = 100 000, Le = 5, n = -2

region of flow reversal intrudes further into the cavity displacing the mass species dominated circulation (figures 6.15 and 6.16). Thus it seems that for n = -2 (previously thought be a mass species buoyancy force dominated flow for all Ra_T) the flow will only be dominated by a mass species buoyancy force for low Ra_T ($Ra_T \leq 20\ 000$). After this point transitional flow occurs and hypothetically for high thermal Rayleigh numbers the flow will be dominated by the thermal buoyancy force. However the present study does not reveal at what point this complete reversal occurs.

The effect of varying the thermal Rayleigh number is further demonstrated on a transitional flow regime (n = -1.2) in figures 6.17 to 6.20. At a low thermal Rayleigh number ($Ra_T = 5000$, fig. 6.17) the majority of the flow is dominated by the mass species buoyancy force apart from the top outer corner of the enclosure where a small thermal eddy exists. Increasing Ra_T to 20 000 results in a substantial increase in size and intensity of this eddy. On examination of figure 6.18 this thermally dominated buoyancy force eddy now occupies approximately half the centre core to the upper outer wall whereas the original flow circulation has been reduced and displaced to a low intensity "L" shaped eddy to the lower left of the enclosure. Further increases in the thermal Rayleigh results in the eventual disappearance of the mass species dominated "L" eddy (figures 6.19 and 6.20). At $Ra_T = 100\ 000$ this eddy is bisected by the more dominant flow circulation resulting in two small eddies in the top left and bottom right corners of the enclosure. For this buoyancy ratio there is more variation in the temperature and concentration contours than in the previous case.

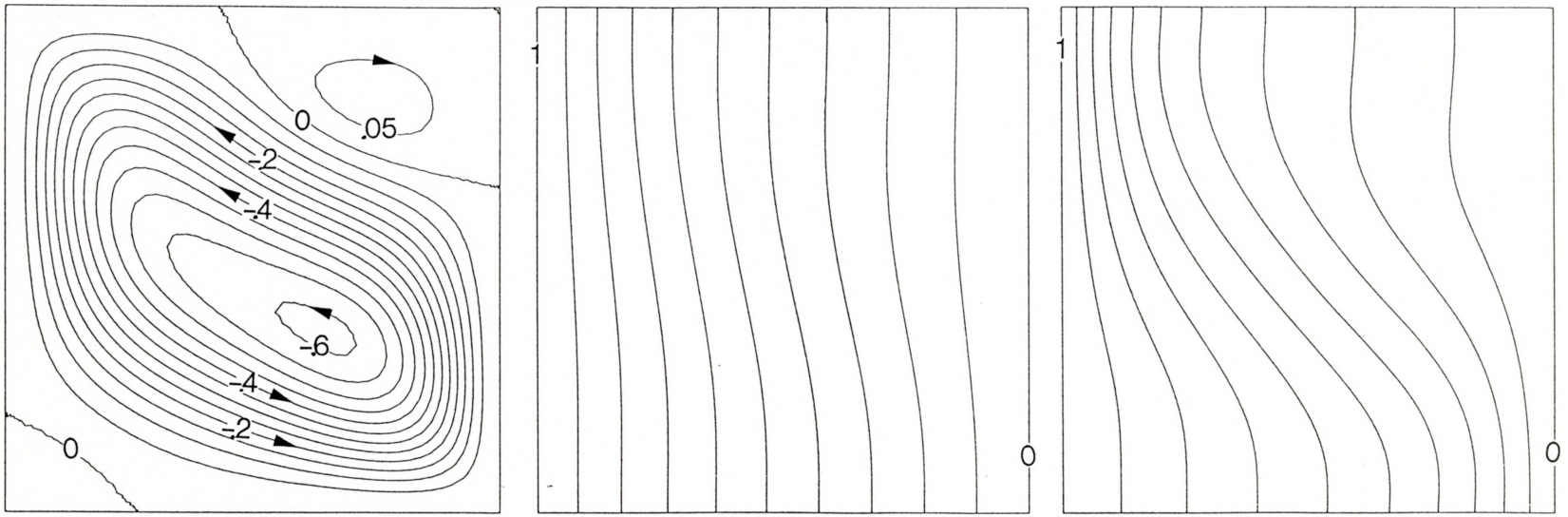

Figure 6.17 Streamfunction, Temperature and Concentration Contours for Ra_T = 5000, Le = 5, n = -1.2

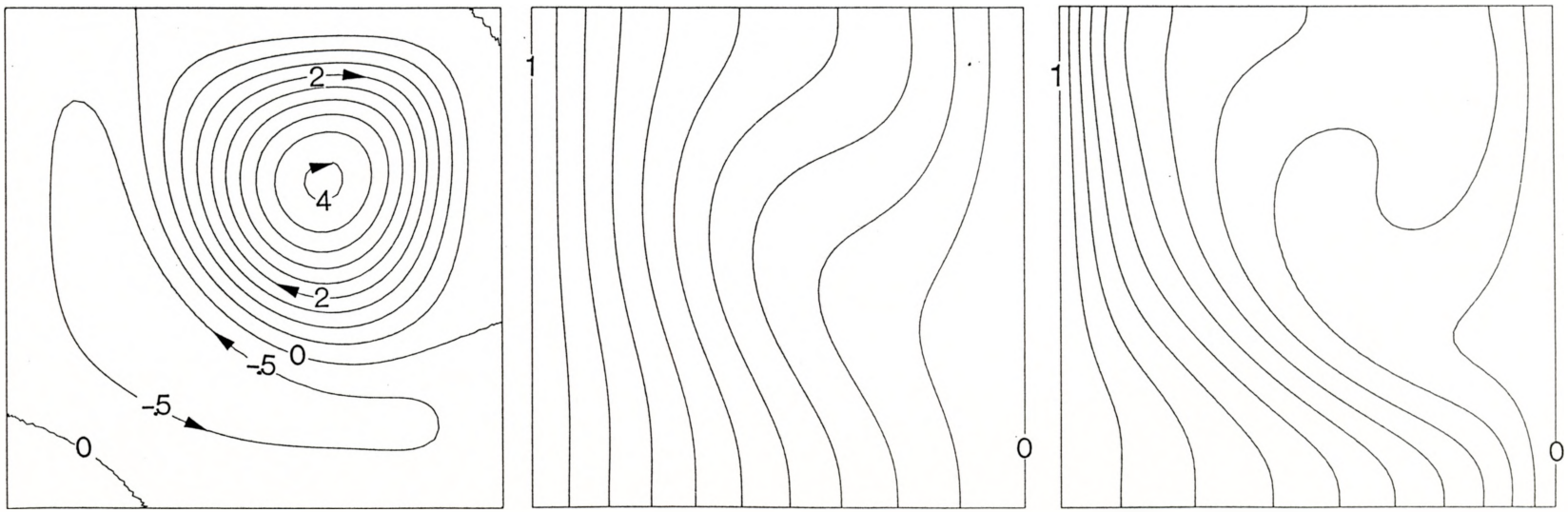

Figure 6.18 Streamfunction, Temperature and Concentration Contours for Ra_T = 20 000, Le = 5, n = -1.2

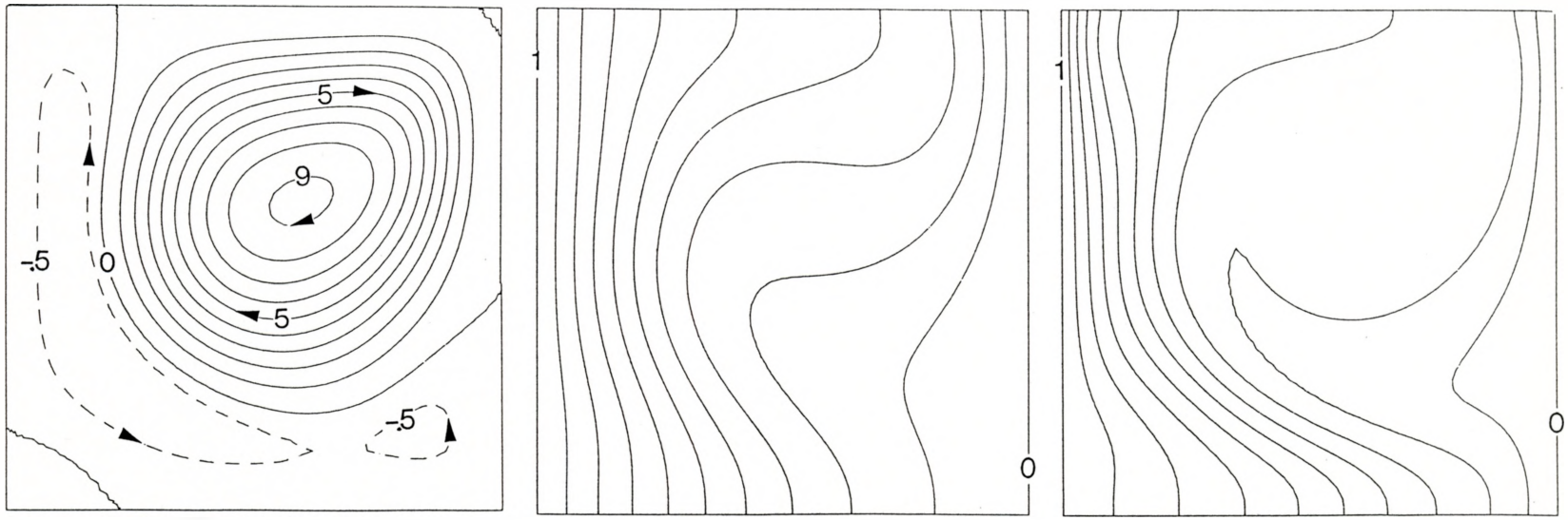

Figure 6.19 Streamfunction, Temperature and Concentration Contours for Ra_T = 50 000, Le = 5, n = -1.2

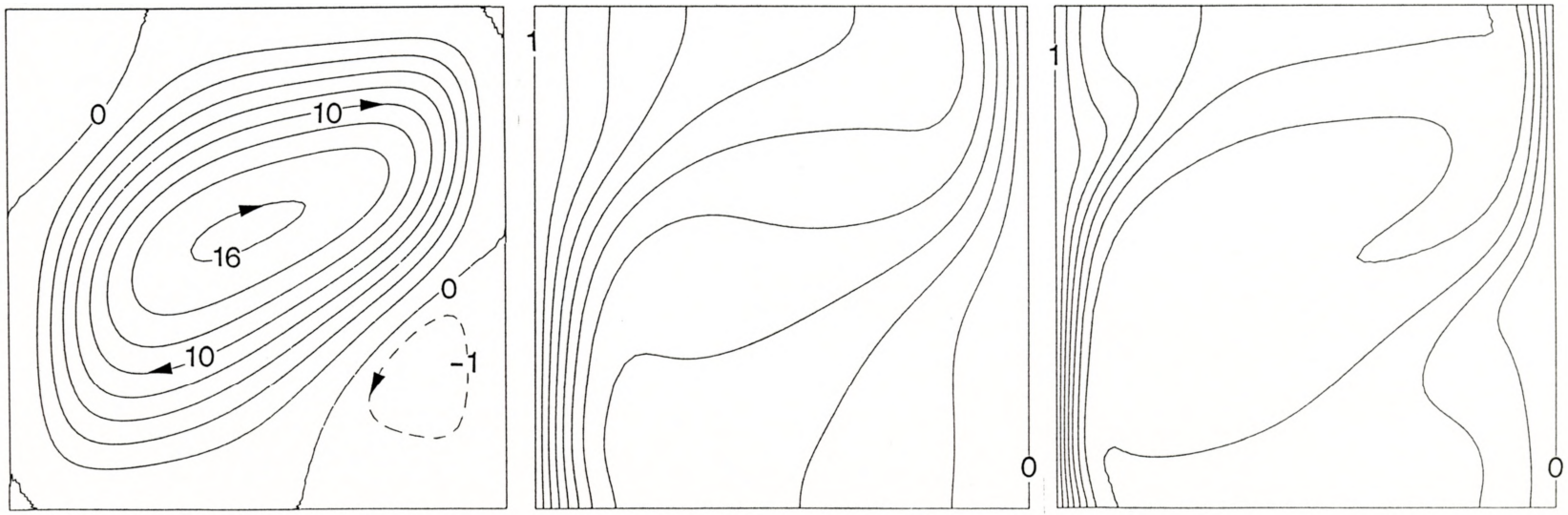

Figure 6.20 Streamfunction, Temperature and Concentration Contours for Ra_T = 100 000, Le = 5, n = -1.2

At a low Ra_T the temperature and concentration contours tend to be distributed horizontally, as Ra_T is increased a distortion is present in both profiles at the location of the stronger thermal dominated vortex. This is more notable in the concentration contours. As the thermal Rayleigh number is increased into the higher values (specifically Ra_T = 100 000, figure 6.20) the distortions result in an almost vertical thermal stratification, while the concentration in the centre on the vortex remains constant. From the observations of this case (n = -1.2) an increase in the thermal Rayleigh number tends to cause transition from a mass species dominated buoyancy flow to a thermal dominated buoyancy flow which further supports the observations for the case of n = -2.

Evaluating the effect of Ra_T at the buoyancy ratio of negative unity is important due to the significance of this value. Figures 6.21 to 6.24 demonstrate the effect of the increase in Ra_T on the flow profiles. At a low Ra_T of 5000 (fig. 6.21) the thermal dominated vortex is somewhat circular in shape. An increase in Ra_T results an expected increase in intensity of motion while the shape of the circulation becomes more box like with the exception of eddies in the top left and bottom right corners. On a point of interest these eddies are not reduced when Ra_T is increased, in fact the opposite is true. From the present observations, it is not known if these corner eddies are a result of shear or a double diffusive characteristic. It is further interesting to note that eddies are not formed in the upper right and low left corners for high Ra_T. This observation will further be discussed for an aiding flow buoyancy ratio. Examination of the

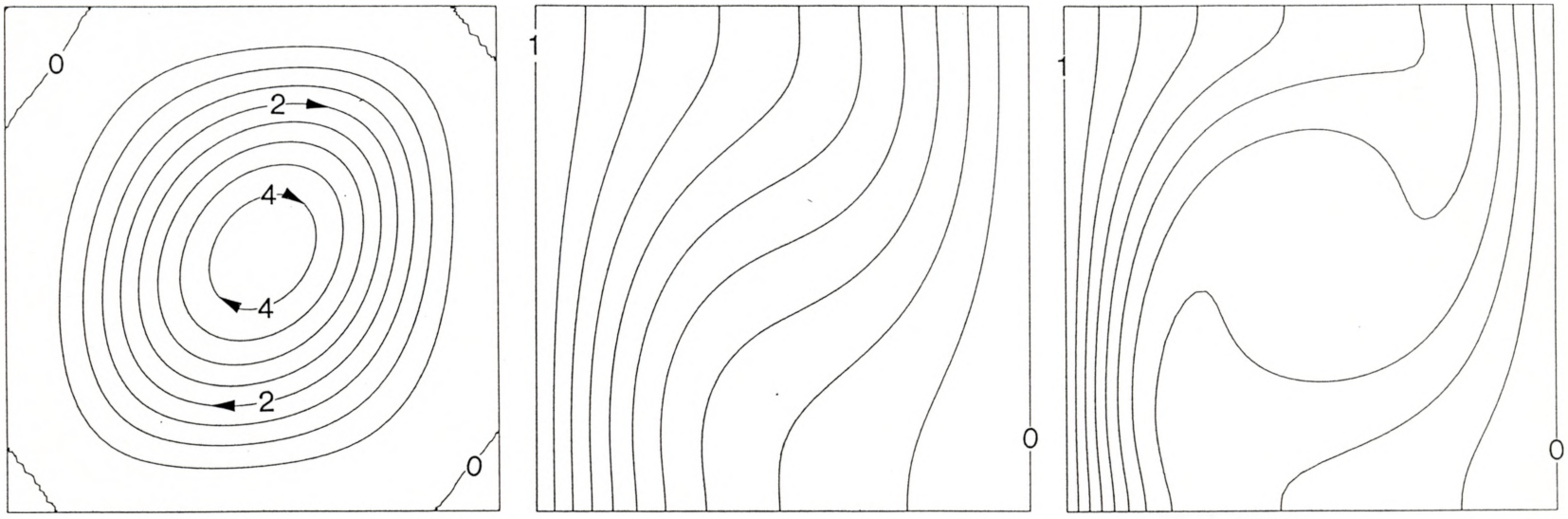

Figure 6.21 Streamfunction, Temperature and Concentration Contours for Ra_T = 5000, Le = 5, n = -1

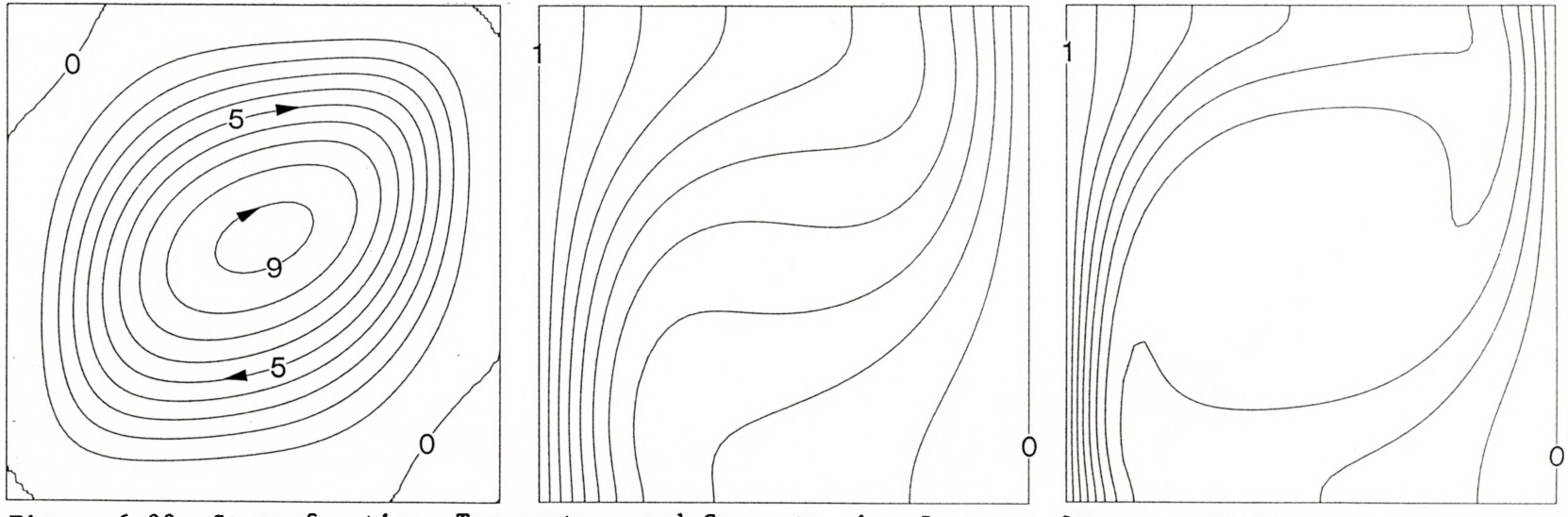

Figure 6.22 Streamfunction, Temperature and Concentration Contours for Ra_T = 20 000, Le = 5, n = -1

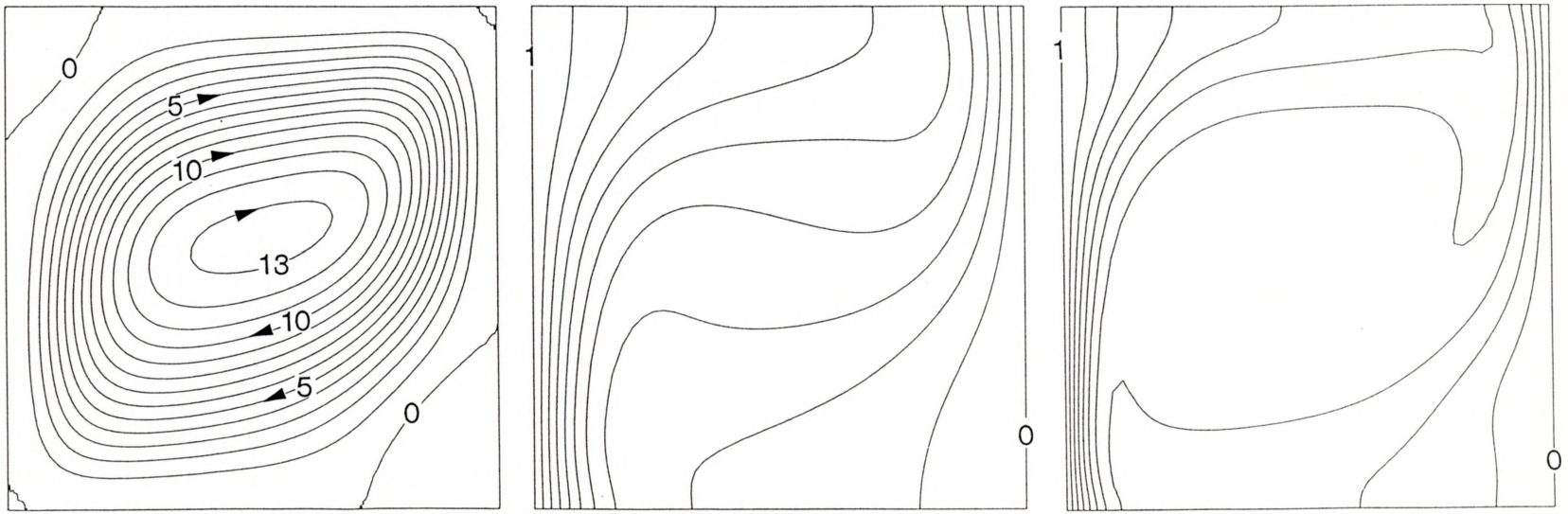

Figure 6.23 Streamfunction, Temperature and Concentration Contours for Ra_T = 50 000, Le = 5, n = -1

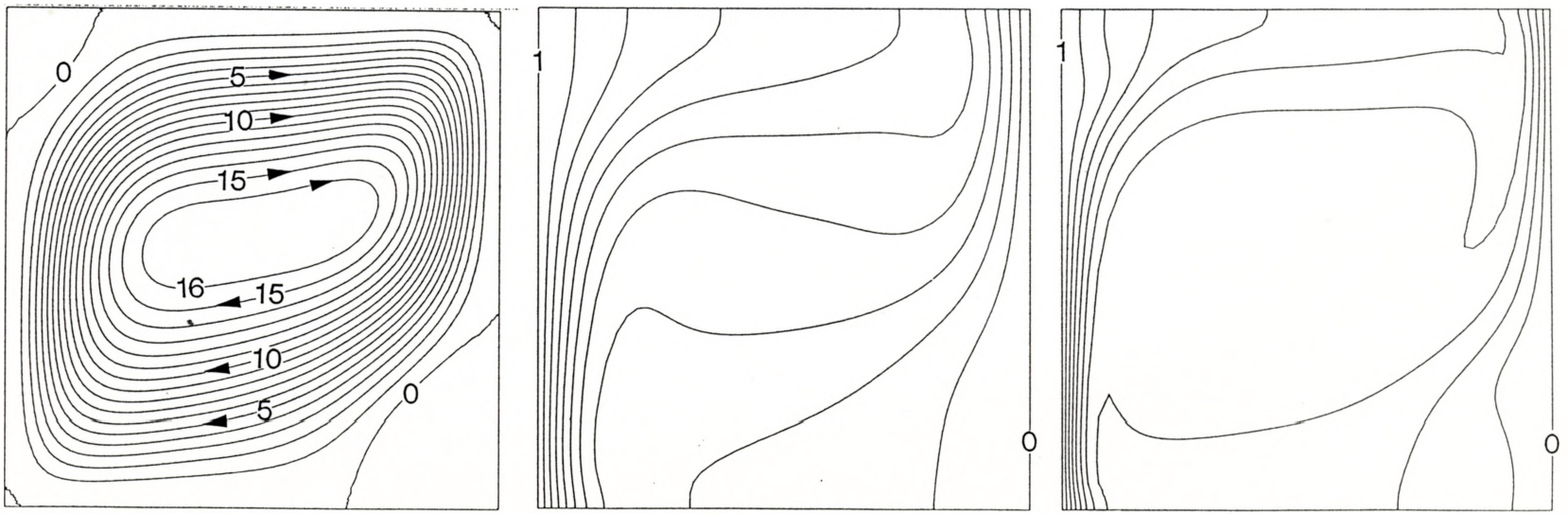

Figure 6.24 Streamfunction, Temperature and Concentration Contours for Ra_T = 100 000, Le = 5, n = -1

temperature and concentration contours for this case reveals that an increase in Ra_T will result in the thinning of the thermal and mass species boundary layers. Consequently a "blob" of uniform temperature and concentration will establish itself in the centre core of the enclosure. This is more noticeable for the concentration contours where the constant concentration "blob" is developing at Ra_T = 5000 (fig. 6.21), however on close examination of the temperature contours for Ra_T = 100 000 (fig. 6.24) the thickening vertical contours at the centre core indicate that a constant temperature "blob" is developing.

Finally, the effect of the thermal Rayleigh number should examined for an aiding buoyancy force case. Figures 6.25 to 6.28 demonstrate this effect for a buoyancy ratio of 2. For low Ra_T the streamfunctions (fig. 6.25, Ra_T = 5000) indicate that the flow is uniformly distributed almost to the centre of the core. However for high Ra_T (fig. 6.28, Ra_T = 100 000) the majority of the flow tends to be in close proximity to the enclosure walls with the core area becoming stagnant. The temperature and concentration contours seem to follow similar relationships with increasing Ra_T as discussed in the previous case (n = -1) with a developing vertical stratified temperature distribution and the growth of a constant concentration "blob" within the core of the enclosure.

Following up on what has been discussed in the previous paragraph, it is interesting to note that no corner eddies have been formed for the case of aiding flow. This leads us to believe that corner eddies are a double-diffusive characteristic and are not caused by shear, otherwise they would have appeared for this case since the

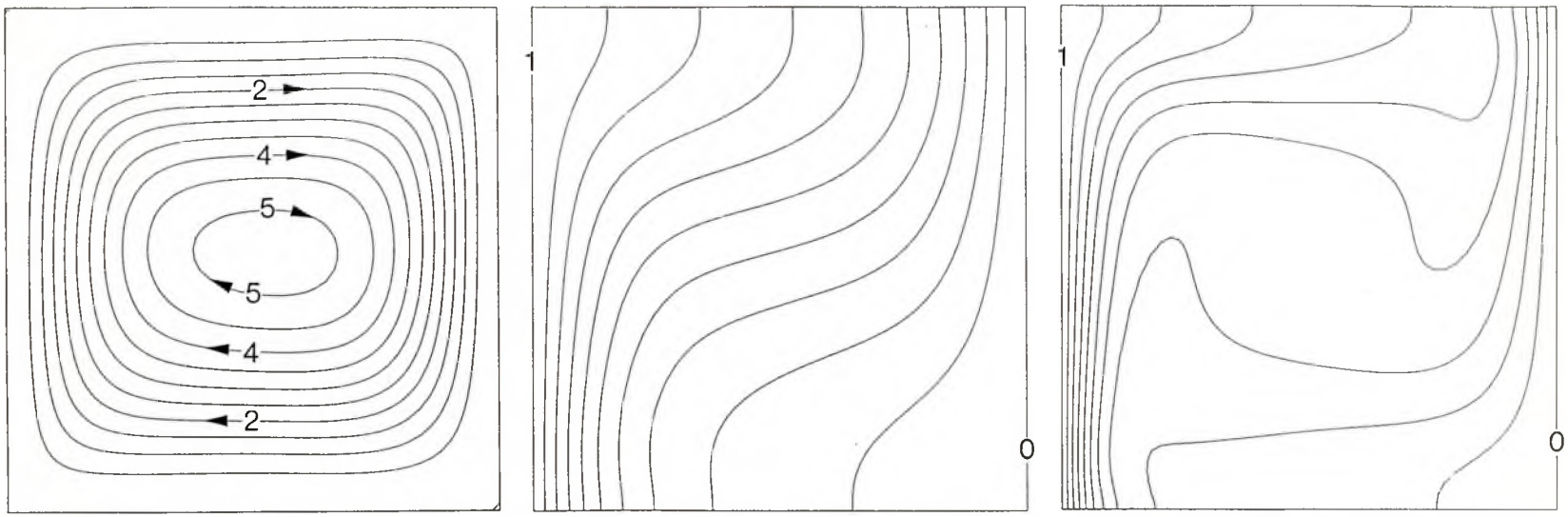

Figure 6.25 Streamfunction, Temperature and Concentration Contours for Ra_T = 5000, Le = 5, n = 2

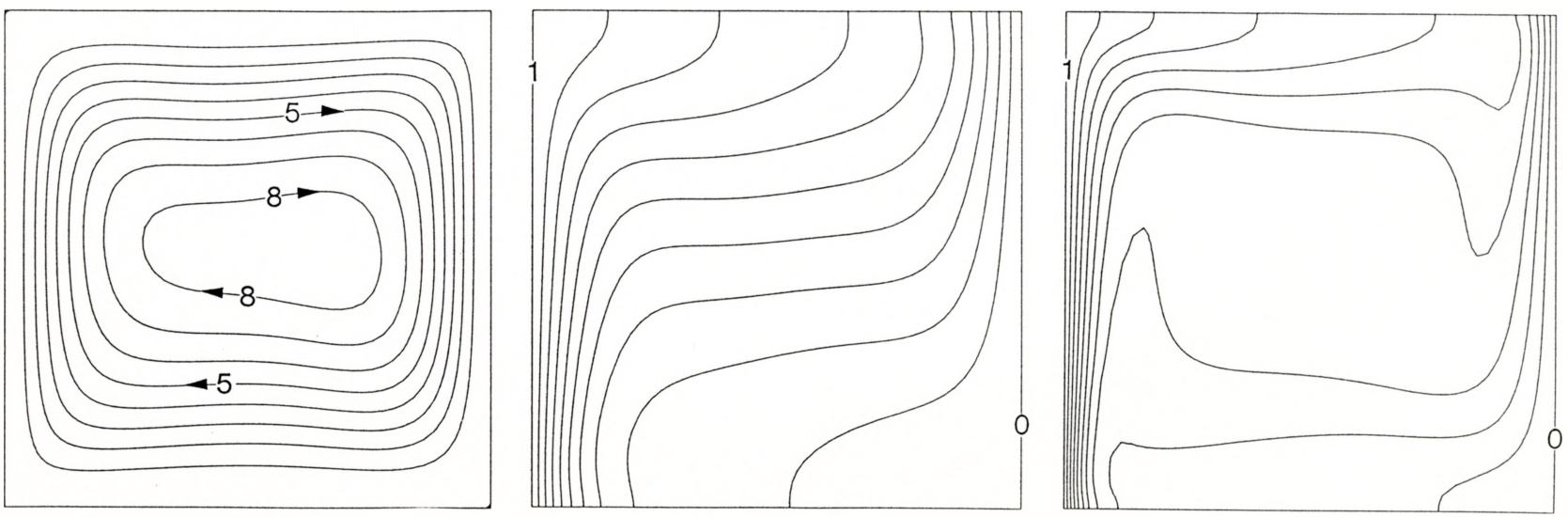

Figure 6.26 Streamfunction, Temperature and Concentration Contours for Ra_T = 20 000, Le = 5, n = 2

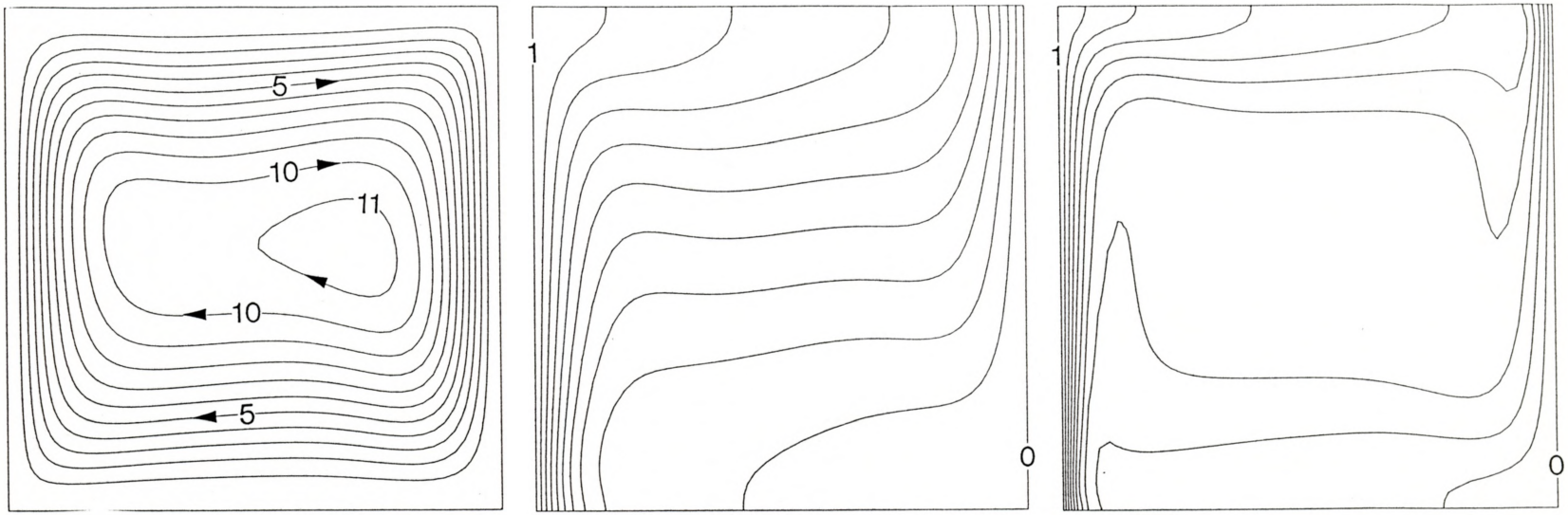

Figure 6.27 Streamfunction, Temperature and Concentration Contours for Ra_T = 50 000, Le = 5, n = 2

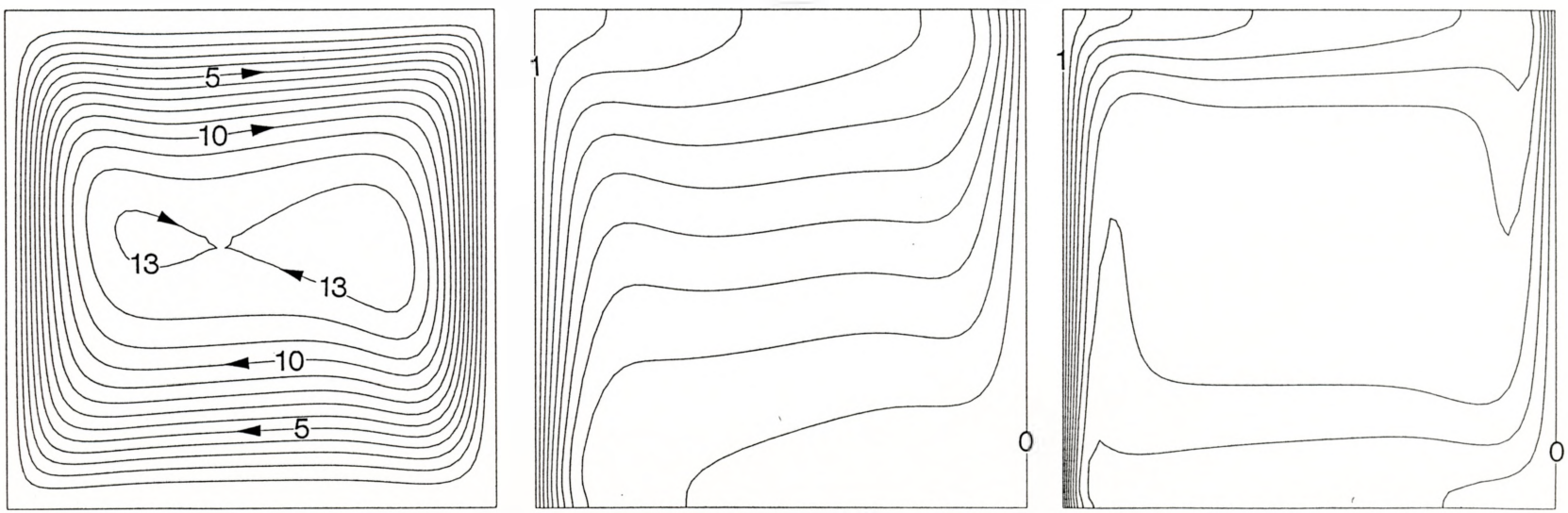

Figure 6.28 Streamfunction, Temperature and Concentration Contours for Ra_T = 100 000, Le = 5, n = 2

intensity of the flow is in the same order as for the case of n = -1. Another interesting note about these eddies is that they only seem to occur in the range of n = -1 to the point before transition from thermal dominated to mass species dominated opposing flows. This indicates that the mass species buoyancy force still has a minor but visible effect on the flow even though the opposing thermal buoyancy force influences the main flow circulation.

6.4 Effect of the Lewis Number on Convection

The effect of Le on convection is also examined for a few specific buoyancy ratios to obtain a brief insight into this relationship. To provide a standard comparison with the previous effect of the thermal Rayleigh number, the flows are examined for similar buoyancy ratios: n = -2, -1.2, -1 and 2, reflecting conditions for mass species dominated opposing, transitional, unity buoyancy ratio, and mass species dominated aiding flows respectively. For these cases the thermal Rayleigh number is held constant at 50 000.

The effect of Le on convection for a buoyancy ratio of -2 can be examined in figures 6.29 to 6.32 for Lewis numbers of 1, 2, 5 and 10 respectively. At a Lewis number of 1 (fig. 6.29) the temperature and concentration profiles are exactly the same as expected, the resulting flow is definitely mass species dominated with a high flow rate circulation. As Le is doubled (fig.6.30) a significant change occurs in the stream functions, the maximum dimensionless stream function decreases the flow circulation from -13 to -5. It is evident at this point that as the Lewis number is increased the effect of the mass species buoyancy force for a constant buoyancy ratio is reduced. This

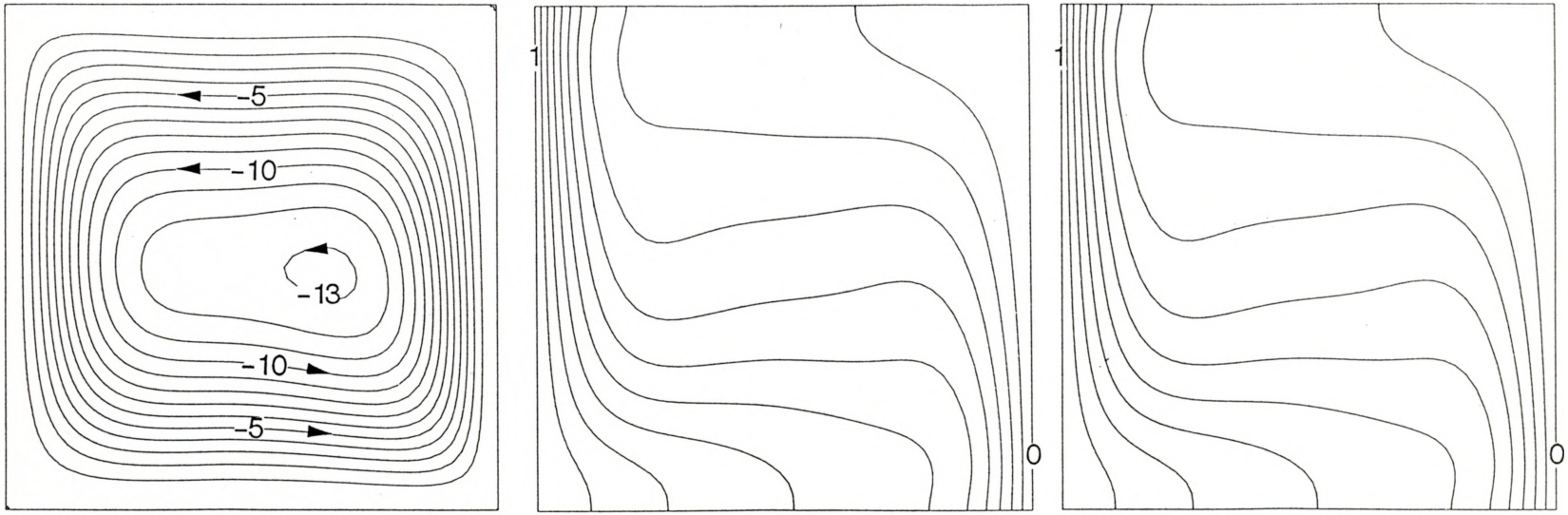

Figure 6.29 Streamfunction, Temperature and Concentration Contours for Ra_T = 50 000, Le = 1, n = -2

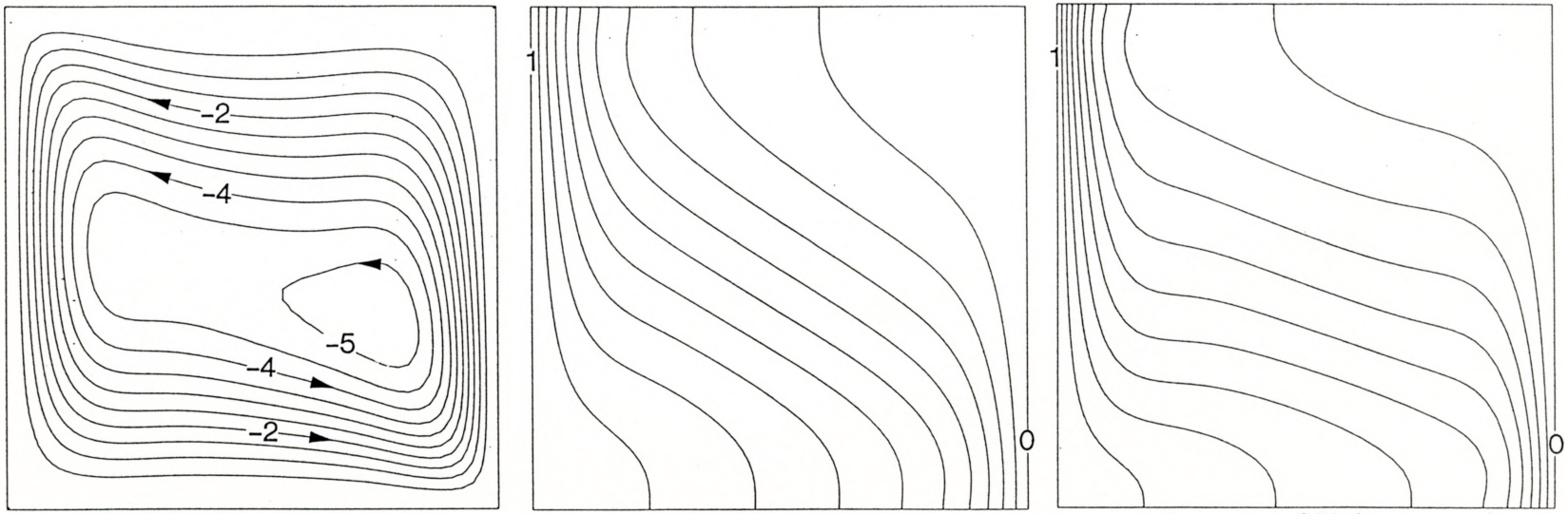

Figure 6.30 Streamfunction, Temperature and Concentration Contours for Ra_T = 50 000, Le = 2, n = -2

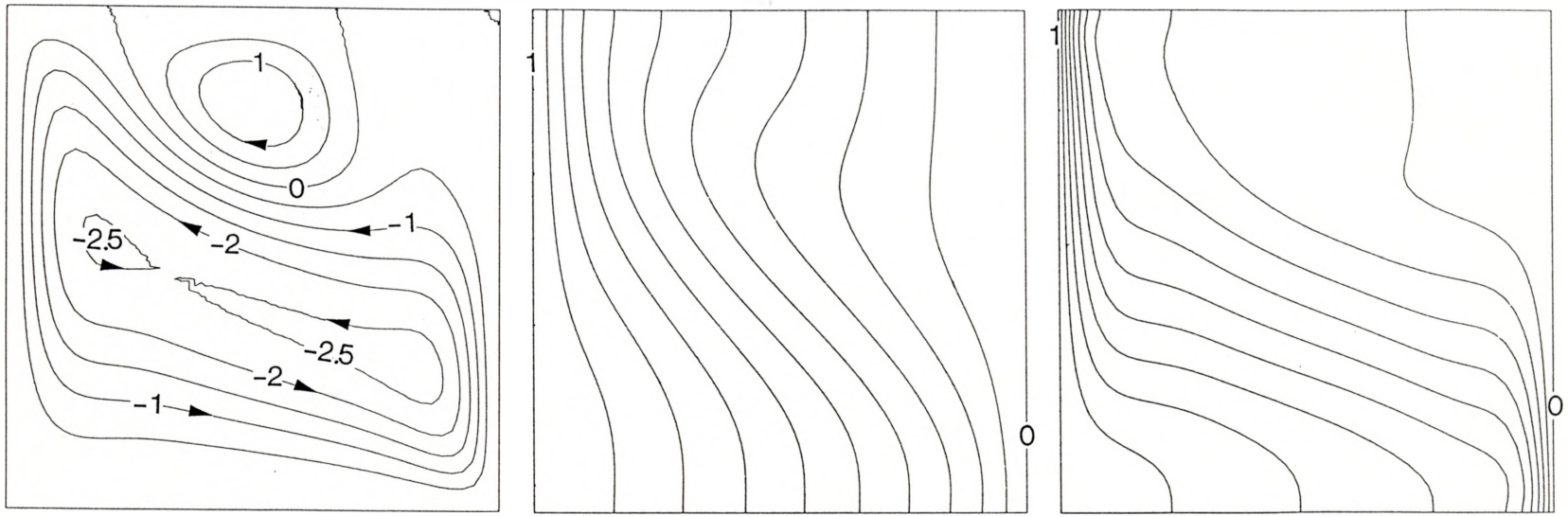

Figure 6.31 Streamfunction, Temperature and Concentration Contours for Ra_T = 50 000, Le = 5, n = -2

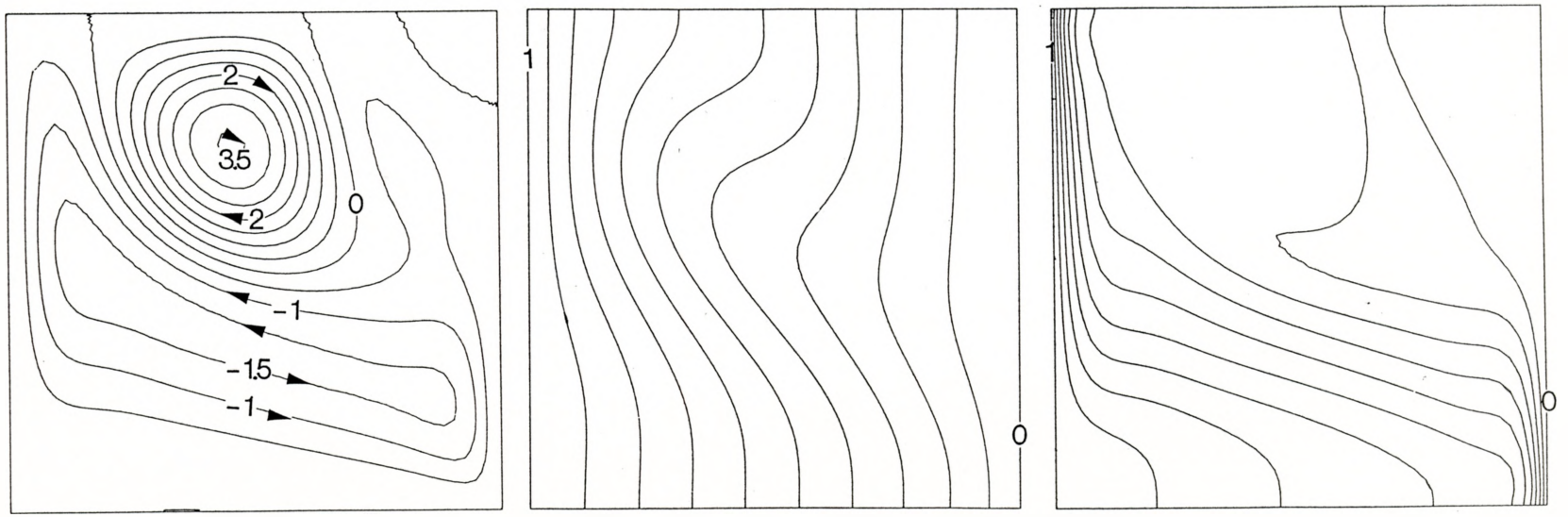

Figure 6.32 Streamfunction, Temperature and Concentration Contours for Ra_T = 50 000, Le = 10, n = -2

is due to the decreased diffusivity of the mass species, which results in the thinning of the mass species boundary layers. Consequently the effect the mass species on the fluid density does not penetrate as a far as the thermal fluid density effect. Further increases in the Lewis number results in the onset of transitional flow (figures 6.31 and 6.32) where a thermal dominated vortex intrudes from the top centre of the enclosure.

The effect of the Lewis number on transitional flow is further demonstrated for a buoyancy ratio of -1.2 in figures 6.33 to 6.36. At a Lewis number of 1, the flow is clearly dominated by the mass species buoyancy force. However as Le is doubled (fig. 6.34), transitional flow starts to develop. Compared to the previous case (n = -2) separation at the top of the enclosure starts for a lower Lewis number, consequently if the buoyancy ratio is increased transitional flow will start to occur at a lower Lewis number. Further increases in the Lewis number (figures 6.35 and 6.36) results in the reduction and eventual disappearance of the mass species dominated "L" shaped eddy. Examination of the temperature contours indicate that as the Lewis number is increased, the layers at the vertical centreline go from an unstable to a stable stratified condition (unstable being the condition where warmer lighter fluid is covered by colder heavier fluid). When the flow circulation is reversed by the dominating opposing thermal buoyancy force (fig. 6.36) the concentration in the centre of the enclosure exhibits the previously mentioned "blob" like characteristic as opposed to the reverse pattern of fig. 6.33. This is due to the lower diffusivity of the mass species at the higher Lewis number.

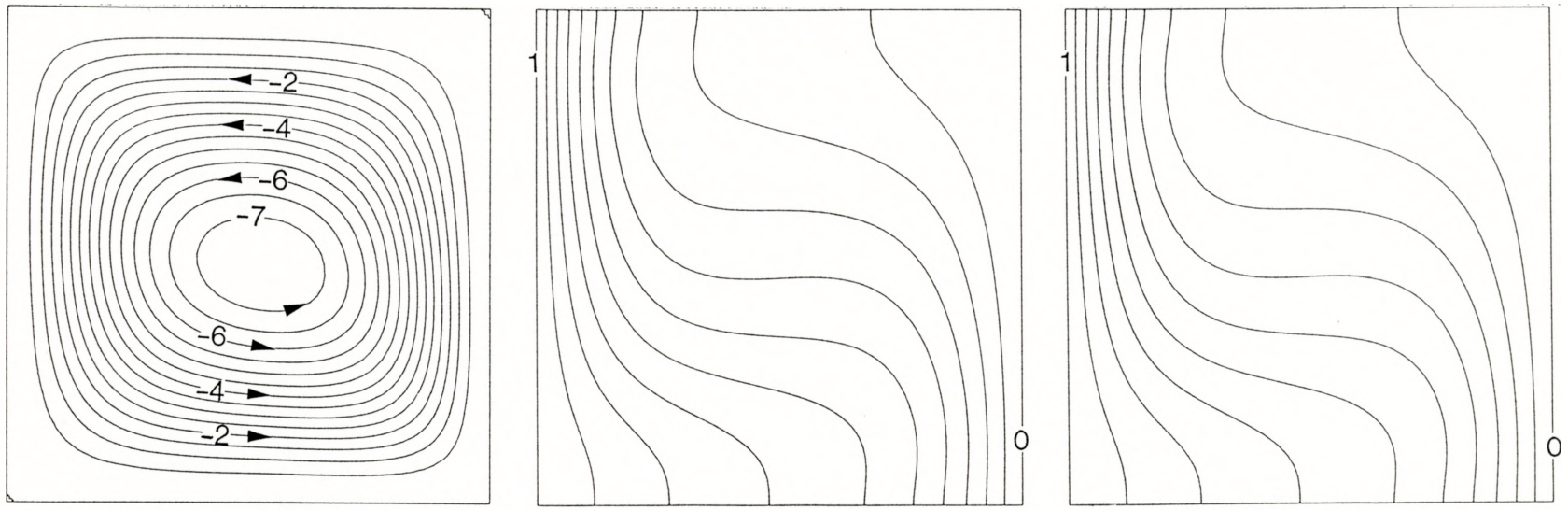

Figure 6.33 Streamfunction, Temperature and Concentration Contours for Ra_T = 50 000, Le = 1, n = -1.2

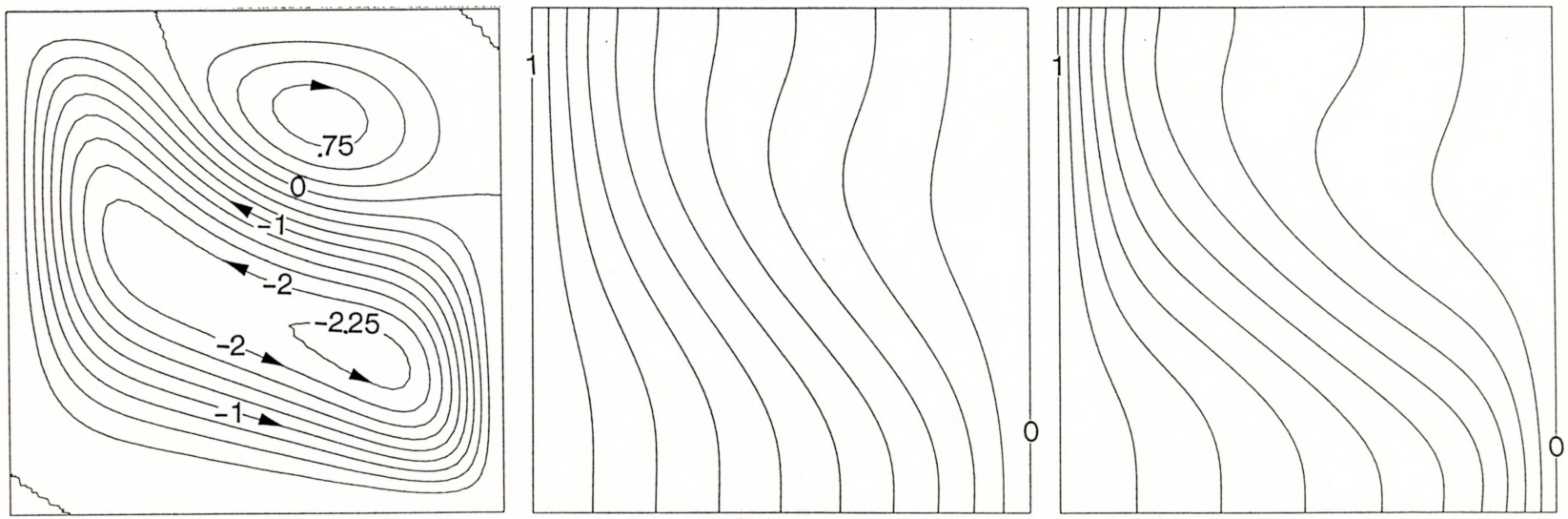

Figure 6.34 Streamfunction, Temperature and Concentration Contours for Ra_T = 50 000, Le = 2, n = -1.2

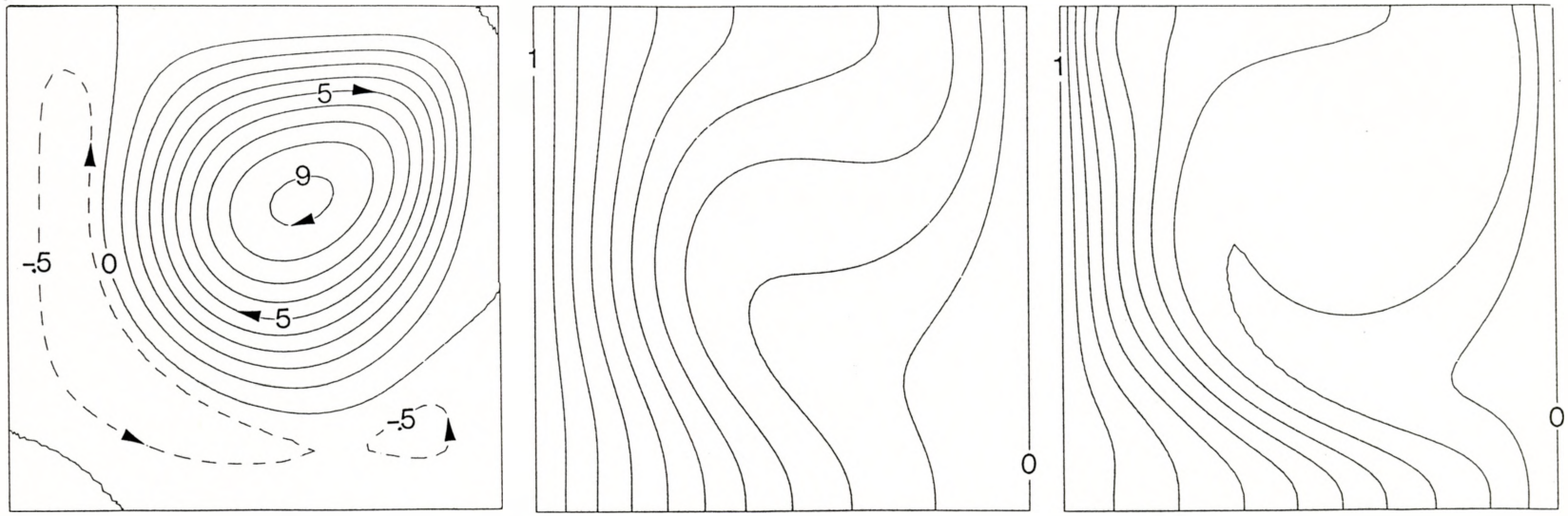

Figure 6.35 Streamfunction, Temperature and Concentration Contours for Ra_T = 50 000, Le = 5, n = -1.2

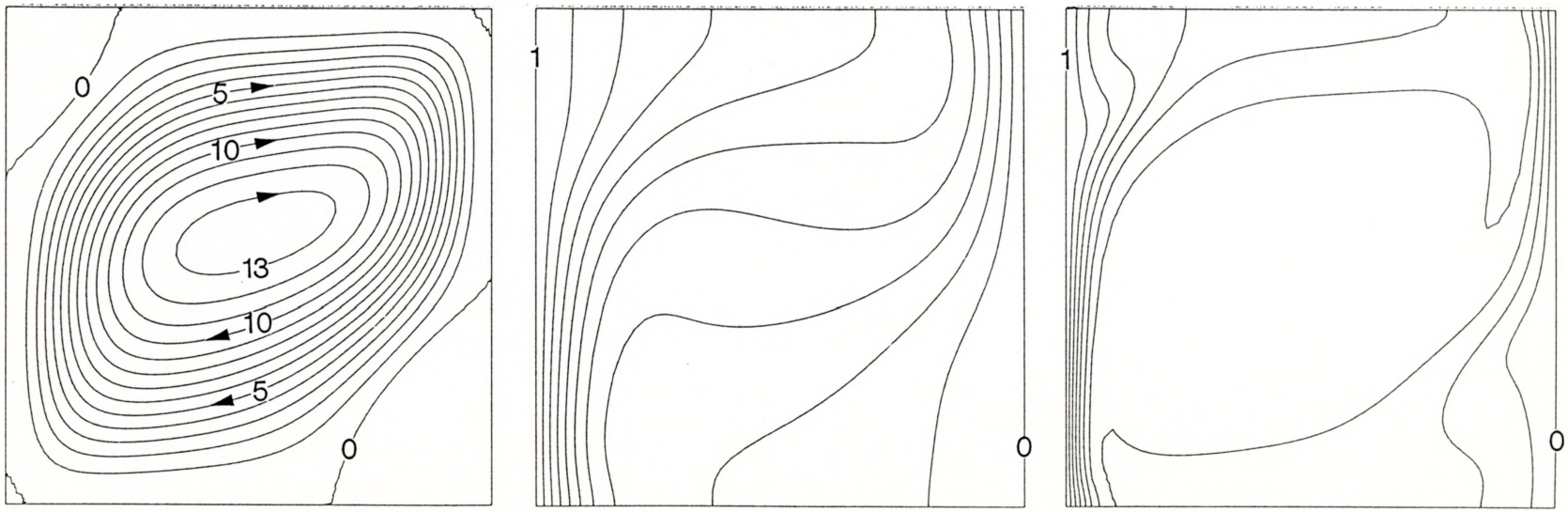

Figure 6.36 Streamfunction, Temperature and Concentration Contours for Ra_T = 50 000, Le = 10, n = -1.2

For the buoyancy ratio of -1 the flow characteristics are established in figures 6.37 through 6.40. At Le = 1 figure 6.37 indicates a no flow situation where the temperature and concentration contours emulate pure heat conduction and solid diffusion. Doubling the Lewis number creates a drastically different flow profile (fig 6.38). A strong thermal buoyancy force dominated vortex has been created. However further increases in the Lewis number does not result in a significantly large increase in the intensity. One may notice again that separation occurs at the upper left and lower right corners in which these eddies are caused by a weak mass species buoyancy force. Upon close examination of the separation points along the enclosure walls it is determined that these secondary eddies are shrinking with increasing Le, such that at very high Lewis numbers (very small mass species diffusivities) the size of the separation area will become insignificantly small. At this point the effect of the concentration on the buoyancy force will be negligible, since the diffusion of the mass species will be almost nonexistent. As a result, the concentration within the enclosure will be uniform, such that gradients are nonexistent, thus there is no mass species buoyancy force.

Figures 6.41 through 6.44 show a very interesting relationship between the Lewis number and the flow profiles for the aiding flow case of n = 2. The most notable feature is that as the Lewis number is increased, the intensity of the flow decreases and then levels off slightly oscillating around a dimensionless streamfunction value of 12. The explanation for this trend is reasonable. The boundary thickness of the mass species layer is shrinking, such that the extent of the

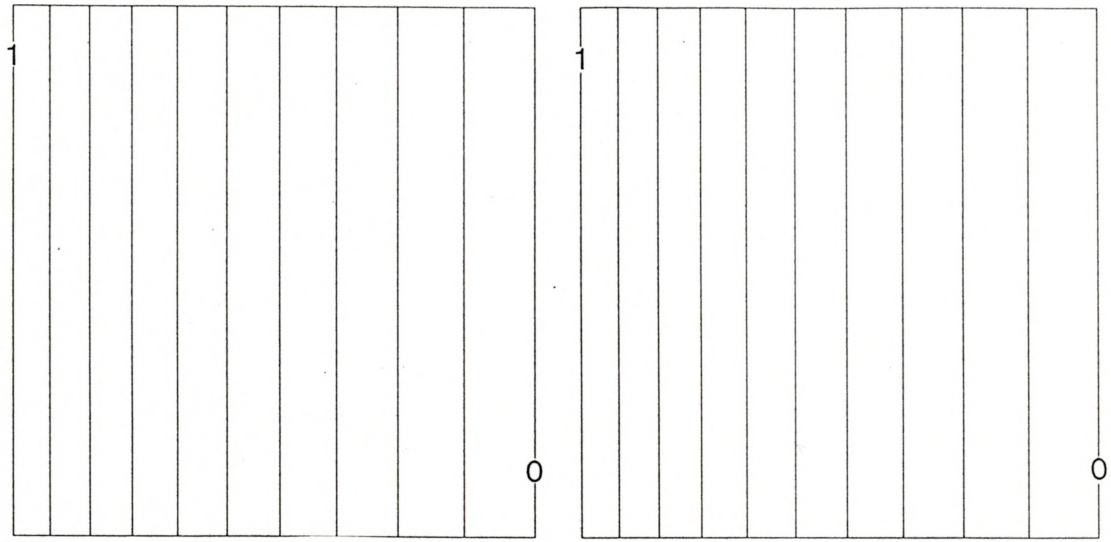

Figure 6.37 Temperature and Concentration Contours for Ra_T = 50 000, Le = 1, n = -1

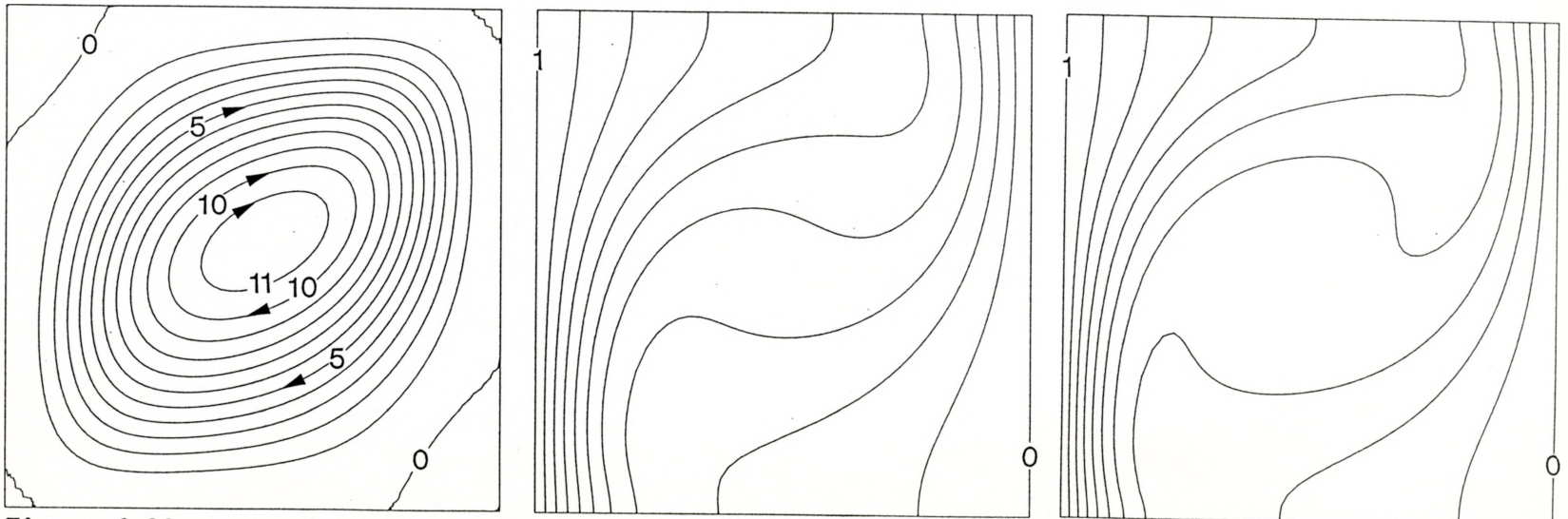

Figure 6.38 Streamfunction, Temperature and Concentration Contours for Ra_T = 50 000, Le = 2, n = -1

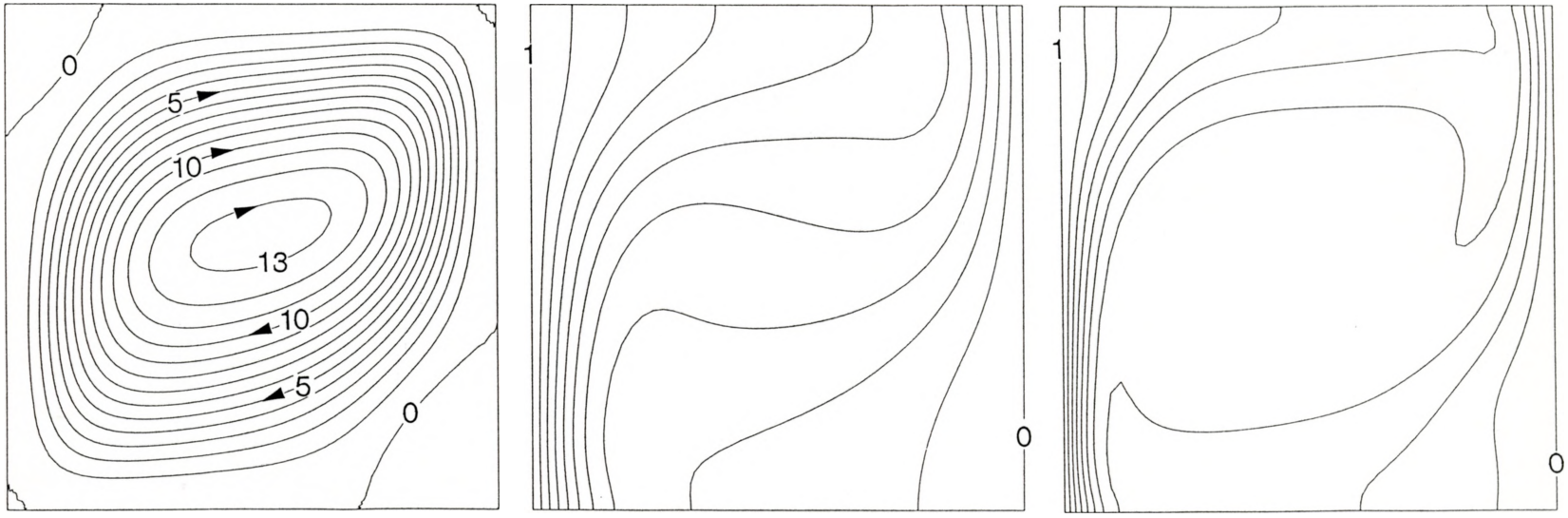

Figure 6.39 Streamfunction, Temperature and Concentration Contours for Ra_T = 50 000, Le = 5, n = -1

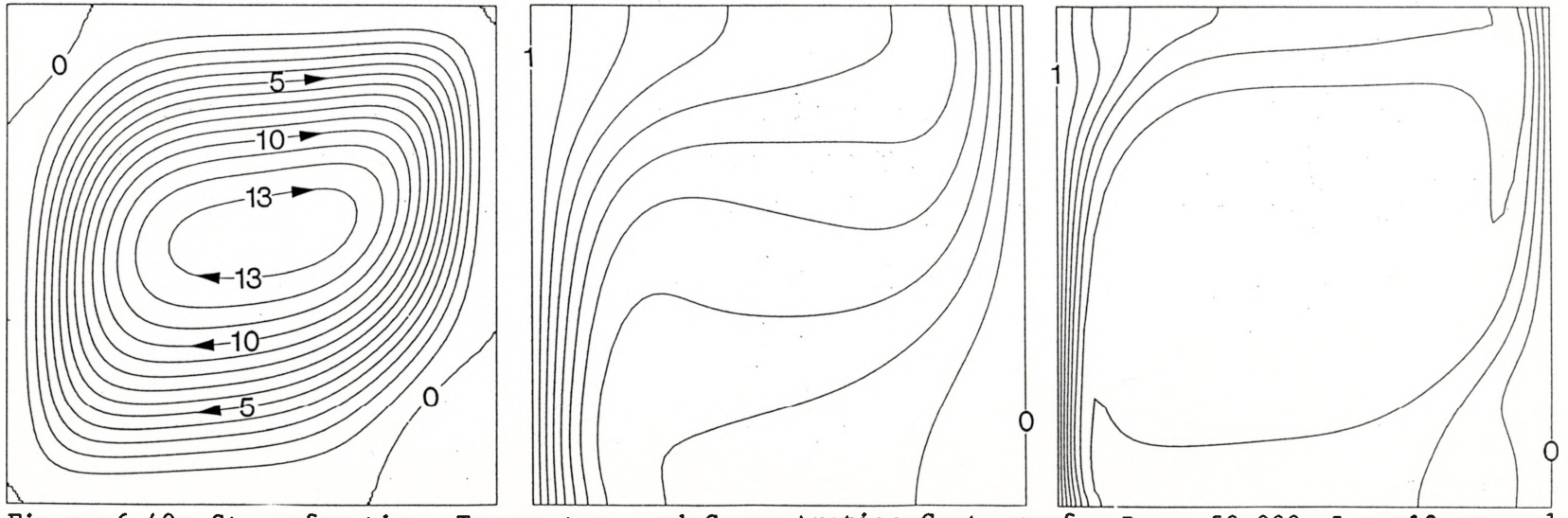

Figure 6.40 Streamfunction, Temperature and Concentration Contours for Ra_T = 50 000, Le = 10, n = -1

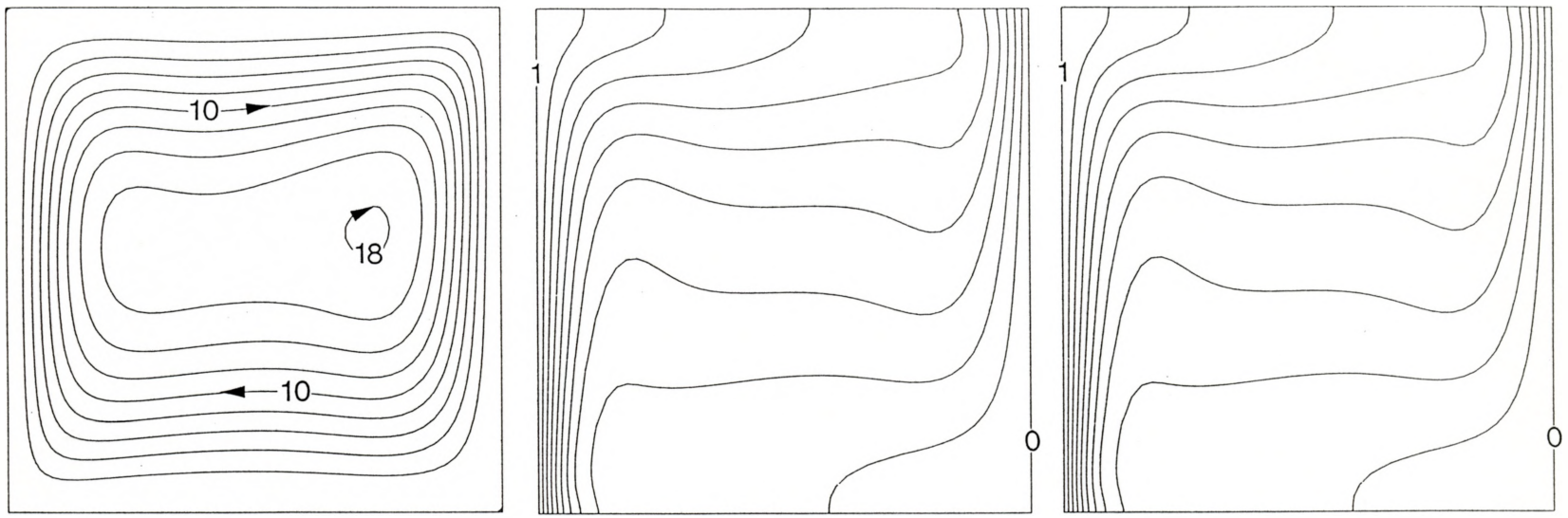

Figure 6.41 Streamfunction, Temperature and Concentration Contours for Ra_T = 50 000, Le = 1, n = 2

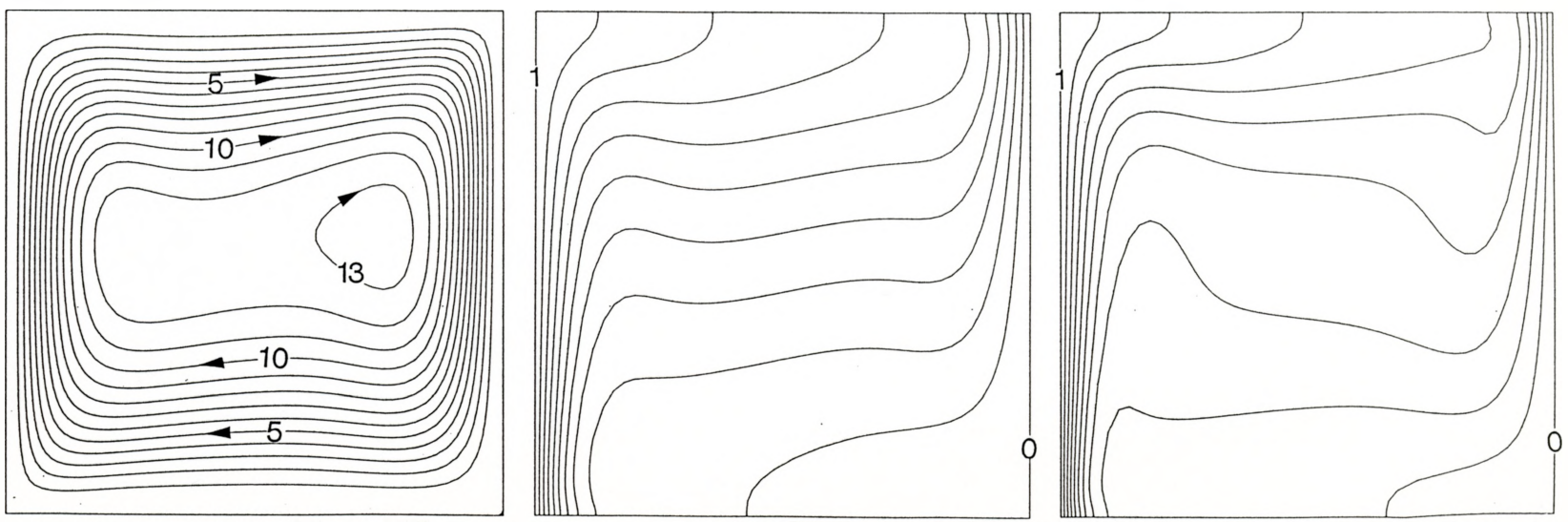

Figure 6.42 Streamfunction, Temperature and Concentration Contours for Ra_T = 50 000, Le = 2, n = 2

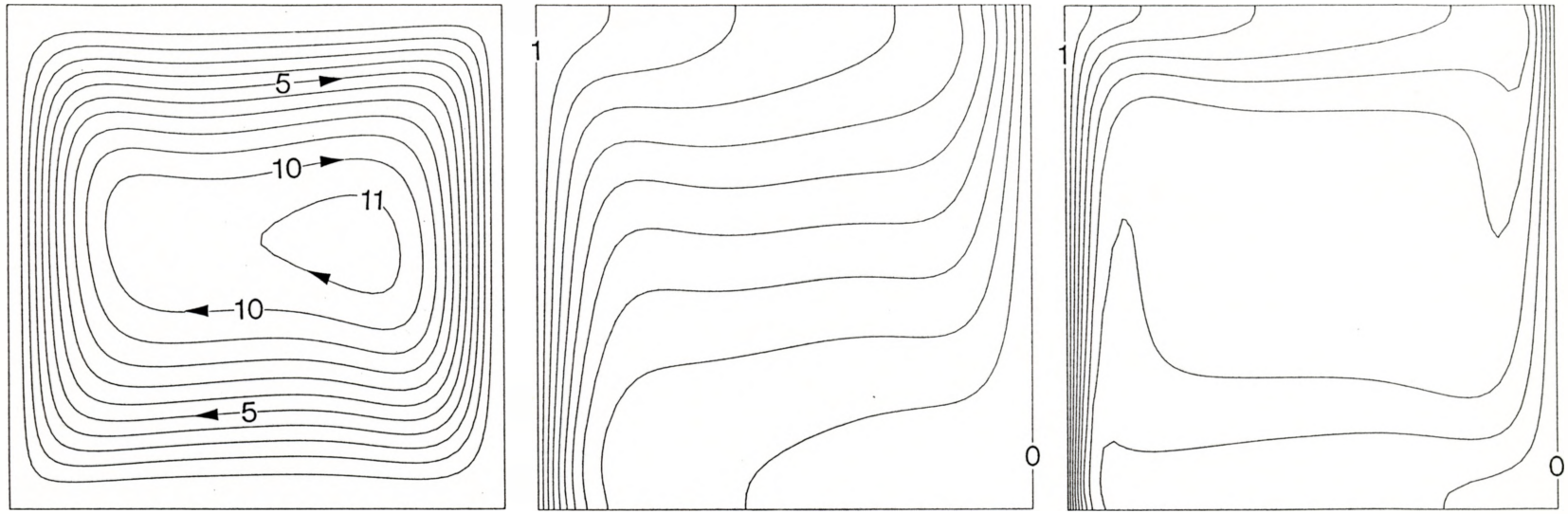

Figure 6.43 Streamfunction, Temperature and Concentration Contours for Ra_T = 50 000, Le = 5, n = 2

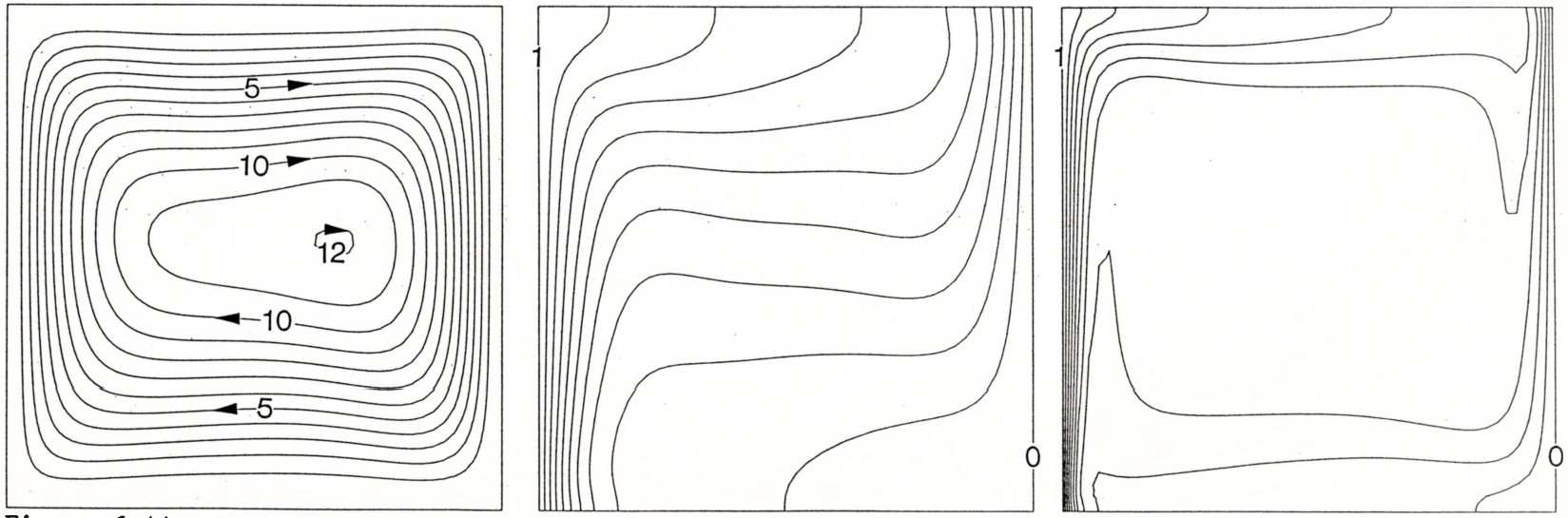

Figure 6.44 Streamfunction, Temperature and Concentration Contours for Ra_T = 50 000, Le = 10, n = 2

buoyancy effect is becoming closer and closer to the wall. Thus the net aiding buoyancy force is reduced to a value primarily influenced by the stable thermal buoyancy force (indicated by the almost consistent temperature contours). Extrapolating from the present observations, further increases in Le will not greatly effect the flow profiles apart from a thinning of the concentration contours. This is due to the same reasons as mentioned in the latter part of the previous paragraph.

6.5 Effect of Ra_T on the Average Sherwood and Nusselt Numbers

The effect of the thermal Rayleigh number on the average Nusselt and Sherwood numbers for a buoyancy ratio range of $-10 \leq n \leq 10$ can be examined in figures 6.45 and 6.46. Generally, the average Nusselt and Sherwood number increases with the thermal Rayleigh number for constant n. However, $\overline{Nu}$ and $\overline{Sh}$ tend to be minimized in the transitional range of flow reversal for constant Ra_T. In general the average Nusselt numbers are less in the opposing flow area ($n < 0$) than for the corresponding n in the aiding flow range ($n > 1$). This is also true for $\overline{Sh}$, however the relative difference for corresponding aiding and opposing buoyancy ratios is lower. This difference is attributed to the fact that opposing flow has a lower flowrate adjacent to the enclosure walls than for the corresponding aiding flow case.

6.6 Effect of Le on the Average Sherwood and Nusselt Numbers

The general effect of the Lewis number on $\overline{Nu}$ and $\overline{Sh}$ for the buoyancy ratio range of $-10 \leq n \leq 10$ is shown in figures 6.47 and 6.48. Examining figure 6.47 reveals that an increase in the Lewis number tends to decrease the average Nusselt number, except for the thermal dominated opposing flow range of $n = 0$ to the onset of flow reversal. On the

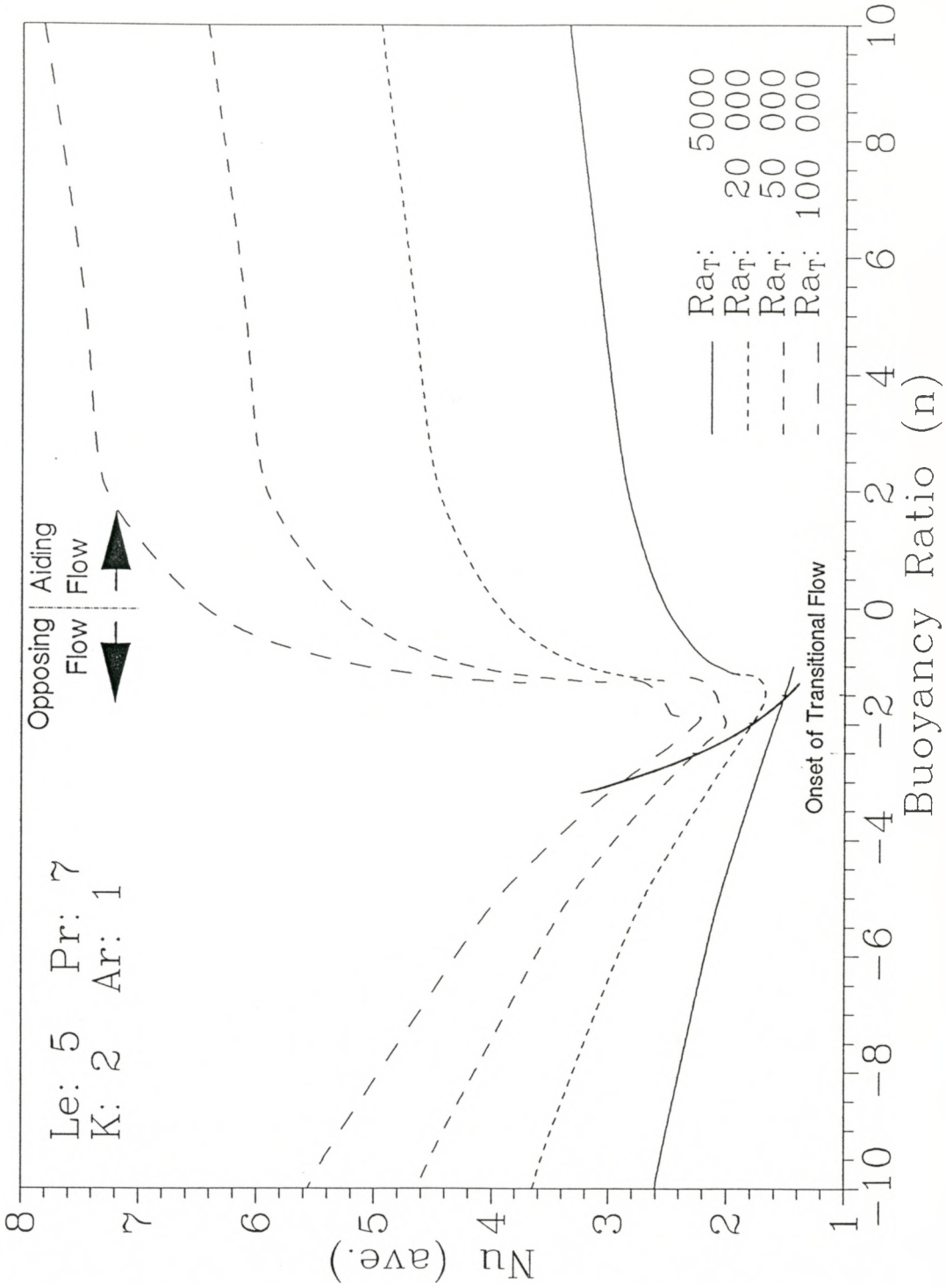

Figure 6.45 Effect of Ra_T on $\overline{Nu}$ for $-10 \leq n \leq 10$

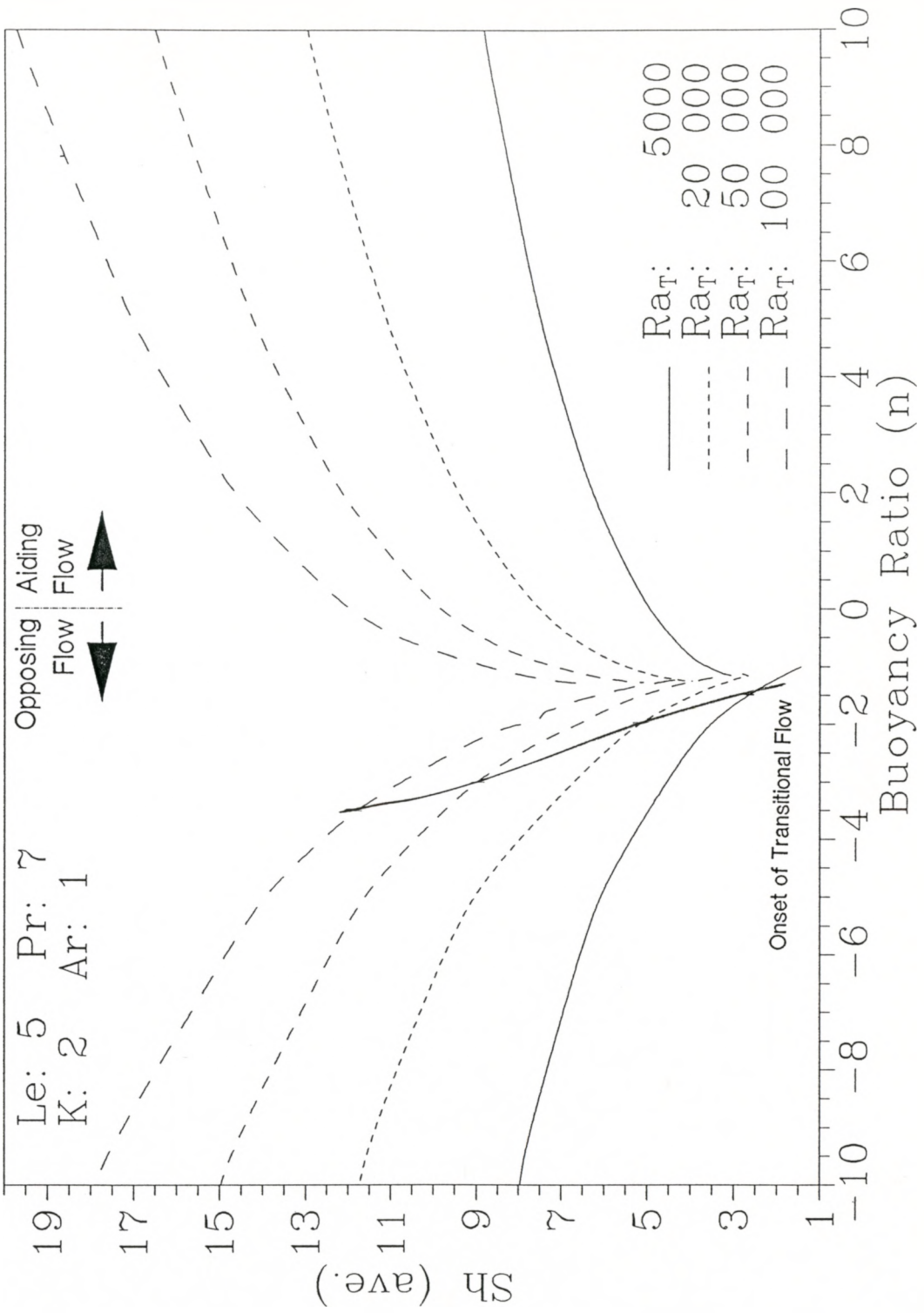

Figure 6.46 Effect of Ra_T on $\overline{Sh}$ for $-10 \leq n \leq 10$

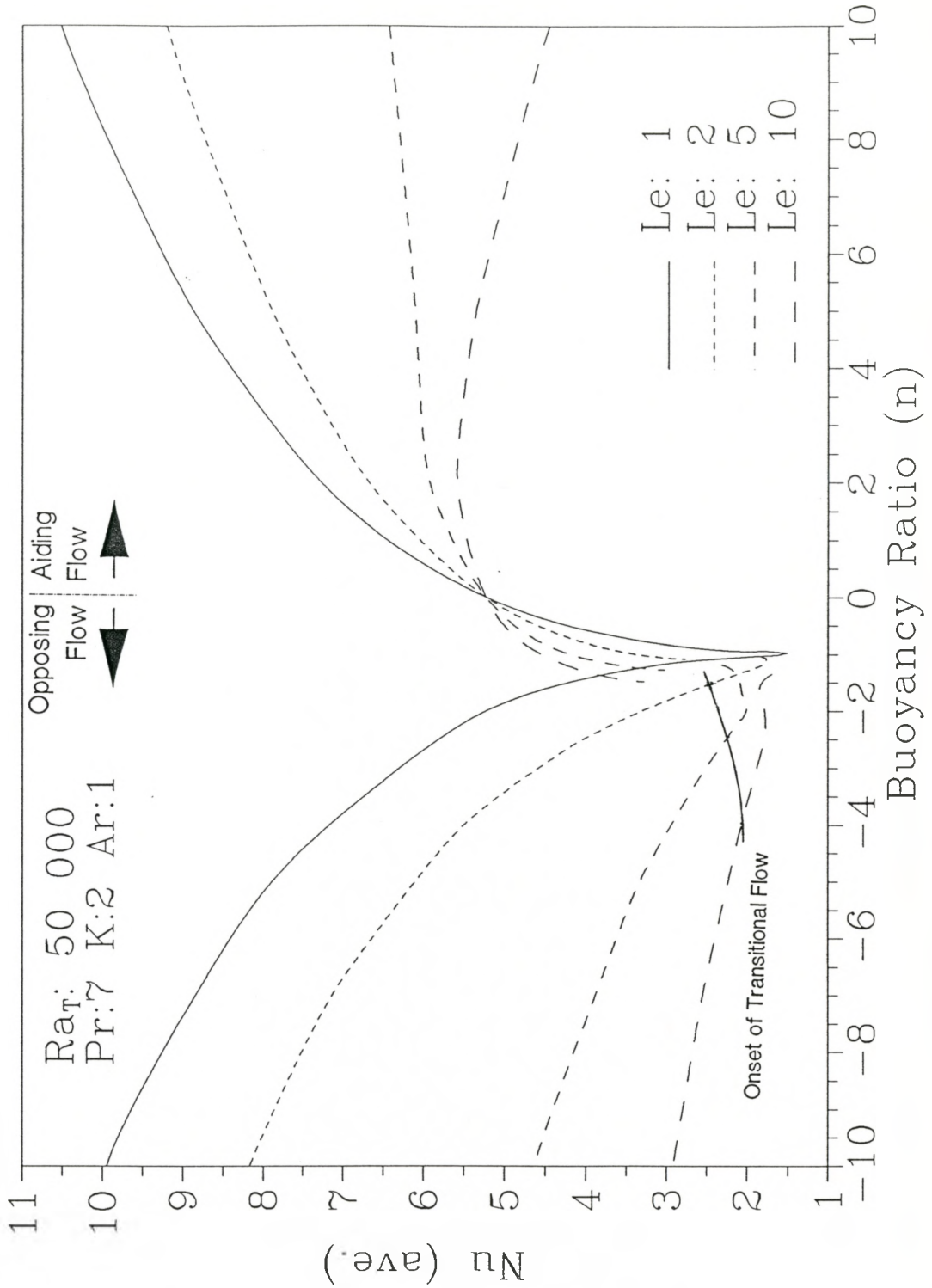

Figure 6.47 Effect of Le on $\overline{Nu}$ for $-10 \leq n \leq 10$

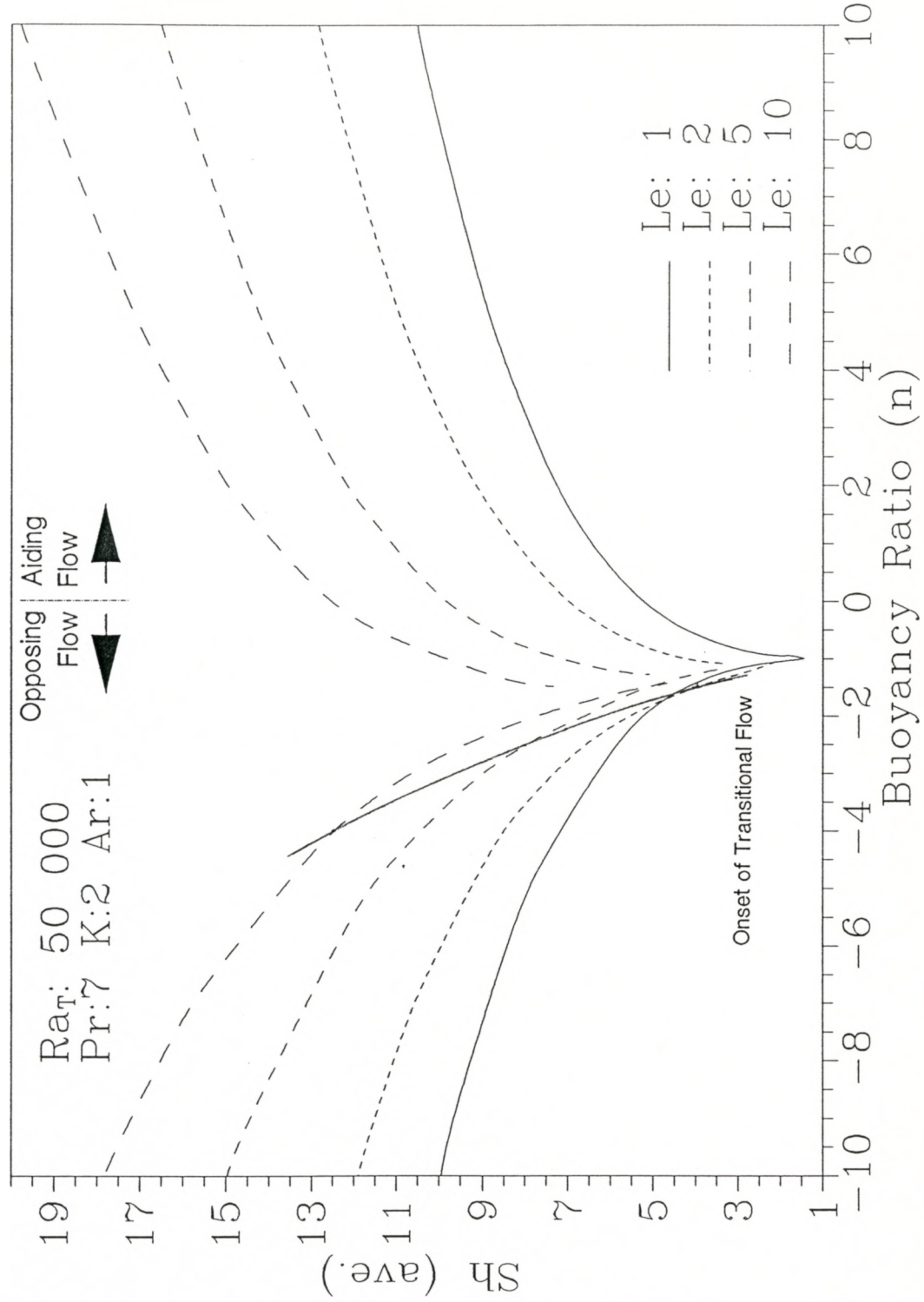

Figure 6.48 Effect of Le on $\overline{Sh}$ for $-10 \leq n \leq 10$

other hand, the average Sherwood number increases for the whole buoyancy ratio range for an increase in the Lewis number for a given buoyancy ratio. The increase in the Sherwood number is simple to explain. An increase in the Lewis number represents a decrease in the mass species diffusivity. This results in the thinning of the mass species boundary layer, consequently the concentration gradients at the vertical enclosure walls will increase. The explanation for the $\overline{Nu}$-Le relationship is slightly more complex. In the thermal dominated opposing flow region between n = 0 and flow reversal (min. $\overline{Nu}$), the flow is enhanced with increasing Le as shown in figures 6.33 to 6.40. This increase in flow circulation is responsible for the increase in heat transfer rate. However, outside this region, flow circulation intensity is reduced as the Lewis number is increased. This is demonstrated in figures 6.41 to 6.44 and discussed in section 6.4.

An interesting relationship between the aiding buoyancy ratio (n > 0) and the average Nusselt number occurs for Le = 10. As the buoyancy ratio is increased the average Nusselt number decreases, whereas for other Le (1, 2 and 5), the average Nusselt number tends to increase for the same region. Since the mass species boundary layer is much thinner than the thermal boundary layer for Le = 10, the mass species buoyancy force tends to dominate the flow very close to the vertical walls. The influence of the thermal dominated buoyancy force extends further out. At low buoyancy ratios (n $\simeq$ 2, fig. 6.48) the axial velocity between the vertical wall and the centre of the enclosure tends to smoothly distributed. However as n increases the flow adjacent to the wall tends to be highly dominated by the mass species buoyancy force such that the

majority of the flow occurs within this region. Thus the axial velocity distribution is very high in a small region very close to the wall, whereas the velocity outside the mass species boundary layer, but within the thermal boundary layer, is quite low if not close to stagnant. This has the effect of reducing the rate of heat transfer from the vertical walls, consequently the average Nusselt number is reduced.

A special case exists for Le = 1 where the solutions are symmetric with respect to n = -1. For example, the streamfunction, thermal and mass species equation solutions for n = -2, 0 will be symmetric with a horizontal line of reflection. This is expected for this Lewis number due to the similar dimensionless mass species and thermal distributions in which the only difference between the corresponding solutions is the change in the sign of the buoyancy force. Notice in figures 6.47 and 6.48 that the average Nusselt and Sherwood numbers for the case of n = -1 are a minimum of 1.44 as predicted by equation 5.3 for a no flow situation. The solutions for this specific Lewis number are referred to as simple additive flow in which similar solutions can be obtained provided the following criteria is met:

$$\text{Le} = 1 \qquad \left(\text{Ra}_T + \text{Ra}_C \right) = \text{Ra}_T \left(n + 1 \right) = \text{Constant} \qquad (6.1)$$

Symmetric solutions will be obtained when $|n + 1| = \text{Constant}$.

Finally it should be observed that at n = 0 all solutions, regardless of the Lewis number, intersect at the same average Nusselt number ($\overline{\text{Nu}} = 5.2313$, fig. 6.47). Since the buoyancy ratio is zero, mass species has absolutely no effect on the convection, consequently the

problem is considered to be single diffusive for this point even though separate solutions exist for the concentration distribution (see fig. 6.48).

6.7 Flow Transition and Flow Reversal Ranges

The flow transition range only covers a small part of the buoyancy ratio spectrum studied, however it is important in the understanding of flow reversal. There are three major points in the buoyancy ratio: *onset of flow transition*, the *upper critical buoyancy ratio* and the *lower critical buoyancy ratio*. The onset of flow transition is the point at which the mass species buoyancy force dominated vortex experiences intrusion by the thermal dominated vortex. The upper critical buoyancy ratio is the point at which the transitional flow changes to thermal dominated flow, which is associated with a sudden rise in $\overline{Nu}$. The corresponding lower critical buoyancy ratio is the point at which a thermal dominated opposing flow jumps to a transitional flow, which is associated with a sudden decrease in $\overline{Nu}$. The upper critical buoyancy ratio is obtained by increasing n, whereas the lower critical buoyancy ratio is obtained by decreasing n. The difference between the upper and lower limits of the critical buoyancy ratio is defined as the *critical buoyancy ratio range*. It can be argued that a fourth major point exists at the opposing-aiding flow boundary (n = 0), however since this point does not vary with the thermal Rayleigh number and the Lewis number it is not discussed here.

6.7.1 Effect of Ra_T on Transition Onset and Critical Buoyancy Ratios

The effect of the thermal Rayleigh number on the onset of transitional flow can be examined in the streamfunction plots for Le =

5, n = -2 (figures 6.13 - 6.16) in which increasing Ra_T results in the intrusion and expansion of a thermal dominated vortex (see section 6.3). The onset of transition for a constant Lewis number is plotted in figures 6.49 and 6.50. Examination of these plots reveals that an increase in the thermal Rayleigh number results in the lowering of the buoyancy ratio at which the onset of transitional flow occurs. The actual buoyancy ratio values for the onset of transitional flow can be found in table 6.1.

Table 6.1 Transition Onset Point and Critical Buoyancy Ratios for $5000 \leq Ra_T \leq 100\ 000$ at Le = 5.

Ra_T	Onset of Transition	Lower Critical n	Upper Critical n	Δn
5000	-1.5	-1.15	-1.00	0.15
20 000	-2	-1.25	-1.13	0.12
50 000	-2.5	-1.275	-1.19	0.085
100 000	-3	-1.29	-1.23	0.06

Figures 6.49 and 6.50 show the average Nusselt and Sherwood numbers in the region of flow reversal, in which the relationship between the two critical buoyancy ratios and the thermal Rayleigh number can be observed. It may be noted that as Ra_T increases both the lower and upper critical buoyancy ratios decrease. From table 6.1 it may also be noticed that the critical buoyancy range or the difference between the upper and lower critical buoyancy ratios (Δn) is decreasing with increasing Ra_T. From the present observations one would hypothesize

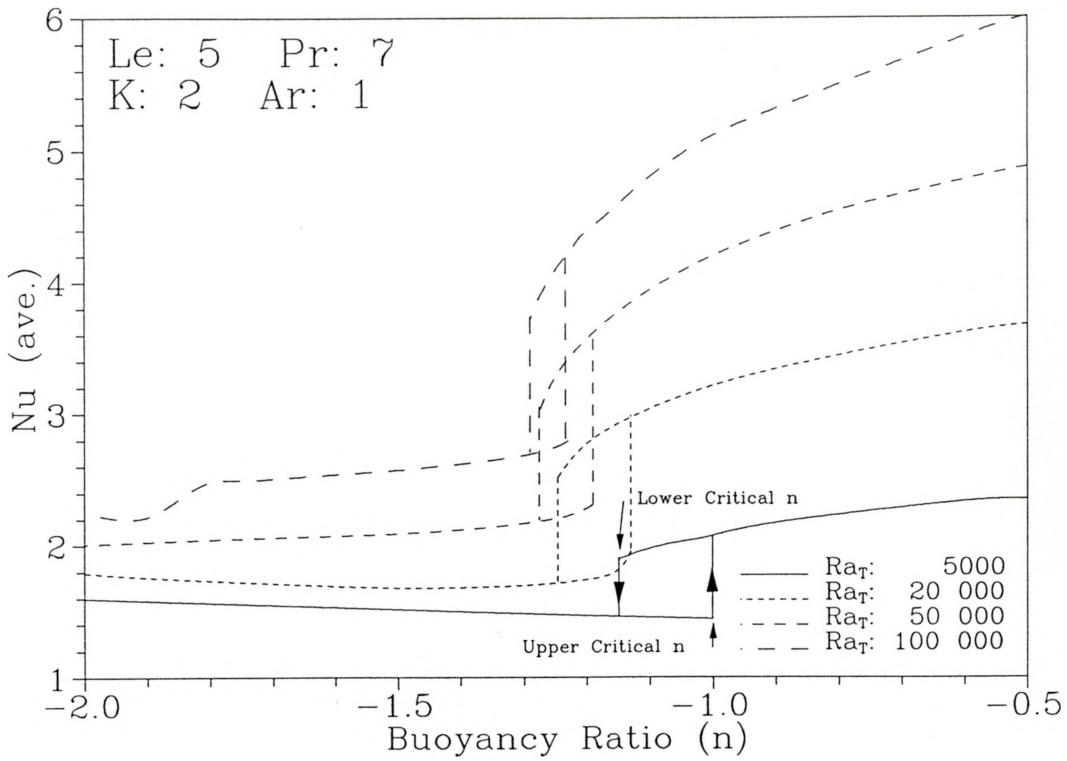

Figure 6.49 Effect of Ra_T on $\overline{Nu}$ and on the Critical Buoyancy Ratios

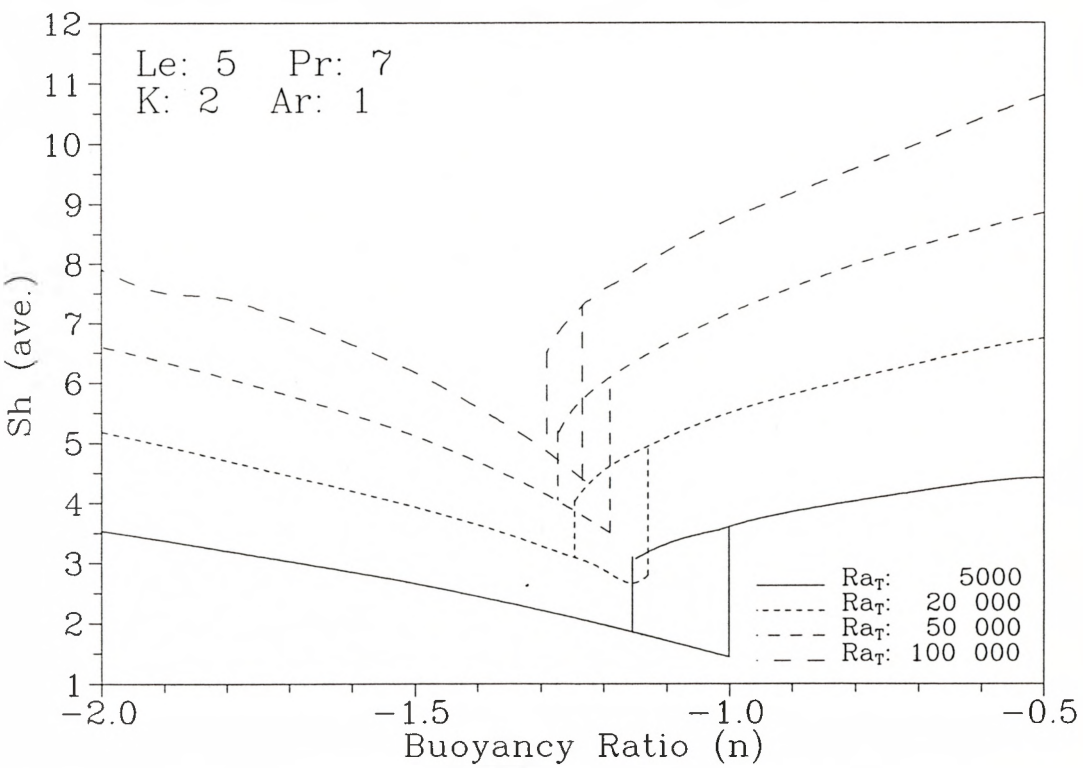

Figure 6.50 Effect of Ra_T on $\overline{Sh}$ and on the Critical Buoyancy Ratios

that a further increase in the thermal Rayleigh number would result in the further shrinkage of the critical buoyancy range to a point where only one critical buoyancy ratio exists. However if this point exists, it is more likely that there will be a step difference or discontinuity in the solutions than a smooth flow reversal since the difference between the average Nusselt number solutions along with the average Sherwood number solutions is increasing. For Ra_T beyond this value it is uncertain if the single step difference will remain or that there may be region of instability or transient flow between the transitional and thermal dominated flow solutions. In fact the region for a high Ra_T may be turbulent as opposed to laminar such that the present speculations may not be applicable.

6.7.2 Effect of Le on Transition Onset and Critical Buoyancy Ratios

The effect of the Lewis number on the onset of transitional flow can be examined in figures 6.47 and 6.48 in which an increasing Lewis number will advance this onset when the buoyancy ratio is increased through the opposing flow range. This agrees with the observations in figures 6.29 through 6.32 for a constant Ra_T of 50 000 (the buoyancy ratio is held at -2), where an increasing Lewis number is documented by the intrusion of the thermal buoyancy force dominated vortex. The actual values of the onset of transition flow may found in table 6.2. Transitional flow is not applicable to Le = 1, since the flow can only be dominated by either the mass species or thermal buoyancy force, not both. It can be argued that the no flow condition (n = -1) could be considered the point of flow transition. This is not the case since

transitional flow requires that there be separate vortices governed separately by the two diffusive buoyancy forces.

Table 6.2 Transition Onset Point and Critical Buoyancy Ratios for $1 \leq Le \leq 10$ at $Ra = 50\ 000$.

Le	Onset of Transition	Lower Critical n	Upper Critical n	Δn
1	n/a	-1.	-1.	0.
2	-1.5	-1.085	-1.05	0.035
5	-2.5	-1.275	-1.19	0.085
10	-4	-1.485	-1.35	0.135

Figures 6.51 and 6.52 examine the average Nusselt and Sherwood numbers in the critical buoyancy ratio range. These plots also enable us to examine the effect of the Lewis number on the critical buoyancy ratios and other reversal phenomena. Curves are plotted for $Le = 2$, 5, and 10 for a constant thermal Rayleigh number of 50 000. The curve for $Le = 1$ is not included since it does not have a discontinuity and therefore does not need to be closely examined in this specific range. Examination of this range reveals that as the Lewis Number is increased the upper and lower critical buoyancy ratios decrease. Furthermore, table 6.2 indicates that the critical buoyancy ratio range (Δn) increases with the Lewis number. A special case exists for $Le = 10$ in which three separate solutions can exist during flow reversal. In this case one solution exists for thermal dominated opposing flow ($n \geq -1.485$, upper curve), however two separate solutions exist for the transition region ($-2.15 \leq n \leq -1.375$, middle curve; $n \leq -1.35$, lower

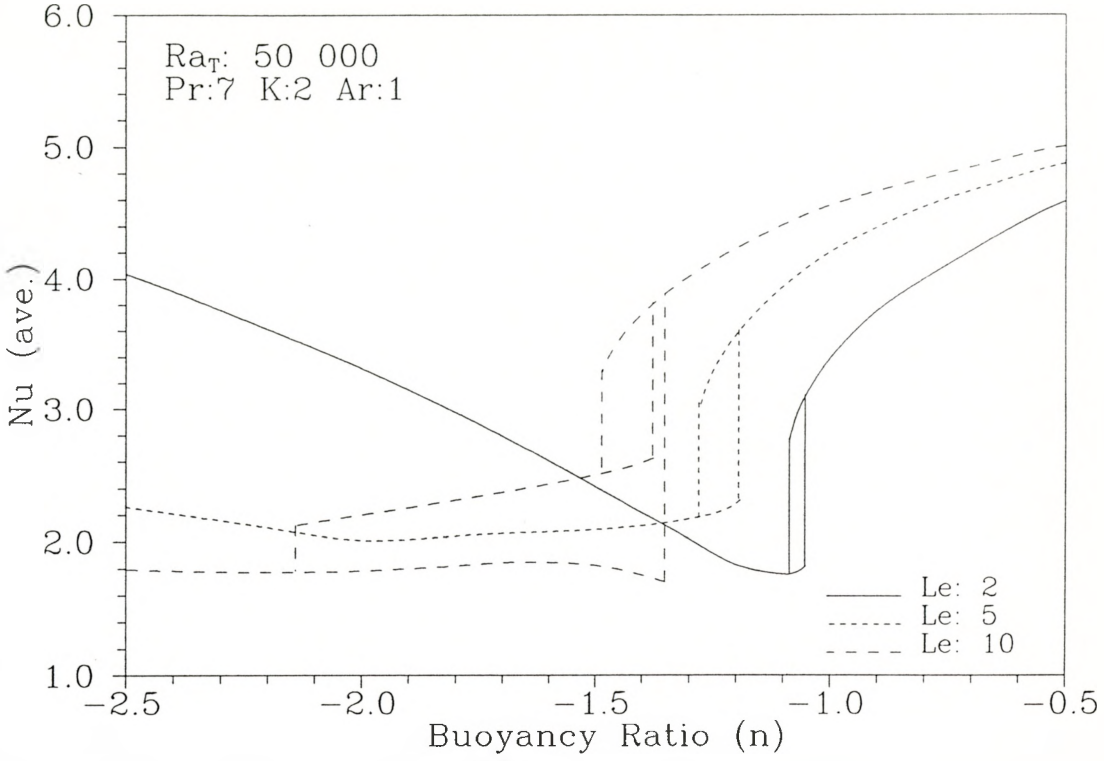

Figure 6.51 Effect of Le on $\overline{Nu}$ and on the Critical Buoyancy Ratios

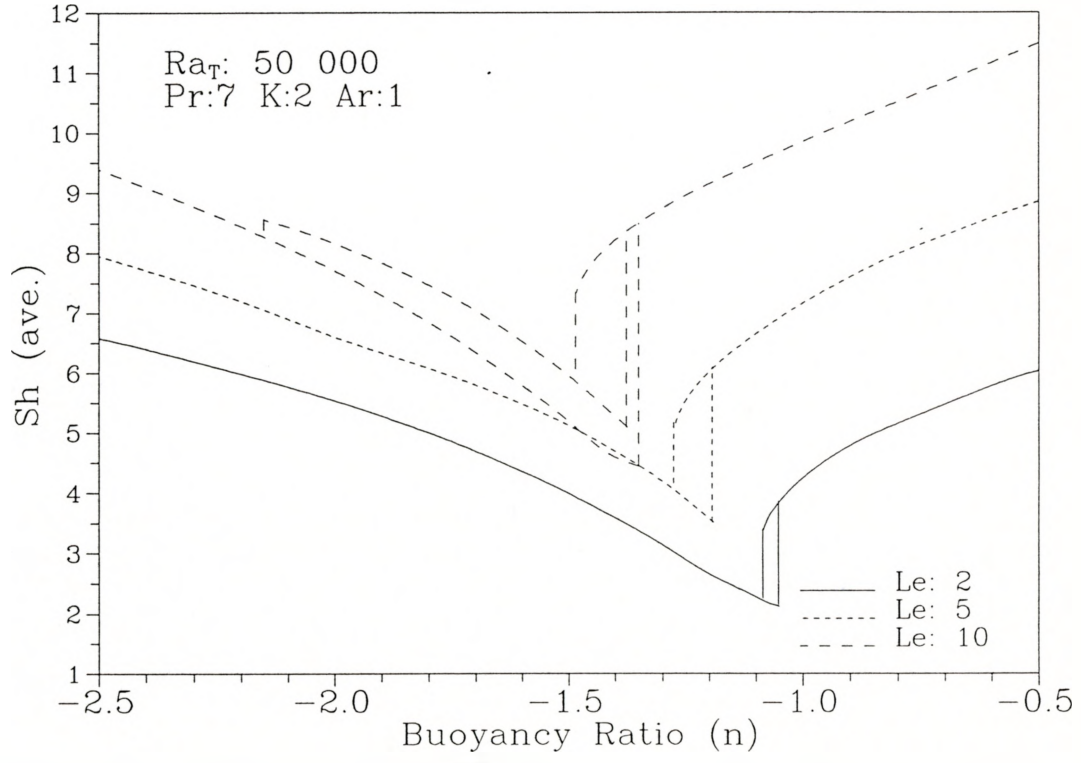

Figure 6.52 Effect of Le on $\overline{Sh}$ and on the Critical Buoyancy Ratios

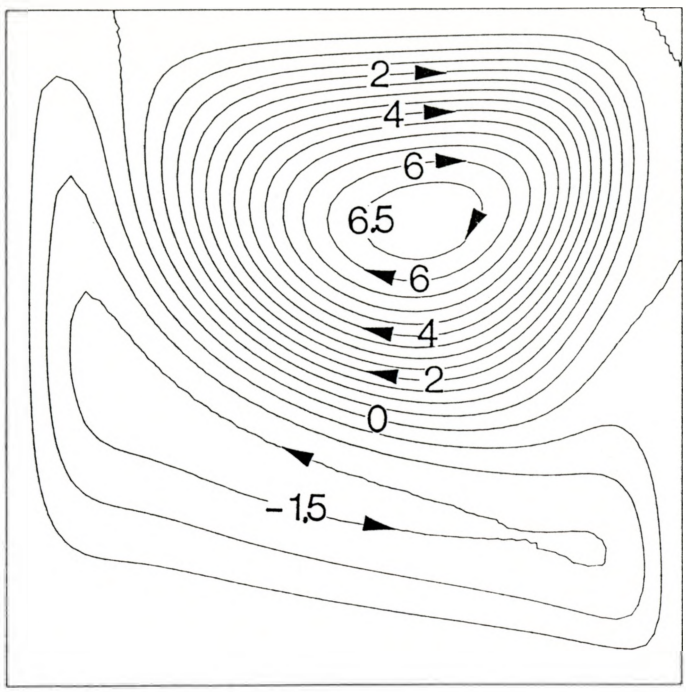

Figure 6.53 Streamfunctions for Middle Solution Curve for Ra_T = 50 000, Le = 10 and n = -2.

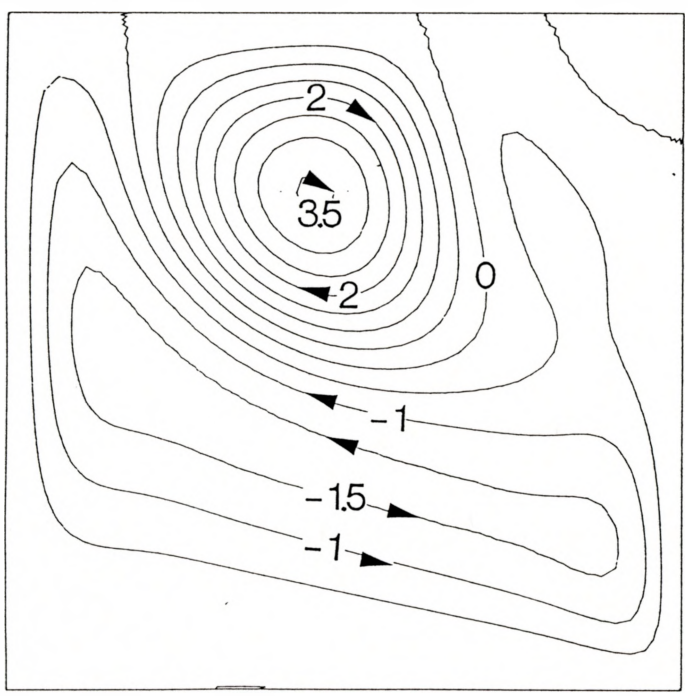

Figure 6.54 Streamfunctions for Lower Solution Curve for Ra_T = 50 000, Le = 10 and n = -2.

curve) depending on the initial flow conditions. The difference between the two transition solutions is shown in figures 6.53 and 6.54 for n = -2 at Le = 10 and Ra_T = 50 000. The difference between the two plots is that the thermal buoyancy force governed vortex has separated from the outer radial wall (fig. 6.54) for the lower solution curve. Referring to figure 6.51, the relationship between the buoyancy ratio and the solution curves will be explained. If the buoyancy ratio is increased from n < -2.15, the solution will follow the lower curve where the thermal dominated vortex is clear of the radial walls. Once the buoyancy ratio surpasses n = -1.35, the solution steps to the upper solution curve where thermal dominated circulation encompasses the enclosure from the lower inner wall to the upper outer wall (fig. 6.36). If n is now decreased, the solution will not revert to transitional flow until a lower critical buoyancy ratio (n < -1.485) is reached. Beyond this point the buoyancy ratio can be increased or decreased along the middle solution curve, for which the thermal dominated vortex is attached to the outer radial wall. If n is increased the flow will revert to thermal dominated flow at n > -1.375; if n is decreased the thermal dominated vortex will separate from the outer radial at n < -2.15 and then follow the lower transitional flow curve.

6.7.3 Comparison of Critical Buoyancy Ratio with Other Studies

In Chapter Two it was discussed that other numerical studies have found critical buoyancy ratios for flow reversal. Comparisons with the other studies are difficult on two accounts. First, the physical configurations are different, but more importantly the values of the fluid parameters such as Pr and Ra_T are different if not unknown.

However, the same general relationships between the Lewis number and the critical buoyancy ratios are present for the studies.

Taunton *et al.* [14] have found numerically that two separation points exist for a vertical flat plate in which, if the buoyancy ratio is decreased from a small negative buoyancy ratio, counter current flow will result until a second buoyancy ratio is reached, beyond which flow occurs entirely in the opposite direction. Comparing to the present study, Taunton's first separation point may represent the lower critical buoyancy ratio, whereas the second separation point represents the onset (or in Taunton's case the termination) of transitional flow. There is no mention of results due to an increase in n from the other end of the spectrum, thus the existence of an upper critical buoyancy ratio was not established. In fact, one critical buoyancy ratio may exist as opposed to two critical buoyancy ratios (upper and lower) if the solutions for vertical flat plates are unique. The first separation points (critical buoyancy ratios) are listed in table 6.3.

Table 6.3 First Separation Point (Critical Buoyancy Ratio) for a Vertical Flat Plate. (Note: Ra is unknown for Taunton's study)

Pr	Le	First Separation Point
0.35	2	-1.13
0.14	5	-1.29
0.7	10	-1.69
0.01	10	-2.00
0.1	100	-3.88
1.0	1000	-6.86

Nilson [17,18] also found a domain of counterflow between two domains of opposite unidirectional flows for double-diffusive flow along a vertical flat plate. The author determined relationships for the domain boundaries for Le $\gg$ 1 and Pr $\gg$ 1.

(i) unidirectional downflow for $n \leq -Le$ (opposing mass species dominated convection)

(ii) unidirectional upflow for $n \geq -Le^{1/3}$ (thermal dominated convection)

(iii) bidirectional counterflow for $-Le \geq n \geq -Le^{1/3}$ (transitional flow)

The parentheses represent the equivalent flows in the present study. Similar to Taunton, Nilson assumes there are unique solutions for any given buoyancy ratio and no other flow parameters have an effect (Ra_T and Pr). Nilson's correlations are compared to the present study in table 6.4. Since Nilson's criteria (Le $\gg$ 1 and Pr $\gg$ 1) do not exactly match, one would not expect good results. However the large differences may also be due to the fact that Ra_T and geometry parameters have not been considered.

Table 6.4 Comparison of the Nilson and Present Studies for Critical Buoyancy Ratios and Onset of Transition

Le	Critical Buoyancy Ratio(s)		Onset of Transiton	
	Nilson	Present	Nilson	Present
2	-1.25	-1.085, -1.05	-2	-1.5
5	-1.7	-1.275, -1.19	-5	-2.5
10	-2.15	-1.485, -1.35	-10	-4

Han [4] found critical points similar to the present study in his examination of numerical double-diffusive flow in a square two dimension cavity. From Han's streamfunction plots, transitional flow represented by the intrusion of thermal buoyancy force dominated vortices are similar to the present study. However in Han's two dimensional study the intrusion occurs centro-symmetrically, intrusion occurs from both the top and the bottom of the enclosure. The absence of centro-symmetry in the present study is most likely due to the axi-symmetry of the problem in which the physical geometry prevents symmetric conditions with respect to the coordinate centre of the enclosure ($r^* = 1.5$, $z^* = 0.5$). Han found that upper and lower critical buoyancy ratios for flow reversal exist, in which the solutions are dependent on the initial conditions. He also determined that as the Lewis number is increased the critical buoyancy ratio will decrease, however no relationship between the critical buoyancy ratios and the thermal Rayleigh number was investigated. Table 6.5 shows the upper and lower critical buoyancy ratios documented by Han.

Table 6.5 Critical Buoyancy Ratios for a Square Two-Dimensional Enclosure: $Pr = 1$, $Ra_T = 100\ 000$ (Han)

Le	Upper Critical Buoyancy Ratio	Lower Critical Buoyancy Ratio
2	-1.14	-1.13
10	-1.8	-2.13

CHAPTER SEVEN

CONCLUSIONS & RECOMMENDATIONS

7.1 Conclusions

A computer code has been developed to study double-diffusive flow in cartesian and axi-symmetric coordinates. The code was verified against a numerical two dimensional double-diffusivity study and a numerical axi-symmetric convective heat transfer study. Grid independence was found for a semi-uniform grid structure for an arbitrary case. Numerical results are presented for steady laminar natural convection of a fluid in a vertical annulus with a constant temperature and concentration applied across the vertical walls. Both opposing and aiding buoyancy force conditions are examined. Depending on the relative magnitude of the buoyancy forces, three flow domains may exist:

i) mass species buoyancy force dominated circulation

ii) thermal buoyancy force dominated circulation

iii) transitional flow (combination of the above flow domains)

Three main parameters have been investigated to determine their effect on the flow structure and the average heat and mass transfer rates. These include the *buoyancy ratio* (n), the *Lewis number* (Le) and the *thermal Rayleigh number* (Ra_T). The *aspect ratio* (Ar), *curvature* (K) and the *Prandtl number* (Pr) have remained constant for the entire study.

The buoyancy ratio strongly determines the flow domain due to the fact that this ratio determines the relative strengths and directions of the buoyancy forces. At low n, the flow is opposed and mass species dominated. For high n, the flow structure is aided and again mass species dominated. For $-1 < n < 1$ the flow structure is dominated by the thermal buoyancy force for $Le > 1$. The transitional domain is generally located in the region of $-4 < n < -1$ for the parameters studied, in which the points of flow reversal are dependent on the Lewis and thermal Rayleigh numbers. The average Nusselt and Sherwood numbers tend to be minimized at the points of flow reversal.

Solutions in the flow reversal range are not unique, as two or three different solutions could be found for the same parameters depending on the initial flow conditions. The extent of this flow reversal range is defined by upper and lower critical buoyancy ratios.

An increase in Ra_T tends to increase the heat and mass transfer rates. The thermal Rayleigh number also affects the critical buoyancy ratios. An increase in Ra_T will decrease the values of the critical buoyancy ratios and will also decrease the difference between these two points.

The Lewis number has a slightly more complex relationship with the Nusselt and Sherwood numbers. For all flow structures an increase in Le will result in an increase in $\overline{Sh}$. For flow structures in the opposing mass species dominating domain and all aiding flow conditions, $\overline{Nu}$ decreases with an increase in Le. However for buoyancy ratios in the thermal dominated buoyancy force region, the average Nusselt number

increases with an increase in Le. The critical buoyancy ratios are decreased by an increase in Le, however the range between the ratios is increased.

Similar findings with flow domains and critical buoyancy ratios have been found in other numerical studies. In fact the general relationship between the Lewis number and the critical buoyancy ratios has been documented, however the relationship between flow reversal and other parameters have not been as well analyzed in previous studies.

7.2 Recommendations for Further Studies

Due to the number of system parameters it is necessary to investigate the effect of the parameters neglected in this study. The range of the present parameters should also be extended especially the Lewis number. The following future work should be considered

i) Effect of aspect ratio (Ar)

ii) Effect of curvature (K)

iii) Effect of Prandtl number (Pr)

iv) Extension of the Lewis number range ($1 < Le < 2000$)

v) Tall enclosures with high Le to examine possible multicell flow structures

vi) Transient flows (including the study of periodic flows, bifurcation and chaos)

vii) Turbulent flows

viii) Soret effects near the density inversion temperature using a nonlinear temperature-concentration-density relationship.

ix) Examination of different boundary conditions such as uniform heat and mass transfer.

A corresponding experimental study is required in order for the results to be fully confirmed. In fact the mechanics of flow reversal should be experimentally examined to verify the existence of upper and lower buoyancy ratios. Other "hysteresis" effects have been experimentally established such as the different onset and termination points for circulation in single-diffusive natural convection systems. Thus it is plausible that such a physical phenomenon exists in the present case.

REFERENCES

1 Turner, J. S.,"Double-Diffusive Phenomena," *Annual Review of Fluid Mechanics*, vol. 6., 1974, pp. 37-56.

2 Ostrach, S., "Natural Convection with Combined Driving Forces," *PhysicoChemical Hydrodynamics*, vol. 1, No. 4, 1980, pp. 233-247.

3 Hansen, U., and Yuen, D. A., "Subcritical Double-Diffusive Convection at Infinite Prandtl Number," *Geophysics Astrophysics Fluid Dynamics*, vol. 47, 1989, pp.199-224.

4 Han, H, "Double-Diffusive Natural Convection in a Vertical Rectangular Enclosure," Ph. D. Thesis, University of Minnesota, 1988.

5 Ostrach, S., "Fluid Mechanics in Crystal Growth - The 1982 Freeman Scholar Lecture," *Journal of Fluids Engineering*, vol. 105, 1983, pp. 5-20.

6 Kuehn, T. H., "Natural Convection Heat Transfer from a Horizontal Circular Cylinder to a Surrounding Cylindrical Enclosure," Ph. D. Thesis, University of Minnesota, 1976.

7 Patankar, S. V., Numerical Heat Transfer and Fluid Flow, Hemisphere, Washington D.C., 1980.

8 Stommel, H., Arons, A. B., Blanchard, D., "An Oceanographical Curiosity: The Perpetual Salt Fountain," *Deep-Sea Research* vol. 3, 1956 pp. 152-153.

9 Martin, S., "The Amateur Scientist - Experiments with Salt Fountains and Related Instabilities in Water," *Scientific American*, vol. 224, 1971, pp. 124-128.

10 Stern, M. E., "The "Salt-Fountain" and Thermohaline Convection," *Tellus*, vol. 12, 1960, pp. 172-175.

11 Somers, E. V., "Theoretical Considerations of Combined Thermal and Mass Transfer from a Vertical Flat Plate," *Journal of Applied Mechanics*, vol. 23, 1956, pp. 295-301.

12 Wilcox, W. R., "Simultaneous Heat and Mass Transfer in Free Convection," *Chemical Engineering Science*, vol. 13, 1961, pp. 113-119.

13 Gill, W. N., Casal, E. D., and Zeh, D. W., "Binary Diffusion and Heat Transfer in Laminar Free Convection Boundary Layers on a Vertical Plate," *International Journal of Heat and Mass Transfer*, vol. 8, 1965, pp. 1135 -1151.

14 Taunton, J. W., Lightfoot, E. N., and Stewart, W. E., "Simultaneous Free-Convection Heat and Mass Transfer in Laminar Boundary Layers," *Chemical Engineering Science*, vol. 25, 1970, pp. 1927-1937.

15 Gebhart, B. and Pera, L., "The Nature of Vertical Natural Convection Flows Resulting from the Combined Buoyancy Effects of Thermal and Mass Diffusion," *International Journal of Heat and Mass Transfer*, vol. 14, 1971, pp. 2025 -2050.

16 Schenk, J., Altman, R., and De Wit, J. P. A., "Interaction between Heat and Mass Transfer in Simultaneous Natural Convection about an Isothermal Vertical Flat Plate," *Applied Scientific Research*, vol. 32, 1976, pp. 599-606.

17 Nilson, R. H., "Countercurrent Convection in a Double -Diffusive Boundary Layer," *Journal of Fluid Mechanics*, vol. 160, 1985, pp. 181-210.

18 Nilson, R. H., and Baer, M. P., "Double-Diffusive Counterbouyant Boundary Layer in Laminar Natural Convection," *International Journal of Heat and Mass Transfer*, vol. 25, No. 2, 1982, pp. 285-287.

19 Chen, T. S. and Yuh, C. F., "Combined Heat and Mass Transfer in Natural Convection on Inclined Surfaces," *Numerical Heat Transfer*, vol. 2, 1979, pp. 233-250.

20 Chen, T. S. and Yuh, C. F., "Combined Heat and Mass Transfer in Natural Convection along a Vertical Cylinder," *International Journal of Heat and Mass Transfer*, vol. 23, 1980, pp. 451-461.

21 Bottemanne, F. A., "Experimental Results of Pure and Simultaneous Heat and Mass Transfer by Free Convection about a Vertical Cylinder for $Pr = 0.71$ and $Sc = 0.63$," *Applied Scientific Research*, vol. 25, 1972, pp. 372-382.

22 Hasan, M. and Mujumdar, A. S., "Simultaneous Heat and Mass Transfer in Free Convection from a Horizontal Cylinder," *American Institute of Aeronautics and Astronautics Journal*, vol. 23, 1985, pp. 1602-1608.

23 Trevisan, O. V., and Bejan, A. "Combined Heat and Mass Transfer by Natural Convection in a Vertical Enclosure," *Journal of Heat Transfer*, vol. 109, 1987, pp. 104-112.

24 Kimura, S., and Bejan, A., "The Boundary Layer Natural Convection Regime in a Rectangular Cavity with Uniform Heat Flux from the Side," *Journal of Heat Transfer*, vol. 106, 1984, pp. 98-103.

25 Adams, J. A. and McFadden, P. W., "Simultaneous Heat and Mass Transfer in Free Convection with Opposing Body Forces," *American Institute of Chemical Engineers Journal*, vol. 12, No. 4, 1966, pp. 642 -547.

26 De Leeuw Den Bouter, J. A., De Munnik, B., and Heerties, P. M., "Simultaneous Heat and Mass Transfer in Laminar Free Convection from a Vertical Plate", *Chemical Engineering Science*, vol. 23, 1968, pp. 1185 -1190.

27 Bottemanne, F. A., "Theoretical Solution of Simultaneous Heat and Mass Transfer by Free Convection about a Vertical Flat Plate," *Applied Scientific Research*, vol. 25, 1971, pp. 137-149.

28 Mendenhall, C. E., and Mason, M., "The Stratified Subsidence of Fine Particles," *Proceedings from the National Academy of Sciences of the U.S.A*, vol. 9, 1924, pp. 199-207.

29 Thorpe, S. A., Hutt, P. K., and Soulsby, R., "The Effect of Horizontal Gradients on Thermohaline Convection," *Journal of Fluid Mechanics*, vol. 38, part 2, 1969, pp. 375-400.

30 Chen, C. F., Briggs, D. G., and Wirtz, R. A., "Stability of Thermal Convection in a Salinity Gradient due to Lateral Heating," *International Journal of Heat and Mass Transfer*, vol. 14, 1971, pp. 57 -65.

31 Wirtz, R. A., Briggs, D. G., and Chen, C. F., "Physical and Numerical Experiments on Layered Convection in a Density-Stratified Fluid", *Geophysical Fluid Dynamics*, vol. 3, 1972, pp. 265-288.

32 Bergman, T. L., Incropera, F. P., and Viskanta, R., "Correlation of Mixed Layer Growth in a Double-Diffusive, Salt-Stratified System Heated from Below," *Journal of Heat Transfer*, vol. 108, 1986, pp. 206-211.

33 Bergman, T. L., and Ungan, A., "Experimental and Numerical Investigation of Double-Diffusive Convection Induced by a Discrete Heat Source," *International Journal of Heat and Mass Transfer*, vol. 29, No. 11, 1986, pp. 1695-1709.

34 Kamotani, Y., Wang, L. W., Ostrach, S., and Jiang, H. D., "Experimental Study of Natural Convection in Shallow Enclosures with Horizontal Temperature and Concentration Gradients," *International Journal of Heat and Mass Transfer*, vol. 28, No. 1, 1985, pp. 165-173

35 Lee, T. S., Parikh, P. G., Acrivos, A., and Bershader, D., "Natural Convection in a Vertical Channel with Opposing Buoyancy Forces", *International Journal of Heat and Mass Transfer*, vol. 25, No. 4, 1982, pp. 499-511.

36 Roušar, I., and Cezner, V., "Simultaneous Flow of Heat and Ions in the Region of Natural Convection," *International Chemical Engineering*, vol. 15, No. 2, 1975, pp. 219-228.

37 Wirtz, R. A., "The Effect of Solute Layering on Lateral Heat Transfer in an Enclosure," *International Journal of Heat and Mass Transfer*, vol. 20, 1977, pp. 841-846.

38 Hassab, M. A., Tag, I. A., and Kamal, W. A., "Double-Diffusive Stability of Salinity Stratified Layers with Vertical Motion," Natural Circulation, HTD-vol. 92, ASME, 1987, pp. 299-306.

39 Moore, D. R., Toomre, J., Knobloch, E. and Weiss, N. O., "Period Doubling and Chaos in Partial Differential Equations for Thermosolutal Convection," *Nature*, vol. 303, 1983, pp. 663-667.

40 Bergman, T. L., and Srinivasan, R., "Numerical Simulation of Soret-Induced Double-Diffusion in an Initially Uniform Concentration Binary Liquid," *International Journal of Heat and Mass Transfer*, vol. 32, No. 4, 1989, pp. 679-687.

41 Lai, W. T., and Ramsey, J. W., "Natural Heat and Mass Transfer in a Rectangular Enclosure," Natural Circulation, HTD-vol. 92, ASME, 1987, pp. 361-372.

42 Ranganathan, P., Viskanta, R., "Natural Convection in a Square Cavity due to Combined Driving Forces," *Numerical Heat Transfer*, vol. 14, 1986, pp. 35-59.

43 Han, H., and Kuehn, T. H., "A Numerical Simulation for Double-Diffusive Natural Convection in a Vertical Rectangular Enclosure," Heat Transfer in Convective Flows (ed. Shah, R. K.), HTD-vol. 107, ASME, 1989, pp. 149-159.

44 Benard, C., Gobin, D., and Thevenin, J., "Thermosolutal Natural Convection in a Rectangular Enclosure: Numerical Results," Heat Transfer in Convective Flows (ed. Shah, R. K.), HTD-vol. 107, ASME, 1989, pp. 249-254.

45 Krishnan, R., "A Numerical Study of the Instability of Double-Diffusive Convection in a Square Enclosure with Horizontal Temperature and Concentration Gradients," Heat Transfer in Convective Flows (ed. Shah, R. K.), HTD-vol. 107, ASME, 1989, pp. 357-368.

46 Patankar, S. V., "A Calculation Procedure for Two-Dimensional Elliptic Situations," *Numerical Heat Transfer*, vol. 4, 1981, pp. 409 -425.

47 Raithby, G. D. and Schneider, G. E., "Ch. 6. Elliptic Systems: Finite-Difference Method II," Handbook of Numerical Heat Transfer, (Eds.: Minkowycz, W. J., Sparrow, E. M., Schneider, G. E., and Pletcher, R. H.), John Wiley & Sons, Inc., 1988.

48 "Private communication from Dr. Hrymak", Department of Chemical Engineering, McMaster University, 1990.

49 de Vahl Davis, G. and Mallinson, G. D., "False Diffusion in Numerical Fluid Mechanics," School of Mech. and Ind. Eng. Rept., Univ. Of New South Wales, 1972/FMT/1.

50 Thomas, R. W., and de Vahl Davis, G., "Natural Convection in Annular and Rectangular Cavities, A Numerical Study," Fourth International Heat Transfer Conference, Paris-Versailles, vol. 4, NC 2.4, 1970.

51 Thomas, L. H., "Elliptic Problems in Linear Difference Equations over a Network," Watson Sci. Comput. Lab. Rept., Columbia University, New York, 1949.

APPENDIX A

TABULATIONS OF NUMERICAL RUNS

Table A-1 Grid Independence Runs for Non-Uniform Grids (Ar = 1, K = 1, Pr = 1, n = -1, Le = 4 and Ra_T = 20 000)

m	*i*	$\overline{Nu}$	$\overline{Sh}$	Max. Cell size
11	0	3.1854	5.2596	0.0909
11	10	3.1137	4.9931	0.1280
11	20	3.0641	4.8713	0.1719
11	30	3.0223	4.7785	0.2214
21	0	3.1174	5.0059	0.0476
21	5	3.0960	4.9504	0.0639
21	10	3.0782	4.9068	0.0828
21	15	3.0620	4.8686	0.1042
21	20	3.0462	4.8332	0.1279
21	30	3.0146	4.7666	0.1810
31	0	3.1065	4.9860	0.0323
31	5	3.0914	4.9477	0.0483
31	10	3.0783	4.9147	0.0679
31	15	3.0643	4.8808	0.0906
31	20	3.0493	4.8458	0.1159
41	0	3.1038	4.9829	0.0244
41	5	3.0925	4.9540	0.0405
41	10	3.0807	4.9241	0.0610
41	15	3.0670	4.8900	0.0851
41	20	3.0506	4.8513	0.1117
41	30	3.0182	4.7781	0.1703
51	0	3.1038	4.9836	0.0196
61	0	3.1009	4.9807	0.0164
61	10	3.0931	4.9528	0.0554
101	0	3.0584	4.8801	0.0528

Table A-2 Grid Independence Runs for Semi-Uniform Grids (Ar = 1, K = 1, Pr = 1, n = -1, Le = 4 and Ra_T = 20 000)

m	s	$\overline{Nu}$	$\overline{Sh}$	Core Cell Size
11	1	3.1854	5.2596	0.0909
11	2	3.0048	4.6492	0.1111
11	3	2.8472	4.4463	0.1429
11	5	2.9886	4.8867	0.3333
21	1	3.1174	5.0059	0.0476
21	3	3.1298	4.9749	0.0588
21	5	3.1180	4.8680	0.0769
21	7	2.9598	4.4877	0.1111
21	10	2.9527	4.8067	0.3333
31	1	3.1065	4.9860	0.0323
31	3	3.1125	4.9897	0.0370
31	5	3.1185	4.9907	0.0435
31	7	3.1256	4.9826	0.0526
31	10	3.1171	4.8630	0.0769
41	1	3.1038	4.9829	0.0244
41	3	3.1058	4.9855	0.0270
41	5	3.1083	4.9881	0.0303
41	7	3.1121	4.9916	0.0345
41	10	3.1210	4.9958	0.0435
51	1	3.1038	4.9836	0.0196
51	3	3.1001	4.9791	0.0213
51	5	3.1049	4.9860	0.0233
51	7	3.1067	4.9884	0.0256
51	10	3.1112	4.9948	0.0303
61	1	3.1009	4.9807	0.0164
61	3	3.0976	4.9766	0.0175
61	5	3.1046	4.9869	0.0189
61	7	3.1047	4.9868	0.0204
61	10	3.1079	4.9929	0.0233

Table A-3 Numerical Runs

Filename	Pr	Le	Ra_T	n	$\overline{Nu}$	$\overline{Sh}$	Max.ψ^*	Min.ψ^*
F13_L0-1	1	0.1	20000	-1	1.4430	1.4430	0.000	0.000
F13_L0-2	1	0.2	20000	-1	1.4430	1.4430	0.000	0.000
F13_L0-25	1	0.25	20000	-1	1.4430	1.4430	0.000	0.000
F13_L0-5	1	0.5	20000	-1	1.4430	1.4430	0.000	0.000
F13_L2	1	2	20000	-1	2.6023	3.3037	7.524	-0.017
F13_L5	1	5	20000	-1	3.2043	5.5584	9.224	-0.084
f13_L10	1	10	20000	-1	3.4312	7.5601	9.510	-0.138
F16_L0-1	1	0.1	80000	-1	5.3414	2.3923	0.506	-57.527
F19_L0-1	0.1	10	80000	-1	4.1975	9.7107	11.578	-0.766
F16_L10	1	10	80000	-1	5.0784	11.1982	14.715	-0.647
F19_L0-1B	0.1	10	8000	-1	2.2365	5.0400	4.920	-0.050
F21R_1E04	7	5	10000	-1	2.5918	4.4708	6.643	-0.021
F28N10_1P5	7	5	10000	-1.5	1.5564	3.1818	0.174	-1.242
F21R_2E05	7	5	200000	-1	6.2537	10.7277	21.399	-1.261
F21R_2E03	7	5	2000	-1	1.5906	2.6090	1.890	-0.005
MY16_PL10	7	5	5000	10	3.3482	8.8286	4.933	0.000
MY16_PL5	7	5	5000	5	3.0529	7.5083	4.827	0.000
MY16_PL2	7	5	5000	2	2.8444	6.2753	5.235	0.000
F27N5_P1	7	5	5000	-0.1	2.4876	4.8528	5.279	0.000
F27N5_P25	7	5	5000	-0.25	2.4413	4.7027	5.212	0.000
F27N5_P5	7	5	5000	-0.5	2.3507	4.4195	5.052	0.000
MR13_P995	7	5	5000	-.995	2.0755	3.6106	4.390	-0.007
MR13_1P0	7	5	5000	-1	1.4426	1.4426	0.000	0.000
F21R_5E03	7	5	5000	-1	2.0754	3.6068	4.389	-0.007
MR11_1P0005	7	5	5000	-1.000	1.4427	1.4442	0.017	-0.035
MR5N5_1P005	7	5	5000	-1.005	1.4432	1.4563	0.042	-0.101
MR14_1P005	7	5	5000	-1.005	2.0686	3.5897	4.365	-0.008
MR5N5_1P05	7	5	5000	-1.05	1.4485	1.5790	0.089	-0.306
MR14_1P05	7	5	5000	-1.05	2.0290	3.4753	4.384	-0.007
MR15_1P1	7	5	5000	-1.1	1.9763	3.3219	4.102	-0.027
MR16_1P15	7	5	5000	-1.15	1.8929	3.0714	3.865	-0.061
MR18_1P175	7	5	5000	-1.175	1.4650	1.9121	0.078	-0.573
F28N5_1P2	7	5	5000	-1.2	1.4686	1.9761	0.073	-0.613
F27N5_1P5	7	5	5000	-1.5	1.5149	2.6622	0.174	-1.242
F27N5_2	7	5	5000	-2	1.5985	3.5296	0.000	-1.396
F27N5_5	7	5	5000	-5	2.0606	6.0833	0.000	-2.657
F27N5_10	7	5	5000	-10	2.6038	7.9690	0.000	-3.610
MY15_PL10	7	5	20000	10	4.9546	12.9663	6.843	0.000
MY15_PL5	7	5	20000	5	4.6636	11.1284	7.125	0.000
MY15_PL2	7	5	20000	2	4.4561	9.4167	8.656	0.000
MY15_0	7	5	20000	0	3.9382	7.5205	9.794	0.000
MY29_P5	7	5	20000	-0.5	3.6780	6.7462	9.832	0.000

Filename	Pr	Le	Ra_T	n	$\overline{Nu}$	$\overline{Sh}$	Max.ψ^*	Min.ψ^*
F21R_2E04	7	5	20000	-1	3.2118	5.5024	9.294	-0.060
MY16_1P1	7	5	20000	-1.1	3.0350	5.0921	8.899	-0.148
JN6_1P125	7	5	20000	-1.125	2.9807	4.9732	8.767	-0.179
JN5_1P13	7	5	20000	-1.13	1.9580	2.7999	6.491	-0.640
MY29_1P15	7	5	20000	-1.15	1.8130	2.6737	5.400	-0.737
MY31_1P2	7	5	20000	-1.2	1.7397	2.8885	4.598	-0.934
MY16_1P2	7	5	20000	-1.2	2.7720	4.5445	8.201	-0.337
MY16_1P25	7	5	20000	-1.25	2.4850	3.9710	7.462	-0.580
JN1_1P26	7	5	20000	-1.26	1.7082	3.1392	4.046	-1.090
MY29_1P35	7	5	20000	-1.35	1.6860	3.4703	3.367	-1.267
F27N_1P5	7	5	20000	-1.5	1.6777	3.9316	2.403	-1.482
F27N_2	7	5	20000	-2	1.7908	5.1803	0.113	-2.111
F27N_5	7	5	20000	-5	2.7018	9.0415	0.000	-3.737
F27N_10	7	5	20000	-10	3.6493	11.7349	0.000	-4.933
JN26_PL10	7	1	50000	10	10.5203	10.5203	24.990	0.000
JN26_PL5	7	1	50000	5	8.8724	8.8724	21.699	0.000
JN26_PL2	7	1	50000	2	7.2649	7.2649	18.194	0.000
JN26_PL1	7	1	50000	1	6.4466	6.4466	16.257	0.000
JN26_0	7	1	50000	0	5.2313	5.2313	13.185	0.000
JN26_P5	7	1	50000	-0.5	4.2233	4.2233	10.571	0.000
JL5_P8	7	1	50000	-0.8	3.1579	3.1579	7.455	0.000
JN26_P95	7	1	50000	-0.95	2.0027	2.0027	3.464	0.000
JN28_P995	7	1	50000	-0.995	1.4546	1.4546	0.450	0.000
JN15_1	7	1	50000	-1	1.4427	1.4427	0.000	0.000
JN25_1P005	7	1	50000	-1.005	1.4546	1.4546	0.000	-0.450
JN26_1P02	7	1	50000	-1.02	1.6001	1.6001	0.000	-1.688
JN22_1P05	7	1	50000	-1.05	2.0027	2.0027	0.000	-3.464
JN20_1P1	7	1	50000	-1.1	2.5132	2.5132	0.000	-5.301
JN20_1P2	7	1	50000	-1.2	3.1575	3.1575	0.000	-7.452
JN20_1P5	7	1	50000	-1.5	4.2233	4.2233	0.000	-10.571
JN15_2	7	1	50000	-2	5.2313	5.2313	0.000	-13.185
JN15_5	7	1	50000	-5	7.8985	7.8985	0.000	-19.623
JN15_10	7	1	50000	-10	9.9481	9.9481	0.000	-23.878
MY7_PL19	7	2	50000	10	9.2020	12.8425	15.548	0.000
MY7_PL5	7	2	50000	5	7.8926	10.9623	14.308	0.000
MY7_PL2	7	2	50000	2	6.6732	9.1556	13.513	0.000
MY7_0	7	2	50000	0	5.2313	6.9879	13.185	0.000
MY7_P5	7	2	50000	-0.5	4.5900	6.0318	13.177	0.000
MY22_1P9	7	2	50000	-0.9	3.7525	4.7859	12.500	-0.004
MY11_1	7	2	50000	-1	1.4430	1.4430	0.000	0.000
MY7_1	7	2	50000	-1	3.3847	4.2459	11.737	-0.060
MY23_1P02	7	2	50000	-1.02	3.2876	4.1052	11.491	-0.094
MY24_1p04	7	2	50000	-1.04	3.1759	3.9449	11.188	-0.160
MY16_1P05	7	2	50000	-1.05	1.8180	2.1147	6.361	-1.063
MY28_1P075	7	2	50000	-1.075	2.9086	3.5689	10.414	-0.395
MY30_1P085	7	2	50000	-1.085	2.7672	3.3773	10.021	-0.563

Filename	Pr	Le	Ra_T	n	$\overline{Nu}$	$\overline{Sh}$	Max.ψ^*	Min.ψ^*
JN6_1P09	7	2	50000	-1.09	1.7555	2.2315	4.379	-1.536
MY14_1P1	7	2	50000	-1.1	1.7571	2.2722	4.074	-1.622
MY10_1P2	7	2	50000	-1.2	1.8282	2.6529	0.890	-2.374
MY10_1P3	7	2	50000	-1.3	2.0189	3.1339	0.243	-2.931
MY10_1P4	7	2	50000	-1.4	2.2158	3.5798	0.005	-3.380
MY7_1P5	7	2	50000	-1.5	2.4118	3.9855	0.002	-3.781
MY9_1P75	7	2	50000	-1.75	2.8820	4.8463	0.000	-4.637
MY7_2	7	2	50000	-2	3.3108	5.5360	0.000	-5.363
MY8_2P5	7	2	50000	-2.5	4.0371	6.5819	0.000	-6.554
MY8_4	7	2	50000	-4	5.5025	8.4931	0.000	-8.921
MY8_7	7	2	50000	-7	7.1358	10.5732	0.000	-11.453
MY8_10	7	2	50000	-10	8.1667	11.9024	0.000	-12.969
A10_PL10	7	5	50000	10	6.4265	16.5051	8.568	0.000
A10_PL5	7	5	50000	5	6.1063	14.2525	8.944	0.000
A10_PL2	7	5	50000	2	5.9240	12.1640	11.491	0.000
A10_00	7	5	50000	0	5.2313	9.8417	13.185	0.000
A10_P2	7	5	50000	-0.2	5.1071	9.4877	13.304	0.000
A10_P5	7	5	50000	-0.5	4.8769	8.8531	13.445	0.000
A10_P8	7	5	50000	-0.8	4.5483	7.9902	13.500	-0.025
F21R_5E04	7	5	50000	-1	4.1994	7.1654	13.376	-0.325
MR21_1P1	7	5	50000	-1.1	3.9363	6.6489	13.027	-0.654
A10_1P15	7	5	50000	-1.15	3.7717	6.3607	12.696	-0.855
A10_1P175	7	5	50000	-1.175	3.6761	6.1997	12.459	-0.962
A16_1P18	7	5	50000	-1.18	3.6556	6.1655	12.406	-0.983
A16_1P19	7	5	50000	-1.19	2.3119	3.5028	9.428	-0.894
A4_1P2	7	5	50000	-1.2	2.2818	3.5677	9.210	-0.976
A11_1P2	7	5	50000	-1.2	3.5679	6.0203	12.167	-1.066
A11_1P25	7	5	50000	-1.25	3.2806	5.5414	11.275	-1.309
A16_1P275	7	5	50000	-1.275	3.0259	5.0948	10.424	-1.469
A17_1P285	7	5	50000	-1.285	2.1782	4.1003	8.203	-1.398
MR23_1P3	7	5	50000	-1.3	2.1680	4.1852	8.066	-1.449
F28N50_1P5	7	5	50000	-1.5	2.0890	5.1147	6.425	-1.950
MR19_1P5	7	5	50000	-1.5	2.0890	5.1147	6.425	-1.950
A18_1P75	7	5	50000	-1.75	2.0527	5.9401	4.581	-2.320
MR19_2	7	5	50000	-2	2.0087	6.5997	1.478	-2.689
A4_2P2	7	5	50000	-2.2	2.1048	7.1944	0.462	-2.902
A4_2P5	7	5	50000	-2.5	2.2615	7.9515	0.068	-3.164
A4_3	7	5	50000	-3	2.5104	8.9756	0.000	-3.533
MR19_5	7	5	50000	-5	3.3327	11.6136	0.000	-4.568
MR19_10	7	5	50000	-10	4.6289	14.9656	0.000	-6.013
A21_PL10	7	10	50000	10	4.4465	19.7822	5.821	0.000
A21_PL5	7	10	50000	5	5.3483	17.1570	9.110	0.000
A21_PL2	7	10	50000	2	5.5811	14.9571	12.059	0.000
A21_0	7	10	50000	0	5.2313	12.5365	13.185	0.000
A17_P5	7	10	50000	-0.5	5.0064	11.4890	13.430	0.000
A17_1	7	10	50000	-1	4.5552	9.8533	13.639	-0.377

Filename	Pr	Le	Ra_T	n	$\overline{Nu}$	$\overline{Sh}$	Max.ψ^*	Min.ψ^*
JL4_1P1	7	10	50000	-1.1	4.4070	9.5026	13.638	-0.576
D19_1P2	7	10	50000	-1.2	4.2309	9.1474	13.554	-0.794
A21_1P25	7	10	50000	-1.25	4.1294	8.9564	13.452	-0.905
JL9_1P32	7	10	50000	-1.32	3.9662	8.6568	13.194	-1.060
JL5_1P35	7	10	50000	-1.35	1.6982	4.4390	4.524	-0.983
A25_1P35	7	10	50000	-1.35	3.8858	8.5101	13.031	-1.131
MY15_1P375	7	10	50000	-1.375	2.6254	5.0869	10.267	-0.701
JL3_1P4	7	10	50000	-1.4	1.7511	4.5849	5.104	-1.039
MY14_1P4	7	10	50000	-1.4	2.5888	5.2650	10.057	-0.800
MY7_1P4	7	10	50000	-1.4	3.7298	8.2223	12.661	-1.255
MY11_1P45	7	10	50000	-1.45	2.5375	5.6170	9.726	-0.956
MY9_1P45	7	10	50000	-1.45	3.5238	7.8287	12.094	-1.394
MY9_1P475	7	10	50000	-1.475	3.3738	7.5258	11.640	-1.471
MY14_1P485	7	10	50000	-1.485	3.2858	7.3389	11.365	-1.511
JN28_1P5	7	10	50000	-1.5	1.8222	5.1818	5.580	-1.191
A17_1P5	7	10	50000	-1.5	2.4973	5.9477	9.431	-1.080
JN27_1P7	7	10	50000	-1.7	1.8420	6.3371	5.193	-1.476
MY10_1P7	7	10	50000	-1.7	2.3676	7.0366	8.395	-1.437
JN26_1P725	7	10	50000	-1.725	1.8368	6.4681	5.066	-1.507
JN11_1P75	7	10	50000	-1.75	1.8312	6.5956	4.940	-1.535
JL3_1P75	7	10	50000	-1.75	2.3380	7.2590	8.138	-1.504
JN7_1P85	7	10	50000	-1.85	1.8077	7.0729	4.374	-1.635
JL4_1P85	7	10	50000	-1.85	2.2806	7.6577	7.632	-1.616
A17_2	7	10	50000	-2	1.7817	7.7068	0.357	-1.746
JL4_2	7	10	50000	-2	2.1984	8.1613	6.869	-1.745
JL9_2P1	7	10	50000	-2.1	2.1445	8.4393	6.336	-1.811
JL9_2P15	7	10	50000	-2.15	2.1148	8.5498	6.049	-1.842
JL6_2P2	7	10	50000	-2.2	1.7713	8.4441	2.631	-1.836
JN7_2P25	7	10	50000	-2.25	1.7724	8.6134	2.438	-1.851
A17_2P5	7	10	50000	-2.5	1.7934	9.3881	1.562	-1.957
A17_3	7	10	50000	-3	1.8779	10.6507	0.433	-2.138
A17_4	7	10	50000	-4	2.0697	12.4769	0.003	-2.441
A21_7	7	10	50000	-7	2.5492	15.7686	0.000	-3.073
A21_10	7	10	50000	-10	2.9167	17.8203	0.000	-3.531
MY10_PL10	7	5	100000	10	7.8178	19.7138	10.218	0.000
MY10_PL5	7	5	100000	5	7.4562	17.0710	10.556	0.000
MY10_PL2	7	5	100000	2	7.2833	14.6498	13.853	0.000
MY10_0	7	5	100000	0	6.4466	11.9757	16.257	0.000
A18_P5	7	5	100000	-0.5	6.0050	10.8000	16.710	0.000
F21R_1E05	7	5	100000	-1	5.1174	8.7506	16.928	-0.755
MR17_1P1	7	5	100000	-1.1	4.7991	8.2127	16.819	-1.203
A3_1P2	7	5	100000	-1.2	4.3828	7.5700	16.259	-1.689
MY7_1P22	7	5	100000	-1.22	4.2774	7.4087	16.033	-1.791
A18_1P225	7	5	100000	-1.225	4.2488	7.3646	15.965	-1.815
A9_1P225	7	5	100000	-1.225	4.2490	7.3650	15.966	-1.815
MY7_1P23	7	5	100000	-1.23	2.7921	4.3672	12.763	-1.039
A24_1P235	7	5	100000	-1.235	2.7765	4.4077	12.653	-1.047

Filename	Pr	Le	Ra_T	n	$\overline{Nu}$	$\overline{Sh}$	Max.ψ^*	Min.ψ^*
A19_1P235	7	5	100000	-1.235	4.1893	7.2729	15.820	-1.864
A20_1P245	7	5	100000	-1.245	4.1252	7.1734	15.656	-1.918
A3_1P25	7	5	100000	-1.25	2.7439	4.5319	12.392	-1.196
A24_1P25	7	5	100000	-1.25	4.0911	7.1200	15.564	-1.946
MY7_1P26	7	5	100000	-1.26	4.0182	7.0052	15.361	-2.007
MY8_1P27	7	5	100000	-1.27	3.9349	6.8728	15.122	-2.063
MY10_1P28	7	5	100000	-1.28	3.8413	6.7203	14.829	-2.134
MY11_1P29	7	5	100000	-1.29	3.7149	6.5119	14.441	-2.203
MR22_1P3	7	5	100000	-1.3	2.6821	4.9305	11.764	-1.544
MR17_1P5	7	5	100000	-1.5	2.5709	6.1737	9.877	-2.334
JL10_1P7	7	5	100000	-1.7	2.5061	7.0523	8.124	-2.753
A17_1P75	7	5	100000	-1.75	2.4939	7.2367	7.706	-2.830
JL11_1P8	7	5	100000	-1.8	2.4822	7.4078	7.265	-2.901
JL10_1P9	7	5	100000	-1.9	2.2179	7.5076	3.749	-3.060
MR17_2	7	5	100000	-2	2.2585	7.9053	2.971	-3.206
MY10_2P5	7	5	100000	-2.5	2.5612	9.5545	0.435	-3.713
A18_3P5	7	5	100000	-3.5	3.1886	11.7915	0.000	-4.456
MR17_5	7	5	100000	-5	3.9456	13.9458	0.000	-5.296
MR17_10	7	5	100000	-10	4.5626	17.9030	0.000	-7.090

APPENDIX B

SIMPLER ALGORITHM

The governing equations are numerically solved using a finite volume approach. The variables are determined at discrete points on a staggered grid in which Patankar's *S*emi-*I*mplicit *M*ethod for *P*ressure *L*inked *E*quations-*R*evised (SIMPLER) algorithm [7,46] is adopted.

1. Equation Discretization

The governing equations can simply be expressed in a generalized conservation non-dimensional equation form with a dependent variable (ϕ), a diffusion constant (Γ) and a source term (S)

$$\frac{\partial \phi}{\partial t^*} + u^* \frac{\partial \phi}{\partial r^*} + v^* \frac{\partial \phi}{\partial z^*} = \Gamma \left[\frac{\partial}{r^* \partial r^*} \left(r^* \frac{\partial \phi}{\partial r^*} \right) + \frac{\partial^2 \phi}{\partial z^{*2}} \right] + S \tag{B.1}$$

Since we are concerned only with the steady state solution we can neglect the time dependant term. The integration of equ.(B.1) over the control volume in figure B.1 gives

$$J_e - J_w + J_n - J_s = (S_C + S_P \phi_P)\, r_P^*\, \Delta r^*\, \Delta z^* \tag{B.2}$$

where J represents the total flux across each control volume face

$$J_e = u_e^*\, r_e^*\, \phi_e\, \Delta z^* - \Gamma \left(r^* \frac{\partial \phi}{\partial r^*} \right)_e \Delta z^*$$

$$J_w = u_w^*\, r_w^*\, \phi_w\, \Delta z^* - \Gamma \left(r^* \frac{\partial \phi}{\partial r^*} \right)_w \Delta z^* \tag{B.3}$$

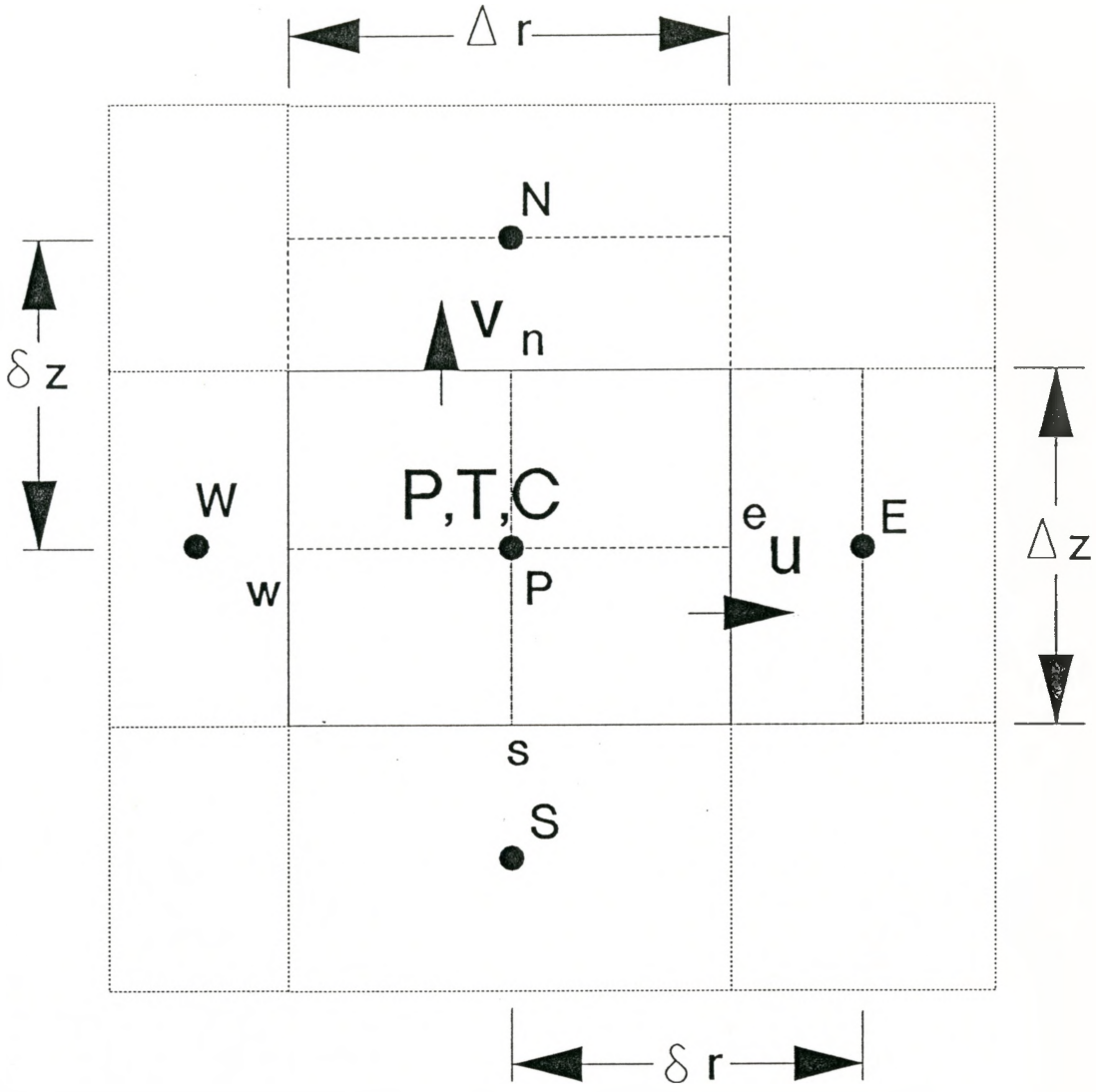

Figure B.1 Layout of a Typical Control Volume and Neighboring Points

$$J_n = v_n^* r_P^* \phi_n \Delta r^* - \Gamma \left(\frac{\partial \phi}{\partial z^*} \right)_n r_P^* \Delta r^*$$

$$J_s = v_s^* r_P^* \phi_s \Delta r^* - \Gamma \left(\frac{\partial \phi}{\partial z^*} \right)_s r_P^* \Delta r^*$$

And $(S_c + S_P \phi_P)$ represents the linearized source term.

The continuity equation is expressed as

$$\frac{\partial (r^* u^*)}{r^* \partial r^*} + \frac{\partial v^*}{\partial z^*} = 0 \qquad \text{(B.4)}$$

Integrating eq. (B.4) over the control volume

$$F_e - F_w + F_n - F_s = 0 \qquad \text{(B.5)}$$

where,

$$F_e = r_e^* u_e^* \Delta z^*, \qquad F_w = r_w^* u_w^* \Delta z^*$$
$$F_n = v_n^* r_P^* \Delta r^*, \qquad F_s = v_s^* r_P^* \Delta r^* \qquad \text{(B.6)}$$

If equation (B.5) is multiplied by ϕ_P and subtracted from equation (B.2), we obtain

$$(J_e - F_e \phi_P) - (J_w - F_w \phi_P) + (J_n - F_n \phi_P) - (J_s - F_s \phi_P)$$
$$= (S_c + S_P \phi_P) r_P^* \Delta r^* \Delta z^* \qquad \text{(B.7)}$$

The terms in the parentheses can be expressed in the following manner:

$$J_e - F_e \phi_P = a_E (\phi_P - \phi_E), \qquad (J_w - F_w \phi_P) = a_W (\phi_W - \phi_P) \qquad \text{(B.8)}$$

with similar expressions for J_n and J_s we can now write the discretization equation as

$$a_P \phi_P = a_E \phi_E + a_W \phi_W + a_N \phi_N + a_S \phi_S + b \qquad \text{(B.9)}$$

where

$$a_E = D_e A(|Pe_e|) + MAX(-F_e, 0)$$
$$a_W = D_w A(|Pe_w|) + MAX(F_w, 0) \qquad (B.10)$$
$$a_N = D_n A(|Pe_n|) + MAX(-F_n, 0)$$
$$a_S = D_s A(|Pe_s|) + MAX(F_s, 0)$$

$$b = S_c \, r_P^* \, \Delta r^* \Delta z^* \qquad (B.11)$$

$$a_P = a_E + a_W + a_N + a_S - S_P \, r_P^* \, \Delta r^* \Delta z^* \qquad (B.12)$$

$$D_e = \frac{\Gamma \, \Delta z^* \, r_e^*}{(\delta r^*)_e}, \qquad D_w = \frac{\Gamma \, \Delta z^* \, r_w^*}{(\delta r^*)_w},$$
$$D_n = \frac{\Gamma \, \Delta r^* \, r_P^*}{(\delta z^*)_n}, \qquad D_s = \frac{\Gamma \, \Delta r^* \, r_P^*}{(\delta z^*)_s} \qquad (B.13)$$

The function A is a weighting function determining the dependant variable (ϕ) value at the control volume walls. This value is determined by the relative strengths of convection and diffusion, also known as the Peclet number.

$$Pe_e = \frac{u_e^* \, (\delta r)_e}{\Gamma}, \qquad Pe_w = \frac{u_w^* \, (\delta r)_w}{\Gamma},$$
$$Pe_n = \frac{v_n^* \, (\delta z)_n}{\Gamma}, \qquad Pe_s = \frac{v_s^* \, (\delta z)_s}{\Gamma} \qquad (B.14)$$

The power law scheme is chosen for interpolating the convective terms at the control volume walls

$$A(|Pe|) = MAX\left[0, \; (1 - 0.1|Pe|)^5\right]. \qquad (B.15)$$

2. Solution Technique

The appropriate control volumes for the velocity components u and v are shown in fig. 4.1. The two faces of the control volume around

the u_e pass through the grid points P and E. The corresponding discretized momentum equation can be written as

$$a_e u_e^* = \sum a_{nb} u_{nb}^* + b + \Delta z^* r_e^* (P_P^* - P_E^*) \tag{B.16}$$

A similar expression can defined for the axial momentum

$$a_n v_n^* = \sum a_{nb} v_{nb}^* + b + \Delta r^* r_p^* (P_P^* - P_N^*) \tag{B.17}$$

It is not directly possible to solve for the velocities using the discretized momentum equation as the pressure field is not known. However we can obtain a velocity field form a guessed pressure field. Let $\bar{u}$ denote the velocity field obtained form the guessed pressure field $\bar{P}$.

$$a_e \bar{u}_e = \sum a_{nb} \bar{u}_{nb} + b + \Delta z^* r_e^* (\bar{P}_P - \bar{P}_E) \tag{B.18}$$

The estimated pressure and velocity field will generally not satisfy the continuity equation. For this purpose the fields may be corrected using a pressure correction (P′) and a corresponding velocity correction (u′)

$$P^* = \bar{P} + P' \tag{B.19}$$

$$u^* = \bar{u} + u' \tag{B.20}$$

$$v^* = \bar{v} + v' \tag{B.21}$$

Subtraction of eq.(B.18) for (B.16) gives

$$a_e u'_e = \sum a_{nb} u'_{nb} + \Delta z^* r_e^* (P'_P - P'_E) \tag{B.22}$$

Assuming that $\sum a_{nb} u'_{nb}$ is negligible, (at convergence, this correction term will be zero, such that its absence does not effect the final solution) equation (B.22) may be rewritten

$$u_e^* = \tilde{u}_e + d_e (P'_P - P'_E), \qquad \text{where} \quad d_e = \frac{\Delta z^* r_e^*}{a_e} \tag{B.23}$$

The pressure-correction equation is obtained by substituting the velocity-correction formulas (B.23) into the discretized continuity equation. The resulting equation can be written as

$$a_P P'_P = a_E P'_E + a_W P'_W + a_N P'_N + a_S P'_S + b \tag{B.24}$$

where

$$a_E = a_e d_e^2, \qquad a_W = a_w d_w^2, \qquad a_N = a_n d_n^2, \qquad a_S = a_s d_s^2 \tag{B.25}$$

$$a_P = a_E + a_W + a_N + a_S \tag{B.26}$$

$$b = \left(\bar{u}_w r^*_w - \bar{u}_e r^*_e \right) \Delta z^* + \left(\bar{v}_s - \bar{v}_n \right) r^*_P \Delta r^* \tag{B.27}$$

It may be noted that the term b in eq. (B.24) represents the residual for the continuity equation when an estimated velocity field is applied.

An equation is required for the pressure field itself. Patankar found that the pressure correction does a good job of correcting the velocities, however it does a relatively poor job of correcting the pressure field. In order to obtain a more efficient algorithm Patankar used a pseudo-velocity field to obtain the pressure field. With reference to eq. (B.16), a pseudo-velocity $\hat{u}_e$ can be defined as

$$\hat{u}_e = \frac{\sum a_{nb} u^*_{nb} + b}{a_e} \tag{B.28}$$

The pressure equation is written as

$$a_P P^*_P = a_E P^*_E + a_W P^*_W + a_N P^*_N + a_S P^*_S + b \tag{B.29}$$

where the coefficients a_E, a_W, a_N, a_S and a_P are given by eqs. (B.25) and (B.26) and b is defined by

$$b = \left(\hat{u}_w r_w^* - \hat{u}_e r_e^* \right) \Delta z^* + \left(\hat{v}_s - \hat{v}_n \right) r_P^* \Delta r^* \qquad (B.30)$$

The only difference between the pressure-correction and pressure equations is that the b term is calculated in terms of the estimated velocity field in one case and the pseudo-velocity field in absence of a pressure force in the other.

The overall calculation procedure is outlined as follows

1. Start with the guessed values for all relevant dependent variables, especially for the velocity components.
2. Calculate the coefficients in the momentum equations and hence evaluate $\hat{u}$ and $\hat{v}$ from equations like (B.28) by substituting the values of the neighbor velocities on the right-hand side.
3. Evaluate the term b from eq. (B.30) and hence solve eq. (B.29) to obtain the pressure field P^*.
4. Regarding this pressure as $\bar{P}$, solve the momentum equation such as (B.18) to obtain $\bar{u}$ and $\bar{v}$.
5. Calculate the term b from eq. (B.27) and hence solve the pressure-correction equation (B.24).
6. Using the P′ field, correct the estimated velocities via equations such as (B.23).
7. Solve the discretization equations for the other ϕ's such as temperature and concentration, provided they influence the flow field.
8. Return to step 2 with the corrected velocity field and the new values of all other ϕ's, and repeat the process until convergence.

APPENDIX C

TRIDIAGONAL MATRIX ALGORITHM (TDMA)

The standard tridiagonal form is given by

$$\begin{bmatrix} d_1 & a_1 & & & & \\ b_2 & d_2 & a_2 & & 0 & \\ & b_3 & d_3 & a_3 & & \\ & & & \ddots & & \\ & 0 & & b_{n-1} & d_{n-1} & a_{n-1} \\ & & & & b_n & d_n \end{bmatrix} \begin{bmatrix} x_1 \\ x_2 \\ x_3 \\ \vdots \\ x_{n-1} \\ x_n \end{bmatrix} = \begin{bmatrix} c_1 \\ c_2 \\ c_3 \\ \vdots \\ c_{n-1} \\ c_n \end{bmatrix}$$

Thomas [50] suggests that the following procedure be used to directly solve this series of equations.

The system is put into upper-triangular form by computing the new d_j according to

$$d_j = d_j - \frac{b_j}{d_{j-1}} a_{j-1}, \qquad j = 2,3,\ldots,n$$

and the new c_j by

$$c_j = c_j - \frac{b_j}{d_{j-1}} c_{j-1}, \qquad j = 2,3,\ldots,n$$

The unknowns are then computed from back-substitution according to $x_n = c_n / d_n$, and then

$$x_k = \frac{c_k - a_k x_{k+1}}{d_k}, \qquad k = n-1,n-2,\ldots,1$$